INFORMATION TO USERS

This manuscript has been reproduced from the microfilm master. UMI films the text directly from the original or copy submitted. Thus, some thesis and dissertation copies are in typewriter face, while others may be from any type of computer printer.

The quality of this reproduction is dependent upon the quality of the copy submitted. Broken or indistinct print, colored or poor quality illustrations and photographs, print bleedthrough, substandard margins, and improper alignment can adversely affect reproduction.

In the unlikely event that the author did not send UMI a complete manuscript and there are missing pages, these will be noted. Also, if unauthorized copyright material had to be removed, a note will indicate the deletion.

Oversize materials (e.g., maps, drawings, charts) are reproduced by sectioning the original, beginning at the upper left-hand corner and continuing from left to right in equal sections with small overlaps.

ProQuest Information and Learning
300 North Zeeb Road, Ann Arbor, MI 48106-1346 USA
800-521-0600

University of Alberta

Effects of Crossflow on Burning Rates of Rectangular Methanol Pool Fires

by

Joshua Anthony Robert Woods

A thesis submitted to the Faculty of Graduate Studies and Research in partial fulfillment of the requirements for the degree of Master of Science.

Department of Mechanical Engineering

Edmonton, Alberta
Spring 2005

ABSTRACT

Methanol pool fires were studied in a closed loop wind tunnel with crossflow speeds ranging from quiescent to 6 m/s. Burning rates for square trays ranging from 7.5 cm x 7.5 cm to 30 cm x 30 cm were measured. Geometry effects were investigated using circular and rectangular fuel trays. Mass fluxes of methanol measured in g/m^2s were found to increase threefold for the smallest square tray through the crossflow range, and remain constant for the largest tray. A transition region at approximately 1 m/s associated with the detachment of the flame off the back lip of the tray was observed to result in a sudden drop in burning rate. Circular tray geometry was found to exhibit the same magnitude of burning rate as its square area equivalent without the transition zone. The orientation of rectangular shaped trays was found to have a significant impact on burning rate, indicating a dependence on stream-wise length.

ACKKNOWLEDGEMENTS

I would like to thank the following people for supporting me and helping me throughout my academic career:

My supervisors Dr. Brian Fleck and Dr. Larry Kostiuk, for letting me take the project wherever I wanted and then providing thoughtful supervision and guidance to make it happen

Bernie Faulkner, Andrew Coward and Terry Nord, for their insight and technical assistance with the design and construction of my experimental apparatus, without them I would not have gotten far

The Mechanical Engineering Department and NSERC for financial support

My friends and colleagues, Kevin, Wayne, T.M., Rob, Dave, and others who made our windowless lab a much more pleasant place to work in

Bob Kievit, for his friendship over the years, interest in all my academic endeavors, and for always encouraging me to burn things

A special thanks to my parents and brother and sisters who have always been there for me and supported everything thing I've done

Most of all, my son Brennan for the joy he brings me, and my wife Jill for her patience, encouragement, love, and support in everything I do.

TABLE OF CONTENTS

LIST OF FIGURES

LIST OF TABLES

NOMENCLATURE

A	surface area
C_p	fuel specific heat (J/g-K)
D	pool diameter
d	freeboard height (m)
Fr	Froude number
h	convection heat transfer coefficient (W/m^2)
H_v	heat of vaporization (J/g)
k	thermal conductivity (W/m-K)
l	heat of fuel vaporization
L	length
m	mass (g)
$\dot{m}$	mass burning rate (g/s)
$\dot{m}''$	mass flux (g/m^2s)
P	pressure
q	heat transfer rate (W)
Q_c	heat of combustion
R	gas constant (J/(kg.K)
Re	Reynold's number
T	temperature
t	time
U	crossflow speed (m/s)
U_c	critical crossflow speed
v	rate of fuel depletion
V	volume (m^3)
$\dot{V}$	volume rate (m^3/s)
W	width
β	scale factor
ε	emissivity
θ	flame angle
κ	absorption coefficient (m^{-1})
ρ	density
σ	Stefan-Boltzmann constant

1. INTRODUCTION

It would not be an exaggeration to say that modern society is highly reliant on hydrocarbon fuels in all their forms. The reason for this dependency is the high energy densities associated with the chemical energies of these substances. For example, methane, which is the main chemical component in natural gas, has stored within its structure approximately 50 MJ[1] of energy in each kilogram as it is converted through oxidation to carbon dioxide and water vapor (Turns, 2000). Similarly, hydrogen, gasoline, methanol and coal respectively have 142, 46, 23, and 25 MJ/kg associated with their burning.

The magnitude of these energy densities becomes more apparent once a comparison is made with other forms of energy. To match the energy density of, for example, methanol with potential energy, a 10 kg mass would have to be lifted over 230 kilometers above the surface of the earth. Similarly, to match the energy density of methanol with kinetic energy, a 10 kg mass would have to be accelerated to a velocity of 2150 m/s, or over Mach 6 in air at standard conditions.

Having this concentrated form of energy makes hydrocarbon fuels very useful in many sectors of society and the economy of the world. Hydrocarbon fuels are used for heating in residential or domestic applications (e.g., home heating, cooking or drying clothes) or in industrial applications (e.g., coke ovens for melting steel). These fuels are also the primary energy source in the transportation sector in the form of gasoline, diesel, methanol and aviation fuel. Electrical power generation also has a large component of its primary energy coming from the burning of coal, and more recently natural gas (Turns, 2000). Clearly, these fuels are integral to our everyday lives and therefore we regularly live and work around them.

Hydrocarbon fuels are available in gas, liquid and solid phases. The focus of this thesis is on the liquid phase of these fuels, which have their own unique and useful properties. Where most hydrocarbon fuels have a relatively high energy density, those in

[1] Based on Lower Heating Value

the condensed phase (liquids and solid) have much higher energy contents per unit volume compared to those in the gas phase under normal conditions. For example, the natural gas delivered to residences is rated at approximately 36 MJ/m^3, while gasoline is over one thousand times greater at 37 GJ/ m^3. When comparing liquid fuels to solid fuels it is important to note that liquids are much easier to handle than solids. These volumetric and material handling issues have historically made liquid hydrocarbons the fuel of choice in the transportation sector. It should be noted as well that liquid hydrocarbons also have many other functions than burning in that they are very good solvents (e.g., acetone) or regularly used as part of food preparation (e.g., vegetable cooking oil) and have found many applications in those roles.

The quantities of liquid fuels produced and used annually in Canada and the United States is remarkable. In Canada, annual oil production in 2003 totaled 3.1 million barrels[2] per day, of which 2.3 million was crude oil. Consumption of these oil products totaled 2.2 million barrels per day with the remainder being exported mainly to the United States. In the United States, oil production in 2003 totaled 7.9 million barrels per day with 5.7 million barrels being crude oil and consumption exceeded production at 20 million barrels per day. In 2002 the consumption of gasoline in the United States approached 9 million barrels per day or 371.6 million gallons per day (Energy Information Administration, 2004).

Liquid hydrocarbons are stored and transported in a variety of volumes. Lamp oils, acetone and cooking oils can be purchased in quantities measured in a few hundreds of millilitres. The fuel tank volumes on cars for gasoline and diesel are typically between 30 to 100 litres (Chevrolet, 2005). The highway transportation of liquid hydrocarbons occurs regularly by articulated truck-trailer units in volumes between 10,000 and 30,000 litres (Lapinetrucks, 2005). Similarly, a Boeing 747 has a fuel capacity of up to 240,000 litres (Boeing, 2005). Still larger volumes of liquid fuels can be found at refineries and tank farms where a single storage tank will hold quantities measured in millions of litres and be part of a collect of many tanks.

[2] One barrel is equal to 42 US gallons or 159 Litres

It would also not be an exaggeration to say that we have come to take the prevalence of the use and handling of liquid hydrocarbons, either as fuels or in their other applications, for granted. It is easy to forget the amount of energies contained within these fuels. Accidental spills of these liquids do occur, many without the incident becoming serious, but when ignited the consequences can be dangerous, if not catastrophic. In these more serious scenarios the spilled liquid fuels tend to collect in pools, creating a danger should they be accidentally ignited. The occurrence of pool fires are an important safety issue in the processing, handling and use of liquid hydrocarbons. Hence, the main motivation for this research is to contribute to a better understand the burning of liquid fuels in pools.

1.1 Pool Fire Background

Over the past few decades the amount of flammable fuels being transported across great distances has increased. Types of fuels include for example, propane, ethanol and liquefied natural gas (LNG) among many others. The increased transport of fuels enlarges the chance of accidental spills and ignition of the transported fuel.

Scientifically, the burning of a free horizontal fuel source is referred to as a pool fire and is essentially the combustion of a flammable material evaporating from a layer of liquid at the base of the fire. The danger and environmental impact of a pool fire can be greatly worsened by the type of fuel as well as surrounding conditions.

There has been a vast amount of pool fire research since the early 1950's with the purpose of understanding flame characteristics and the coupling between air entrainment and heat feedback to the fuel surface. The majority of this work has however, been under ideal quiescent conditions, meaning no crossflow of air.

Quiescent studies are useful for obtaining information about the flame and parameters such as fuel type and tray size. These can be varied readily to determine the impact on the flame such as the burning rate or heat release. In reality however, quiescent flames are rare, especially in the unpredictable case of an accident. It is more often than not that the conditions are least favorable for extinguishing and controlling the

fire. The addition of crossflow to a pool fire simulates more realistically actual pool fires since most spills occur in unpredictable environmental conditions including exposure to wind. However, the addition of a crossflow complicates the fluid mechanics and flame behaviour.

Research of crossflow on pool fires has focused on the physical aspects of the flame such as flame shape, flame tilt and heat release, among others. The danger associated with a pool fire, which is coupled with the heat release rate and the burning rate of the fuel, can be augmented by crossflow.

1.2 Crossflow and Burning Rates of Liquid Fuels

The addition of crossflow has multiple impacts on a fire over a liquid fuel surface. Crossflow increases the influx of needed oxygen to the combustion zone and also the convective heat transfer. The tilting effects of crossflow on the flame enables the flame to spread quicker over the fuel surface and is most often the biggest concern when dealing with large accidental industrial fires or forest fires which behave essentially in the same manner as pool fires.

The amount of fuel consumed in a pool fire is coupled in a positive feedback loop with fuel vaporization from the heat transferred from the flame. While much data have been accumulated for quiescent cases, there is less information on the effects of crossflow on pool fire burning rates. In addition to this, there is a significant amount of confounding and contradictory information between different research sources in the literature. Capener and Alger (1972) observed a decrease in burning rate for 1 m diameter pools of JP-5 fuel under 6 m/s crosswind. They reasoned that the decrease was caused by the shifting of the bulk of the flame downstream from having a centrally located apex, thus decreasing the flame volume and the radiative heat transfer to the fuel. Contrary to this, Lois and Swithenbank (1978) observed an increase in burning rate in hexane pool fires up to a 4 m/s crosswind with no additional rate increase with increasing wind speed.

A thorough review of the literature on pool fires in crossflows (Chapter 2) shows a systematic investigation into the effects of crossflow on pool fires is required. This should be performed by eliminating as many complicating factors as possible, allowing for clear results that explain in isolation each of the physical mechanisms governing the behaviour of this combustion system.

1.3 Objectives of Thesis

The inclusion of crossflow into combustion of pool fires increases the complexity of the system greatly. The problem can be made simpler or more complicated depending on the pool and surrounding geometry, fuel type, transient behaviour (e.g., consumption of the fuel in the pool), obstructions in the pool or air flow, and the characteristics of the crossflow in terms of shear and turbulence. An example of a complication is the height of the lip of the container above the fuel surface, which is called the "freeboard height". When the freeboard height is deep enough and subject to a crossflow it can initiate turbulence near the pool and thus affect the combustion. Reducing the freeboard height to essentially having the fuel container full would reduce these effects, if not eliminate this complication. However, a container with a fixed quantity of fuel results in a constantly increasing freeboard height; as the fuel is consumed the liquid level drops. Changing the geometry of the pool from circular to rectangular produces a much different leading edge when subject to crossflow. Also, a steady uniform crossflow (low turbulence intensity potential flow with a very thin boundary layer), as opposed to a turbulent crossflow may have much different impact on the flame and the consumption of the fuel.

The purpose of this research is to perform a systematic investigation of pool fires, but to limit the work to relatively simple geometries and conditions. It is worth emphasizing that this research is not directed to solving a particular fire or safety scenario. This research addresses the problem from a fundamental perspective to provide a better understanding of the general issues associated with the nature of crossflow on pool fires.

The following four objectives will be sought:

1. **Design, construct and implement a steady-state, steady-flow fuel delivery system to maintain the level of the fuel in burner tray and measure the volume of fuel consumed during combustion.**

In order to obtain valuable information about the characteristics of pool burning, the first objective must be satisfied. The burning rate is a key objective of this research and a high precision method of delivering and monitoring the fuel during the experiments is crucial to obtaining valuable information.

2. **Create "ideal" crossflow conditions across the burner trays to eliminate large complex flow structures and produce controllable simple quasi two-dimensional airflow across the fuel surface.**

Crossflow across a fuel tray with blunt edges would create complex air circulation and unwanted vortices which could confound the results of the experiments. By developing a burner tray which takes advantage of air flow aerodynamics and boundary layer theory, a fully attached crossflow can be produced across the fuel surface and eliminate further complications which would result from unsteady air flow caused by flow separation, recirculation or shedding structures over uneven surfaces.

3. **Use rectangular fuel trays to simplify upstream boundary conditions and to determine the effects of pool surface area and aspect ratio on the burning rate of pool fires.**

The use of a non-uniform leading edge adds further complexity to a pool fire. A circular fuel tray increases the difficulty in understanding lip effects, especially when the flame is pushed back due to crossflow. By using rectangular geometry, the upstream conditions of the flame can be simplified.

4. **Obtain both qualitative and quantitative information about methanol pool fires under quiescent and crossflow conditions in order gain an understanding of how tray size and crossflow conditions affect fuel consumption.**

The combustion of liquid methanol produces a low luminescent blue flame rather than a luminous bright orange flame that would result from a fuel such as acetone or diesel fuel. The use of a non-luminous flame was used in order to reduce the effects of radiation heat feedback to the fuel surface and thus simplify the problem somewhat. The primary objective of this research after eliminating as much complexity as possible is to observe the effects of crossflow on the burning rate of methanol pool fires. Also, to gain an understanding of how the burning rate is influenced by shape, relative size and crossflow conditions. Photographs of flames will be obtained and the coinciding flame shape and burning rate will be compared to determine if there is a significant coupling between flame shape and burning rate.

Information gained in this experimental study will help improve the overall understanding of pool fires and the complex interaction between the flame and the crossflow.

1.4 Thesis Outline

This thesis is composed of six chapters; this first chapter introduces the problem and itemizes the research goals. Chapter 2 is devoted to a review of literature relevant to this study. Chapter 3 is a description of the apparatus, methodology and the equipment used for this investigation. The diagnostics of important measurements are discussed in Chapter 4, and include measurement of crossflow speed and fuel burning rate. The experimental results are presented and analysed in Chapter 5 and conclusions are discussed in Chapter 6.

The literature review discusses fundamentals of liquid fuel combustion. More specifically, the scope is narrowed to diffusion flames and the ignition, flame spread and

flash point associated with diffusion flames. A pool fire overview follows and defines the fundamentals of pool fires and the points of interest relevant to this thesis, including the burning rate and heat transfer mechanisms. Three final literature topics relevant to this study are the effects of freeboard height, tunnel enclosure and more importantly the effects of crossflow.

An experimental apparatus was developed and is discussed following the literature review. By carefully constructing and choosing equipment for the research goals the complexity of the problem will be reduced significantly.

Results presented include burning rate data and trends for burner trays of 7.5 cm x 7.5 cm to as large as 30 cm x 30 cm in order to consider the effects of tray size. A base case tray is chosen with dimensions 15 cm x 15 cm and is compared with trays of equal area but different geometry. Results for rectangular trays 7.5 cm wide by 30 cm long, 30 cm wide by 7.5 cm long and for a circular tray will be presented and compared with the base case tray.

Finally the thesis will be concluded and future work and directions of this research will be proposed.

2. SURVEY OF LITERATURE

2.1 Fundamentals of Liquid Fuel Combustion

In order to better understand the combustion of liquid fuels it is important to first understand the basic principles and fundamentals behind the physical make-up of a flame. Although a combustible fuel can be in any state such as a piece of coal (solid), kerosene (liquid) or propane (gas), the combustion process occurs in the gaseous phase. Liquid fuels vaporize when heated sufficiently and then mix with surrounding ambient air. The mixing of air and fuel vapor depends on such factors such as temperature, pressure, type of fuel and whether the surrounding air is quiescent or in motion. Ignition will occur when the leanness of the fuel and air mixture is above the limit of flammability for the given fuel and exposed to a pilot source. Once ignited, the flame will propagate across the fuel surface and if the generated heat from the flame and products of combustion can cause further vaporization, the flame will become self-sustained (Kanury, 2002).

2.1.1 Diffusion Flames

Liquid fuels are used extensively in combustion applications however when describing the combustion process it is not the liquid fuel which burns rather it is a mixture of air and evaporated fuel vapour. Fristrom and Westenberg (1965) classify liquid-gas flames into three categories. The first occurs when the liquid fuel is dispersed colloidally in air in order that it evaporates entirely in the preheat zone, resulting in a premixed flame. This occurs if the fuel droplets are smaller than approximately $3x10^{-3}$cm in diameter and is found for example in an internal combustion engine. The second mode of liquid-gas burning is droplets in the range of $3x10^{-3}$ cm to 0.1 cm in diameter, which tend to burn as individual diffusion flames. They are called diffusion flames because the

mixture of fuel vapour and oxidant occur by diffusion at the same time as combustion. This behaviour of burning is very much the same as the burning of the wick of a candle. Finally, liquid drops greater than 1 cm in diameter are also diffusion flames but are typically referred to as pools and the relative size and geometry restrict the entrainment of air resulting in flames with large amounts of soot (Fristrom, 1965).

Generally, diffusion flames can be either homogeneous or heterogeneous (Kanury, 1975). In homogeneous diffusion flames the fuel and oxidant are both in vapour phase and are found for example in the combustion of natural gas. Heterogeneous diffusion flames are those involving the combustion of a liquid or solid in an oxidizing gaseous atmosphere such as a candle or pool fire. A diffusion flame has a chemical reaction rate which is limited by the rate of diffusion, mixing, and rate of flow because the air must diffuse into the reaction zone itself and the burning process is governed by heat and mass transfer. Ideal diffusion flames are those with an infinitesimally thin reacting interface that separates the fuel and oxidant streams.

2.1.2 Fuel Ignition and Flame Spread

A pool of liquid fuel contained in a pan can be ignited provided the vapour pressure of the given fuel is at the appropriate conditions. If the vapour pressure is high enough at ambient temperature to form a flammable vapour and air mixture, then an ignition source of high enough energy will allow a flame to spread across the fuel at a speed called the burning velocity (Gaydon, 1970). According to Chomiak (1990), the flame spread of a liquid fuel is similar to that of a porous fuel bed with the added exception that there is surface tension-generated spread. In general however the process of liquid fuel combustion occurs as follows; first the fuel is preheated by existing combustion, the volatile components of the fuel evaporate, mixing of the oxidizer and fuel occurs, finally ignition and combustion of the air-fuel mixture takes place, which in turn adds to the heating of the pool.

2.1.3 Flash Point

The flash point of a fuel is the lowest temperature of a flammable liquid at which vapour is formed at the surface in sufficient amount to allow ignition of the mixture. The flash point temperature is also somewhat dependent on conditions such as ignition source and vessel shape and size. Combustion of less volatile fuels may only be achieved by heating of the fuel prior to ignition and flame spread depends on further heat transfer to the fuel from the flame. If the fuel temperature is raised far enough above the flash point, the flame will be self-sustained (Kanury, 1975).

2.2 Pool Fires Overview

The combustion of a horizontal liquid fuel source or pool fire is a very practical combustion problem and is found namely in the accidental ignition of a spilled flammable substance. Documented pool fire research dates back to the pioneering work done by Emmons (1956) and Blinov and Khudyakov (1957, translated in 1961). Studies on the vast topics that encompass pool fire research include; flame shape, heat feedback from the flame, burning rate, flame pulsation frequency, radiation emitted from the flame to the fuel, and also the effects of parameters ranging from fuel type, tray diameter and the effects of crossflow (Joulain, 1998).

The purpose of this investigation is to narrow the scope of what actually takes place when there is a crossflow present during a pool fire.

2.2.1 Burning Rate of Pool Fires

In many studies the burning rate of a given fuel is often investigated and can be expressed as the rate of fall of the liquid surface or as fuel consumption rate per unit area. The actual burning rate of an ignited fuel depends on the heat transfer from the flame to the fuel surface as well as conditions such as pool size and surrounding conditions. For

small flames and flames which are transparent such as alcohols, the primary mode of heat transfer is through conduction (Gaydon, 1970, Hottel, 1959). For intermediate flames, generally 10 cm diameter and larger, and flames with higher emissivities such as benzene, the main mechanism of heat transfer is radiation. Burning rate also depends on the transfer of heat within the fuel below the surface. Liquid fuels with high flash points can in fact be extinguished by stirring the fuel from below in order to bring cooler fuel with low vapour pressure to the surface (Gaydon, 1970).

In Blinov and Khudyakov's pool fire research, regression rates of fuel levels were analysed to determine the rate v of fuel depletion where $\dot{V}$ is the volume rate with time and A is the surface area

$$v = \frac{\dot{V}}{A} \tag{2.1}$$

The rate of combustion was found to increase at first and then remain constant, with the constant trend being the steady-state burning rate. Conversely, a flammable liquid whose level is not kept constant can show a continuous increase or decrease in burning rate. They concluded that a decrease in burning rate occurs for ethanol-propanol mixtures and a rise occurs when toluene rich, ethanol-toluene mixtures are used. It was found that the initial rise in the burning rate was due to the heating up of the fuel, then a linear trend followed by a rising or falling in burning rate caused by alterations in fuel composition.

Systematic data for the burning rate can only be obtained when steady-state burning is taking place, however transient effects occur between the ignition and steady-state burning. According to Babrauskas (1983) steady-state does not occur immediately due to the following reasons: heat conduction losses into the fuel are still changing, the effects of the tray edge heating may still be present, the bottom of the tray may be increasingly heated if the fuel depth is shallow, and finally, the effects of lip height on the convective and radiative fluxes may increasingly change if the fuel level is not kept constant. Lip height is generally defined by the vertical distance from the pool surface to the lip of the container.

The burning rate of a fuel is commonly expressed by the variable $\dot{m}$ and is represented by

$$\dot{m} = \rho \frac{dV}{dt} \tag{2.2}$$

where ρ is the density and dV/dt is the change in volume per unit time.

The burning rate of a fuel is also often called a mass burning flux and is equivalent to $\dot{m}$ divided by the area of the fuel tray as

$$\dot{m}'' = \frac{\dot{m}}{A} \tag{2.3}$$

The effect of tray diameter has been a topic of interest for many researchers including Blinov and Khudyakov (1957, translated in 1961). Hottel (1959) analysed the work of Blinov and Khudyakov and Figure 2.1 is compiled data he collected which illustrate the effects of tray diameter on burning rate. For small diameter pools the burning rate tends to decrease with increasing diameter leveling out at approximately 10 cm in diameter and subsequently increasing for larger pools to a constant value. Fuels studied in these investigations were gasoline, tractor kerosene, diesel oil and solar oil.

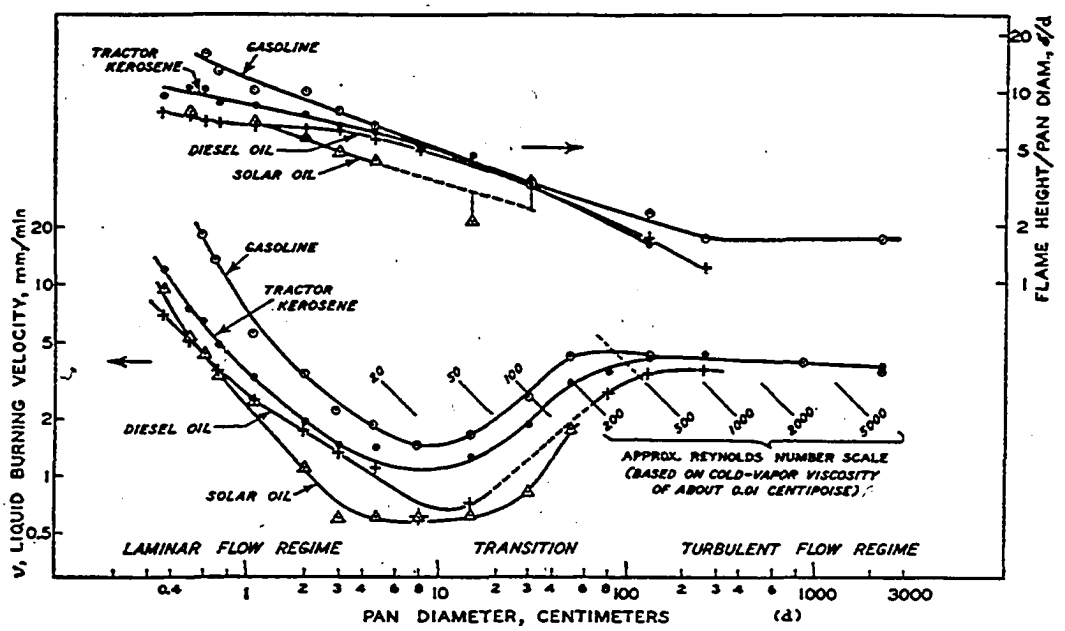

Figure 2.1: Burning rate for varying diameter pool fires (Hottel 1959)

Babrauskas (1983) compiled data for gasoline, liquefied natural gas and methanol, among others. The mass flux of gasoline and methanol are shown in Figure 2.2 to illustrate the relative difference in behaviour due to fuel type. The mass flux of gasoline increases in the manner described by Hottel in Figure 2.1 whereas the mass flux of methanol is essentially constant for increasing tray diameter.

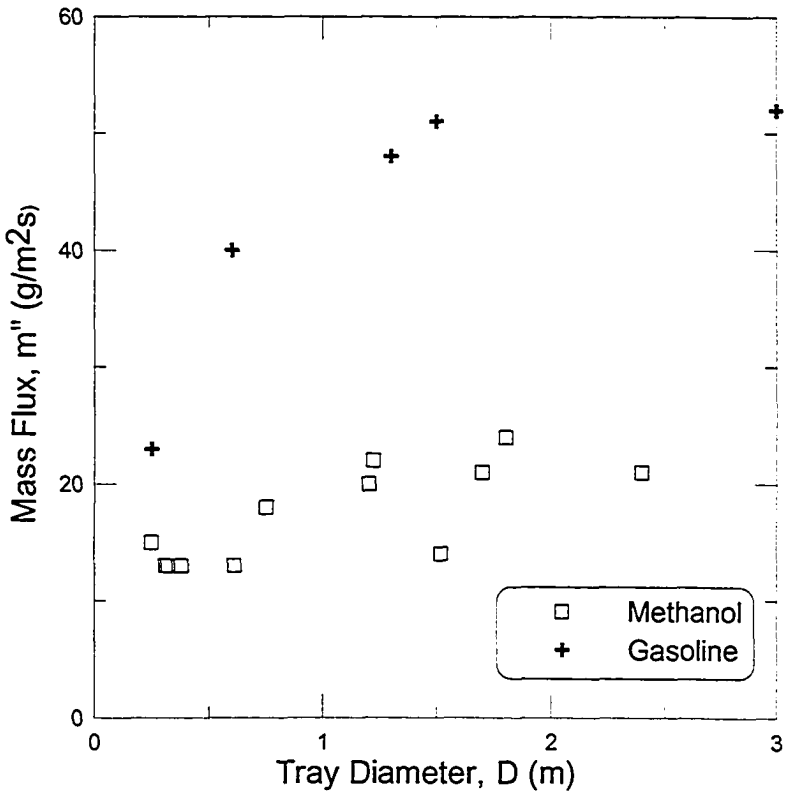

Figure 2.2: Mass flux data compiled by Babrauskas (1983) for varying pool diameters.

Akita and Yumoto (1965), and Klassen and Gore (1994) observed the tendency for mass flux in methanol flames to be highest for diameters of 1 cm and decrease significantly to the same constant value for diameters greater than 10 cm. The increased mass burning flux at small diameters found by these authors is assumed to be due to the increased effects of conduction from tray to the fuel or the laminar convection occurring at small diameters.

2.2.2 Heat Transfer Mechanisms

In the combustion of a liquid fuel pool there is an important coupling of the heat flux transferred to the fuel surface and the mass flux of fuel that is vaporized. The heat flux to the fuel surface and the mass of fuel parting from the surface to participate in combustion are coupled in a positive feedback loop. The rate at which fuel is vaporized

depends on the heat transferred to the fuel surface that causes the vaporization of the fuel. However, the heat fed back to the fuel surface depends on the amount of fuel vaporizing and participating in the combustion.

The heat feedback from the flame back to the pool surface is affected by many factors including the diameter of the pool fire, the flame shape, the flame luminosity and the spatial distribution of temperature and soot inside of the fire (Hammins, 1994). For small diameter pool fires ($D < 0.1$ m), conduction from the container rim to the liquid dominates. For intermediate diameter pool fires (0.1 m $< D <$ 1 m), conduction, convection and radiation are all important. Finally, for large diameter pool fires (1 m $< D$), radiation from the flame to liquid dominates (Hottel 1959).

Figure 2.3 is a diagram of the energy balance in a pool fire for a steady-state system (Hammins, 1994). The size of the arrows indicates the relative amount of heat for each component and therefore their magnitude is a function of pool size. A steady-state system is achieved by adding new fuel through the bottom of the fuel tray such that the level remains constant. Hamins cited that after approximately 5 minutes in a 0.30 m diameter pool fire, the fuel-burning rate $\dot{m}$ is nearly constant.

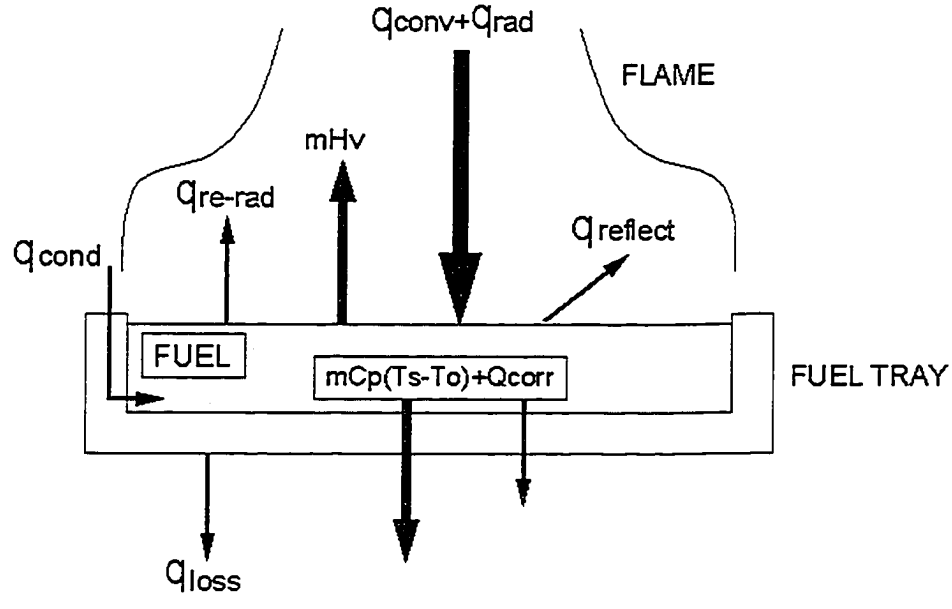

Figure 2.3: Energy balance for a pool fire burning a liquid fuel (Hammins 1994)

For large luminous pool fires the net heat feedback to the fuel surface is dominated by the convective and radiative heat transfer and is balanced primarily by the heat needed to vaporize the fuel. The vaporization heat for the fuel is

$$q_{fuel} = \dot{m}\left[H_v + C_p(T_s - T_o)\right] \tag{2.4}$$

where $\dot{m}$ (g/s) is the mass burning rate, H_v (J/g) is the heat of vaporization, C_p (J/g-K) is the average specific heat of the gaseous fuel, and T_s (K) and T_o (K) are the temperatures of the pool surface and surrounding ambient air temperature, respectively.

A heat balance to the fuel surface yields

$$q_{net} = q_{cond} + q_{conv} + q_{rad} - q_{reflect} \tag{2.5}$$

where q_{cond}, q_{conv} and q_{rad} represent the heat feedback to the fuel surface due to conduction, convection and radiation, respectively. The term $q_{reflect}$ takes into account heat losses due to radiation from the flame to the surroundings.

A heat balance lost from the fuel surface and tray yield

$$q_{net} = q_{fuel} + q_{rerad} + q_{loss} + q_{corr} \tag{2.6}$$

where q_{rerad} and q_{loss} are heat loss terms, q_{fuel} is defined in Equation 2.4, and q_{corr} is included to account for the growing thermal layer within the liquid fuel.

Hamins carried out his measurements in 0.30 m pool fires in order to determine the portion of the energy feedback due to radiation as well as the spatial variation of the radiated energy along the pool surface. Fuels tested were heptane, methanol, PMMA (polymethylmethacrylate) and toluene; he suggested three key conclusions. His first conclusion was that the effects of radiation heat feedback are significant for both luminous and non-luminous fuels in 0.3 m pool fires. Secondly, the net heat flux is

approximately constant for both luminous and non-luminous flames across the pool surface. Finally, radiative heat flux is relatively constant for luminous flames but decreases towards the rim for non-luminous methanol fires.

From Hottel's (1959) review of Blinov and Khudyakov's results he concluded that two burning regimes exist; convectively dominated burning for small diameters pool fires and radiatively dominated burning for large diameters. In addition to this, for convectively dominated burning, the flame can be turbulent or laminar whereas in the radiatively dominated regime the flames are either optically thin or thick and the flow is always turbulent (optically thick flames have significant radiative absorption of their own emission). Based on pool diameter these observations are summarized in Table 2.1.

Table 2.1: Modes of burning for range of pool diameters

D (m)	Burning Mode
<0.05	Convective, laminar
0.05 to 0.2	Convective, turbulent
0.2 to 1.0	Radiative, optically thin
>1.0	Radiative, optically thick

Hottel suggested that the heat transfer from the fire to the liquid pool be represented by the three global flame properties

$$q_{cond} = k\pi D(T_f - T_a) \tag{2.7}$$

$$q_{conv} = hA_s(T_f - T_a) \tag{2.8}$$

$$q_{rad} = \sigma\varepsilon A_s(T_f^4 - T_a^4)(1 - e^{-\kappa D}) \tag{2.9}$$

The subscripts a and f are representative of the flame and ambient temperatures, respectively. The constant k is the thermal conductivity (W/m-K) and the constant h is the convective heat transfer coefficient (W/m^2). The constants σ, ε, and κ are the Stefan-

Boltzmann constant ($1.380658 \cdot 10^{-23}$ J/K-molecule), emissivity and absorption coefficient (m^{-1}), respectively for the radiative component. Hotel's theory neglected the reflective term in the heat balance of Equation 2.5 and the following can be used to describe the mean heat flux from the flame to the fuel surface

$$q_{s,net} = k\pi D(T_f - T_a) + hA_s(T_f - T_a) + \sigma\varepsilon A_s({T_f}^4 - {T_f}^4)(1 - e^{-\kappa D}) \qquad \textbf{(2.10)}$$

The first term on the right represents the conductive heat flux occurring at the lip of the fuel tray, the second term is the convective heat flux and the final term is the radiative heat flux. Equation 2.10 can be used to explain the behaviour of the mass flux shown earlier in Figure 2.1. At small diameters the conductive term dominates since it is proportional to D and the convective and radiative terms are proportional to D^2. When the diameter is large, the conductive term diminishes until the radiation term dominates because the term $e^{-\kappa D}$ becomes large and the radiation term is also proportional to the temperature of the flame to the fourth power. Larger pool fires then exhibit a constant burning rate. This effect of constant burning rate for large pool diameters is also supported by Chomiack (1990), who references the following relationship for burning rate

$$v_p = 0.076\frac{Q_c}{l} \qquad \textbf{(2.11)}$$

where v_p is the burning rate expressed as the rate of fall of fuel (mm/min), Q_c is the heat of combustion and l is the heat of fuel evaporation. Pool fires greater than 50 cm in diameter become turbulent in nature and up to 75-90% dependent on radiative heat feedback. As such the flames become optically thick, as proposed by Hottel, and the luminous combustion zone of the flames do not significantly differ with size, as such the burning rate becomes independent of tray size.

Akita and Yumoto (1965) analysed heat transfer in methanol pool fires using concentric ring trays and concluded the burning rate of the fuel is largest at the rim near the flame base. Hamins attempted to reproduce these experiments but found a decrease

in mass flux towards the rim of the tray. Akita and Yumoto explained that the tendency for the burning rate to decrease from the rim to the center of the tray is more common in smaller trays and causes a certain amount of radial flow of the fuel. They also concluded convective heat transfer contribution in small pool fires decreases towards the center of the tray at an exponential rate whereas the heat transfer due to conduction is confined to the rim of the tray. The effects of radiation when dealing with methanol were noted as negligible and also found to contradict the work of Hamins. Finally, Akita and Yumoto developed an extended version of Hottel's burning rate theory that was modified to fit the burning rate of methanol or non-luminous flames. From their experimental findings they stated that Hottel's theory could in fact be applied to non-luminous liquid fuel flames.

2.3 Lip Height Effects (Freeboard Height)

Babrauskas (1983) states that the effects of having the fuel below the lip of the fuel tray are significant in all pool fires. For large pool fires the following effects can occur if the ratio of freeboard height d (distance below lip of tray) to the diameter D is greater than zero ($d/D > 0$):

- A large enough lip can induce turbulence near the edge of the pool fire thus increasing the convective heat transfer.
- It can cause a change in the distribution of temperature in the walls of the tray thus changing the heat transfer due to conduction.
- Results in a shorter flame with increased emissivity.

Past studies done by Orloff (1980) showed an increase in freeboard height results in an increase in burning rate for the combustion of polymethylmethacrylate (PMMA). In contrast, experiments done by Blinov and Khudyakov showed that the burning rate decreases as the height from the surface of the fuel to the lip of the tank increases. Unfortunately little data exist for the effects of freeboard height.

2.4 Pool Burning in Tunnels and Enclosures

Some interesting research relevant to this review was conducted by Haukur Ingason from the Swedish National Testing and Research Institute (1995). Heptane, methanol and xylen pool fires were studied in a 1.2 m high, 1.08 m wide and 10.95 m long wind tunnel. Tray sizes tested were 0.3 m x 0.3 m and 0.4 m x 0.4 m. Ventilation effects on the release of heat from pool fires were investigated. It was found that air flow varying from stoichiometric ratios ranging from unity to ten times the required amount of air resulted in significant changes in heat release rate. Low ventilation resulted in a smaller flame size and thus a decreased burning rate. Ingason concluded this was due to the result of decreased oxygen in the entrained air thus affecting soot formation in the flame and subsequently reducing the flame radiation to the fuel surface and decreasing the burning rate.

Wind tunnel and tray dimensions used in Ingason's experiments are similar to those used in the experiments conducted for this thesis, which will be discussed in the following chapter. Therefore, the effect of air flow decreasing the flame size and burning rate may be a concern when reviewing results.

The fact that the oxygen concentration could possibly be depleted during combustion was investigated for this study and details are discussed in Chapter 4.

2.5 Crossflow on Pool Fires

There have been numerous studies in the past on the effects of crossflow on pool fires. Generally these studies have been categorized into either quantitative or qualitative observations. Quantitative information related to the combustion of pool fires in the presence of crossflow can be for example heat transfer effects or fuel consumption measurements. From a qualitative point of view, the flame shape and height is of interest. One of the goals of this thesis is to attempt to recognize a coupling between burning rate and flame shape.

2.5.1 Fuel Burning Rate

The effect of crossflow over a pool fire is a very complex problem and strongly dependent on the size of the flame. At small pool fire diameters, the main effect is due to convective heat transfer enhancement (Babrauskas, 1983). At large diameters three phenomena occur. The first is again increased heat transfer due to convection. Secondly the flame temperature is increased due to improved mixing and combustion (Emmons, 1956). Thirdly, the redistribution of radiant heat fluxes occurs causing the flame volume to decrease and be less centered, resulting in lower heating due to radiation.

Capener and Alger (1972) found that for JP-5 pool fires, the burning rate for a 1 m diameter pool in a 6 m/s wind drops to approximately half its quiescent value. They reason that the decrease in burning rate is a result of flame tilt caused by crossflow.

Yumoto (1971) found an increase from about 4 mm/min at quiescent to 6 mm/min at 4 m/s in 0.6 m diameter hexane fires followed by a constant burning rate. Lois and Swithenbank (1978) performed tests to compare with Yumoto using 1 m diameter hexane fires and found a doubling of the burning rate between approximately 2 m/s and 8 m/s wind speeds.

Blinov and Khudiakov (1961) considered the effects of air movement on the burning of liquids in tanks. The experiments consisted of steel tanks of diameters 150 mm, 300 mm, 490 mm and 500 mm with respective heights of 800 mm, 1800 mm, 2000 mm and 4000 mm. Airflow was produced with a large fan in the open and the airflow was not always constant, nor direct and ranged from 70° to 109° with the vertical. Fuel levels were maintained constant and runs lasted 2 to 5 hours. Fuels studied were diesel oil, kerosene and gasoline. Their results fit the form

$$v - v_0 = (v_\infty - v_0)(1 - e^{-\beta U}) \qquad \textbf{(2.11)}$$

The term v is equivalent to the volume rate divided by the surface area. The rate v_0 is the rate of fuel depletion for quiescent conditions, v_∞ is the limit of the rate v, and β is a scale factor. As it stands this equation increases indefinitely, however this is impossible since at some critical wind speed U_c the flame will blow out. Blinov and

Khudyakov reason that crossflow tends to increase the flow of heat from the flame to the liquid. Radiation from the flame and the flow of heat through the tank wall both tend to increase with U and so tend to raise v. Babrauskas reviewed the work of Blinov and Khudyakov and expressed their relationship for pool burning rate in the form

$$\frac{\dot{m}''_{windy}}{\dot{m}''_{still}} = 1 + 0.15\frac{U}{D} \tag{2.12}$$

although, he added, is not appropriate for alcohol fuels.

Lam, Weisinger and Weckman (2003) studied fuel regression rates in 30 cm diameter acetone fires subjected to crossflow. Regression rates were found to be larger in a 0.74 m/s crossflow than at quiescent but further increase in wind speed resulted in a decrease in regression rate. The increase in regression rate is explained as a result of increased air entrainment, and the decrease at higher wind speeds is due to increased flame tilt and hence less radiative heat feed back to the fuel surface.

As can be seen from the different results obtained by these researchers, there is no consistent result to explain increases or decreases in burning rate due to crossflow and it is difficult to replicate experiments done in past work.

2.5.2 Flame Shape

The chief goal of this investigation is to determine the effects of crossflow on the burning rate of pool fires with less emphasis on flame shape. Flame shape remains important however it is expected that there is a coupling between the flame shape at the onset of crossflow to the rate at which fuel is consumed. This has already been evident in past research where the flame tilts from centrally located to being displaced downstream and thus changing the heat feedback to the fuel surface.

Welker, Sliepcevich and Pipkin (1965, 1966) studied the bending of pool fire flames in crossflow and the effects on heat transfer, flame spread rate and fuel burning

rate. Tests were done with methanol, acetone, n-hexane, cyclohexane and benzene as fuels in trays flush with the wind tunnel floor. They devised the following equation as a relation for flame bending

$$\frac{\tan\theta}{\cos\theta} = 3.3 Re^{0.07} Fr^{0.8} \left(\frac{\rho_g}{\rho_a}\right)^{-0.6} \qquad \textbf{(2.13)}$$

The flame angle θ, is the angle between the flame axis tilted downstream and the vertical. The terms *Re* and *Fr* are the Reynolds and Froude numbers, respectively. The densities of the ambient air and that of the fuel gases are represented by the subscripts a and g respectively. The main objective of their work was to obtain geometric correlations for flame bending and flame trailing, but does not extend into the effects of wind on burning rate.

A propane burner was used by Kolb et al. (1997) to simulate a pool fire in a wind tunnel. Flame shape was observed and it was concluded that the flame transitioned from "plume" mode to "boundary layer" mode at crossflow speeds greater than 1 m/s. In plume mode the flame is buoyantly dominated and only slightly affected by the crossflow. Once the crossflow exceeded 1 m/s, the shape of the plume transitioned from buoyancy dominated to inertia dominated and is called boundary layer mode. In boundary layer mode the buoyancy effects are restricted to the flow surrounding the flame. The flame extension length and flame height were observed and for increasing wind speed in plume mode it was found that there was an increase in both length and height. Once the flame transitions to boundary layer mode, the flame height decreases while the flame length continued to increase linearly.

The same transition from plume mode to boundary layer mode was also observed in experiments conducted by Apte et al. (1991). This work however was related to the shape of the flame as it spread across a horizontal polymethylmethacrylate (PMMA) surface. During initial flame spread, the flame was confined to a shape similar to that of a boundary layer. Once the fuel reached the end of the fuel bed, buoyancy effects dominated and the flame rose vertically.

2.6 Summary

Key conclusions arising from this literature are as follows:

1. Under quiescent conditions tray size is important at small sizes, namely less than approximately 1 m in diameter. For diameters less than 10 cm the heat feedback is controlled by conduction from the tray lip to the fuel surface. Larger trays generate turbulent flames, emissivities approach unity and the burning rates become invariant with increasing tray size.
2. Lip height effects have not been well studied but do affect the airflow across the pool fire. Complications that may arise from this effect will be avoided by maintaining the same fuel depth for all tests.
3. Pool fires in enclosed wind tunnels have been shown to be affected by oxygen concentration. This issue will be considered by calculating the available oxygen content of the wind tunnel used in this study and determining if there is a lack of oxygen in the combustion process.
4. Crossflow on pool fires is a topic of much interest, however past results have shown little consistency. No in-depth reference to the effects of tray size or geometry with burning rate experiments under crossflow conditions was found.

3. EXPERIMENTAL APPARATUS

The aim of this experimental investigation is to examine the complex problem of a pool fire under crossflow at a fundamental level. By controlling key variables, namely geometry, fuel depth and crossflow conditions, the randomness of the problem can be simplified. This chapter introduces the design criteria for the experiments and the objectives needed to satisfy each criterion. The methodology for choosing equipment and proceeding in a given direction are discussed. Detailed descriptions are given for the apparatus used and finally the procedure for testing is presented.

3.1 Fuel Delivery and Consumption Measurement

3.1.1 Methodology

The first step in building the apparatus was to design experimental equipment capable of measuring the rate at which methanol was vaporized by part of a combustion process. Without complicating the problem at this stage by involving crossflow and different geometries, a precise fuel delivery system had to be made before the addition of any further conditions. Once fuel could be accurately supplied and measured, the problem could be further developed by adding crossflow and altering tray geometries.

The burning rate of the fuel is the mass of fuel consumed per unit of time. To eliminate the issue of a changing mass of fuel due to the consumption of the fuel in the tray, a system was designed to maintain a steady-state fuel level.

3.1.2 Fuel Delivery System

A steady-state, steady-flow fuel delivery system was designed to simultaneously maintain the fuel level and measure the volume of fuel consumed. Figure 3.1 illustrates the fuel replenishing system.

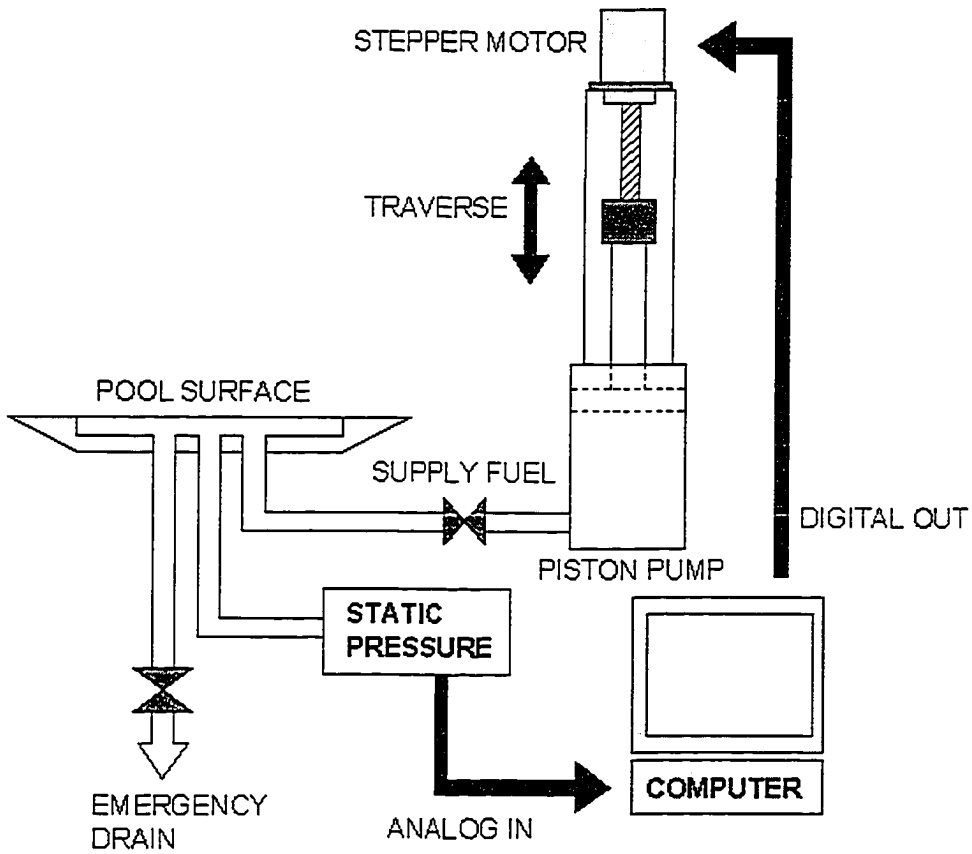

Figure 3.1: Fuel leveling and consumption recording system

The fuel trays were filled with methanol to within 1 mm below the lip of the tray and a static pressure set point was recorded prior to the ignition from below the fuel tray. The fuel was ignited with a hydrogen flame that was promptly extinguished and retracted from the flow so that it would not create any flow disturbances. The liquid level was maintained by measuring the static pressure from the middle port of the pans using a pressure transducer with a pressure range of 0 to 250 Pa (1 inch water column). As fuel was consumed, the static pressure would decrease and the pressure change in the form of a 0 to 10 Volt analog signal was used to control a positive displacement pumping system

that injected the required liquid into the bottom of the pans. The fuel supply system could theoretically control the liquid level within 0.025 mm, however observations suggest that the liquid level varied by as much as 0.5 mm as the pump responded to the dynamics of the fuel consumption. The pumping system was driven by a 1.8°/step, 200 steps/revolution stepper motor which received 5 Volt pulses in response to any change in pressure. The stepper motor drove a traverse that subsequently depressed a piston containing the fuel. A stepper motor was chosen as a driving motor due to the ability to accurately and reliably measure its position and thus the amount of fuel delivered. A high torque stepper motor was used to ensure that skipping of the motor shaft did no occur. The total volume of fuel displaced was calculated by multiplying the stroke of the piston by the area of the piston. A data acquisition system recorded the volume displaced with time and was then used to calculate the mass burning rate of methanol for any set of crossflow and pan area conditions. Chapter 4 discusses the details and uncertainties associated with this measurement.

The fuel level was maintained constant to create a steady-state experiment throughout the test. The duration of the tests were approximately 4 minutes for the largest tray and 20 minutes for the smallest tray. Tests were terminated when a steady burning rate of the fuel was achieved (steady-state occurred after approximately 3 to 5 minutes, depending on tray size). Draining the fuel by reversing the pump and allowing the flame to consume the remaining amount of fuel extinguished the flames at the end of the tests.

3.1.3 Fuel

The fuel chosen for the testing procedure was methyl alcohol, more commonly known as methanol, CH_3OH. Methanol is a clear colourless alcohol which is used in manufacturing many chemical products, a carrier of hydrogen for fuel cells and is becoming a more predominant alternative fuel in the automotive industry.

The combustion of methanol produces a sootless, translucent blue flame with a lower emissivity compared to more radiative flames such as acetone, gasoline or diesel

fuel. The low radiative heat transfer was the main reason for choosing methanol in an attempt to simplify the heat transfer during the analysis of the flames. Removing the majority of the radiative component from the problem significantly reduces the complexity associated with understanding the fundamental impact of crossflow on the flame. There is no method of completely removing the radiative component however, by choosing methanol as a fuel it may be possible to neglect the minimal effects of the heat feedback due to radiation.

3.2 Crossflow Conditions

3.2.1 Methodology

A highly consistent crossflow source was desired for these experiments in order to alleviate the possibility of variable crossflow conditions. Also, uniform steady flow across the burner trays was desired in an attempt to eliminate any randomness or inconsistencies in the crossflow.

3.2.2 Wind Tunnel Facility

All experiments were conducted in a closed-loop wind tunnel which is shown in Figure 3.2. A contraction section upstream of the test section provides uniform low turbulence (turbulence intensity <0.4% (Bourguignon, 1999)) airflow across the burner trays. The test section of the tunnel is 1.2 m high by 2.4 m wide and approximately 11 m long. The total internal volume of the wind tunnel is approximately 350 m^3. The tunnel to flame volume ratio $O(10^4)$ is large enough to assume invariant ambient conditions for the duration of the test. For a typical test in this study when no more than 0.5 litres of methanol is burned, there is a maximum depletion of approximately 0.6% of the total

oxygen volume in the tunnel. The concentration of oxygen in the tunnel is further discussed in Chapter 4.

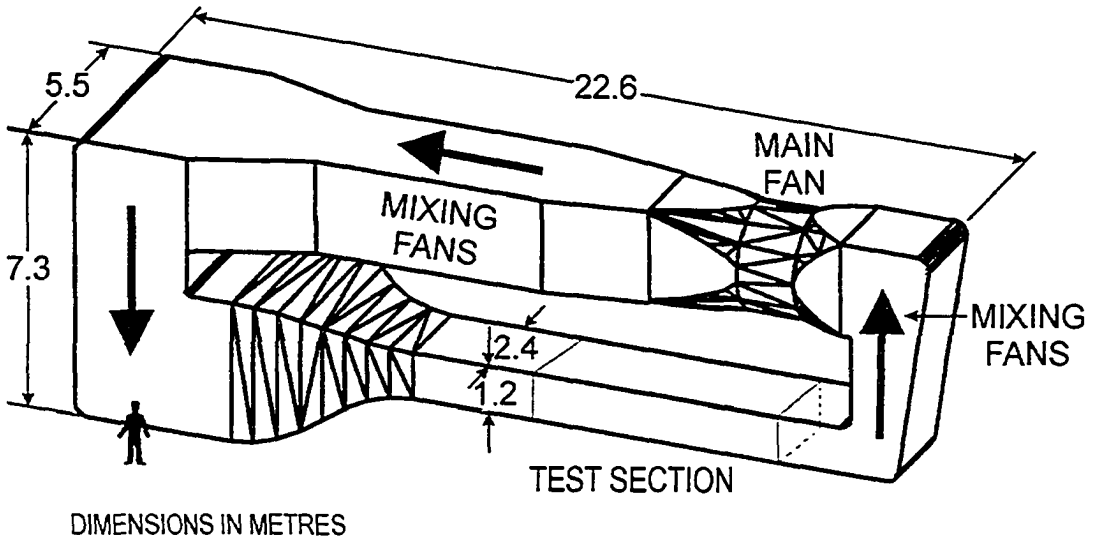

Figure 3.2: University of Alberta Combustion Wind Tunnel Facility

The tunnel fan is driven by a variable speed 150 kW D.C. motor and being a closed-loop tunnel, stable crossflow speeds in the lower test section can be produced from 0.2 m/s to 35 m/s. The mixing fans (see Figure 3.2) do not allow any coherent plume of combustion products to return to the flame. With the tunnel fan turned off, the air surrounding the flames can be made quiescent. After each test the tunnel is completely purged and dampers in the tunnel allow fresh air to be brought into the tunnel.

Crossflow velocities tested were from 0 m/s (quiescent) to 6 m/s and were measured by a Pitot-static tube. The Pitot tube measurement is the result of a pressure difference from the stagnation port and the static port per Equation 3.1. The stagnation and static pressures are represented by P_o and P respectively, and ρ is the ambient air density.

$$U = \sqrt{\frac{2(P_o - P)}{\rho}} \tag{3.1}$$

The pressure transducer was an Ashcroft diaphragm sensor with a range of 17 Pa (0.07" water column) calibrated for a 1 to 5 Volt output. The density of air was calculated from the ideal gas law per:

$$\rho = \frac{P_{atm}}{R_{air} T_{air}} \tag{3.2}$$

During a typical test it was not the indicated crossflow speed which was set to the desired conditions, rather the independent variable was the fan power. Experiments were prepared and the tunnel was set to a given fan power which was represented as percent of the total fan power. The crossflow speeds were recorded and mean values as well as maximum and minimum values for the velocity were calculated in the data acquisition process. Chapter 4 discusses in greater detail this measurement and the corresponding uncertainty.

3.3 Tray Geometry

3.3.1 Methodology

The design of the trays and the support to which they would be fastened was another key issue in designing the experiments. Rectangular trays were chosen because of their two dimensional nature when viewed from the side. This was relevant when crossflow was present, creating a boundary layer at the leading edge of the tray. A circular tray would cause the approaching crossflow to change from uniform to variable as it moved across the leading edge of the circular shaped lip.

The main objective of this study was to observe the effects of crossflow on the burning rate of methanol pool fires. A square "base case" tray was chosen with dimensions 15 cm wide (cross-stream direction) by 15 cm long (stream-wise direction). The effects of increasing and decreasing area and aspect ratio were investigated by using

other rectangular trays with different dimensions. In addition to the rectangular trays, a circular tray was also considered. The circular tray was designed with the same area as the base case in an attempt to compare square and circular geometries. During testing each tray was inserted into an aerodynamically designed streamlined base, mounted above the tunnel's 12 cm boundary layer to maintain uniform attached airflow across the burner trays. The trays were machined so that the upper lip of the recessed volume holding the fluid was flush with the airfoil base.

3.3.2 Rectangular Trays

Rectangular trays were used for the liquid pool to provide a relatively simple upstream boundary condition for the combustion. All trays were milled out of a single 19 mm (0.75 inch) thick plate of aluminum and had the same depth and leading edge dimensions. The plates have identical outside dimensions but vary in the shape of the tray which is milled out of the inside. Figure 3.3 illustrates the tray dimension. All trays were 10 mm deep.

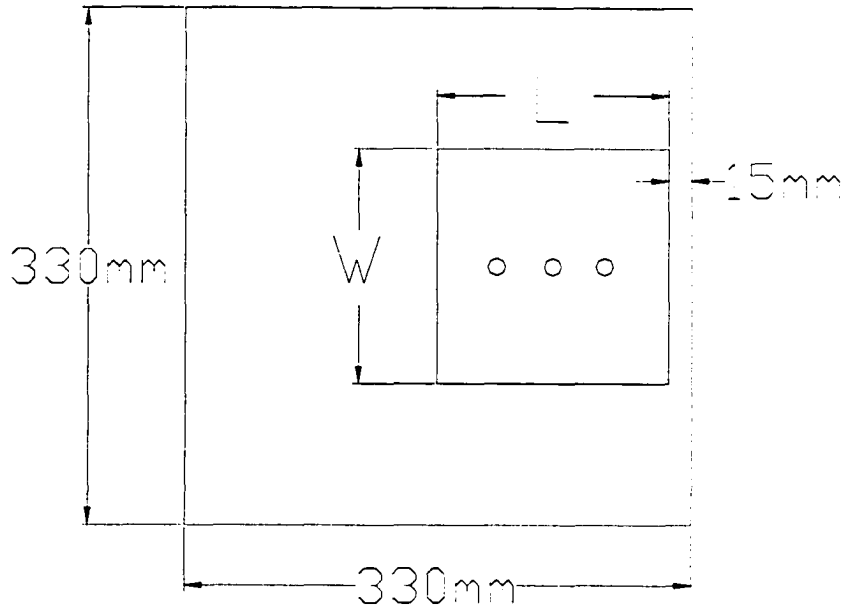

(a)

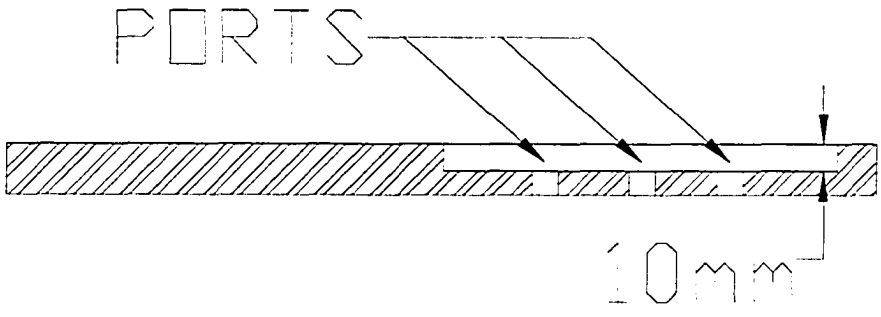

(b)

Figure 3.3: Square tray dimensions

(a) Top view of generic tray. Outside dimensions are constant for all trays tested, stream-wise length "L" and cross-stream width "W" are varied.

(b) Side view of generic tray. All fuel-containing sections are 10 mm deep and have three ports.

The tray construction included three ports for supply fuel, emergency drainage and a pressure port for controlling the fuel level. All lines for fuel supply, drainage and the pressure sensor were 6.35 mm (0.25") stainless steel tubing and were connected using compression fittings. Directly connected to the three ports were 30 cm long stainless steel braided hoses for flexibility and to simplify connection under the airfoil structure. Table 3.1 summarizes the rectangular geometries of the trays tested.

Table 3.1: Geometries of trays tested

Cross-stream Width (cm)	Stream-wise Length (cm)	Area (cm^2)	Aspect Ratio (Length/Width)
30	30	900	1
20	20	400	1
15	15	225	1
10	10	100	1
7.5	7.5	56	1
30	7.5	225	0.25
7.5	30	225	4

3.3.3 Circular Tray

A circular tray with the same area as the base case was also tested and had a diameter of 16.93 cm and is illustrated in Figure 3.4. Similar to the rectangular trays, the circular geometry was milled out of the same size aluminum plate as the other trays. The leading edge of the circle was positioned at the same 15 mm distance as the rectangular trays from the front of the plate.

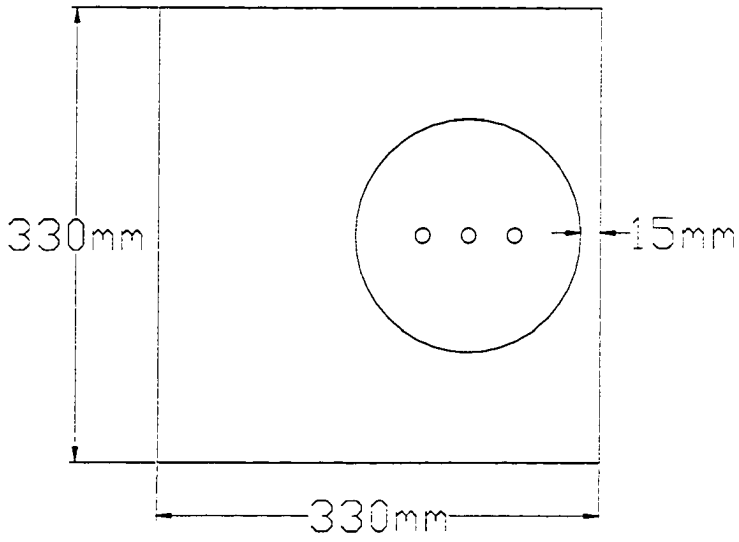

Figure 3.4: Dimensioned top view of circular burner tray

3.3.4 Streamlined Base Structure

In order to create nearly two-dimensional boundary conditions with a thin approaching boundary layer, an airfoil structure with an aerodynamically designed leading edge was constructed to act as a base. The wing-like surface eliminated flow separation upstream of the pool. The wing dimensions were 0.9 m in the stream-wise direction and 1.83 m in the cross-stream direction and was mounted above the tunnel floor's 12 cm boundary layer. Figure 3.5 is a cross sectional view of the wing and tray. The entire structure is constructed out of aluminum except the leading edge that was shaped out of wood and polyurethane, covered in fiberglass, filled and painted with heat resistant paint.

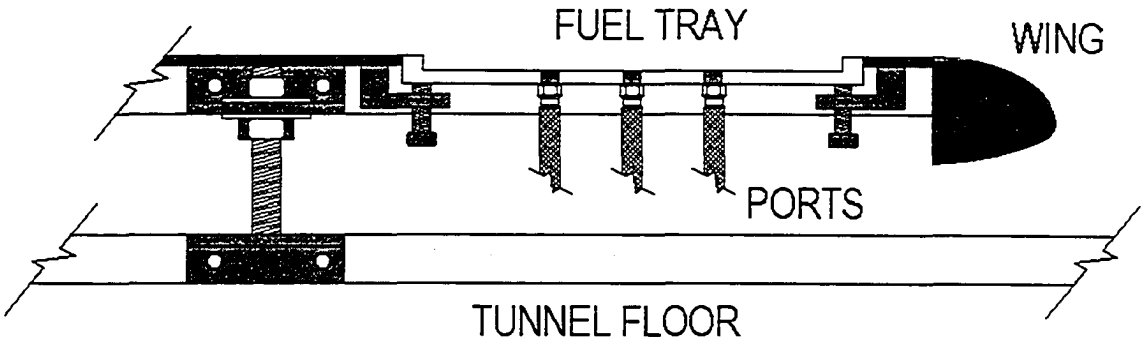

Figure 3.5 Cross-sectional view of wing structure and fuel tray.

The burner trays were mounted with the upper edge flush with the wing surface. The wing surface was constructed out of reinforced 6.35 mm (0.25") aluminum and expansion slots were cut along the length of the surface as shown in Figure 3.6 to allow for expansion caused by heat from the flames. This prevented the surface from buckling and altering the level of the wing surface.

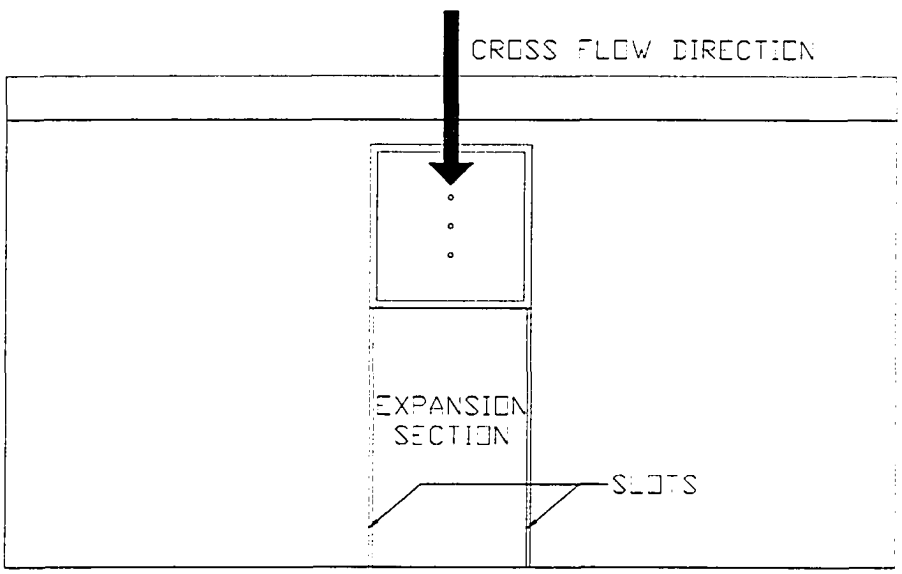

Figure 3.6: Top view of streamlined base.

During the initial testing of the wing and pool trays it was found that for increasing crossflow speeds greater than 1 m/s, the flame would creep upstream from the leading lip of the tray towards the leading edge of the wing, suggesting that boundary layer separation of the crossflow was occurring. Laser sheet visualization was used to observe the crossflow trajectory over the wing. Figure 3.7 illustrates the separation occurring as the crossflow came up over the curved edge of the wing.

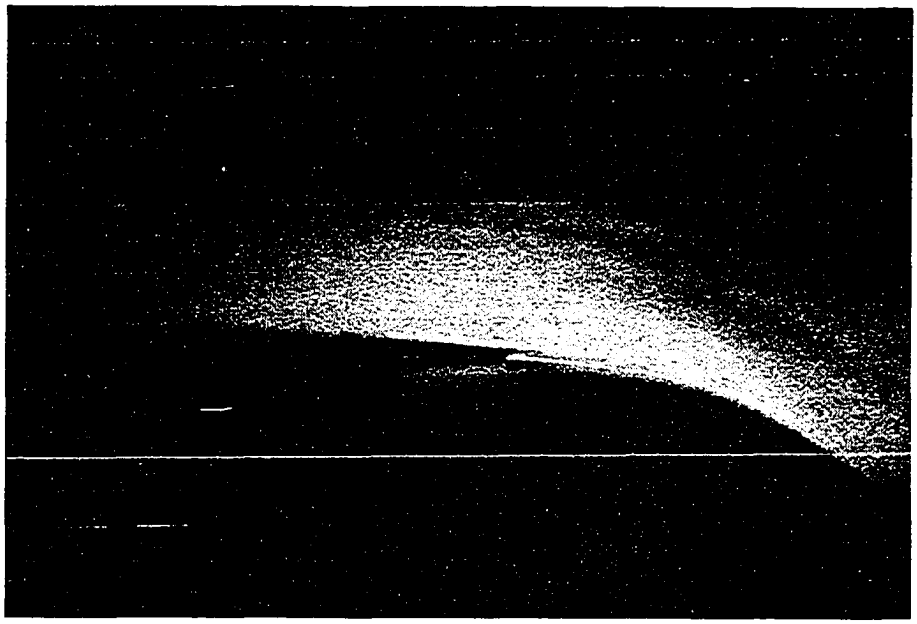

Figure 3.7: Flow visualization of crossflow separation over the wing leading edge

In order to ensure boundary layer attachment for all crossflow velocities, a 1/8" diameter wire was fitted midway down the leading edge to trip flow into becoming turbulent. After this adjustment the methanol flames remained attached to the leading edge of the pool trays until high enough crossflow speed was attained in order to begin to blow the flame off.

3.4 Collection of Qualitative and Quantitative Data

3.4.1 Data Acquisition

The wind tunnel was controlled with a computer system and software developed on National Instruments LabView 6.1.

The pool fire experiments and the fuel delivery system were controlled with a second computer and data were recorded through an E-6032 National Instruments data acquisition board. The program used to communicate with the board was also constructed and executed with National Instruments LabView. Data recorded included the pulse counts sent to the stepper motor, the time in milliseconds, indicated crossflow speed and atmospheric pressure. The atmospheric pressure was read manually from a mercury barometer and entered into the program prior to beginning a test, as it was required to calculate crossflow speed. All data were recorded in a spreadsheet for analysis.

3.4.2 Photography

Photographs were obtained with a 6.1 Mega pixel Nikon D100 digital camera. Lenses used were manual focus Nikon Nikkor lenses with 50 mm and 105 mm focal lengths. Due to the non-luminous nature of methanol flames, photographs were taken without room or strobe lights. For this reason, the aperture settings used for the 50 mm lens and 105 mm lens were F 1.4 and F 2.5 respectively. A digital film speed of ISO 6400 was used to obtain the exposure under the low light conditions. The largest fires were able to take advantage of the smaller focal length and aperture, but with smaller fires the larger focal length was required to obtain a full image of the flame.

3.5 Experimental Procedure

Prior to beginning a test, a standard procedure was followed to ensure repeatable results. Before initiating any test, the wind tunnel was completely purged by opening dampers and running the fan to evacuate remnants of previous tests and impurities in the air.

Initially, a tray would be installed in the airfoil structure and leveled flush with the airfoil in order to decrease the effects of blunt edges on the crossflow. Air was bled from the supply and pressure lines by pushing fuel through until air bubbles were evacuated. The pressure line led to a three-way solenoid valve that was required to equalize both sides of the differential pressure transducer. Figure 3.8 is a detailed outline of the fuel delivery system. Either side of the transducer was open to atmospheric pressure using a sight glass higher than the liquid level of the fuel tray. The use of the equalizing valve and pressure ports being open to atmospheric pressure eliminated the need to remove the bleed screws from the pressure transducer to remove air trapped in the line.

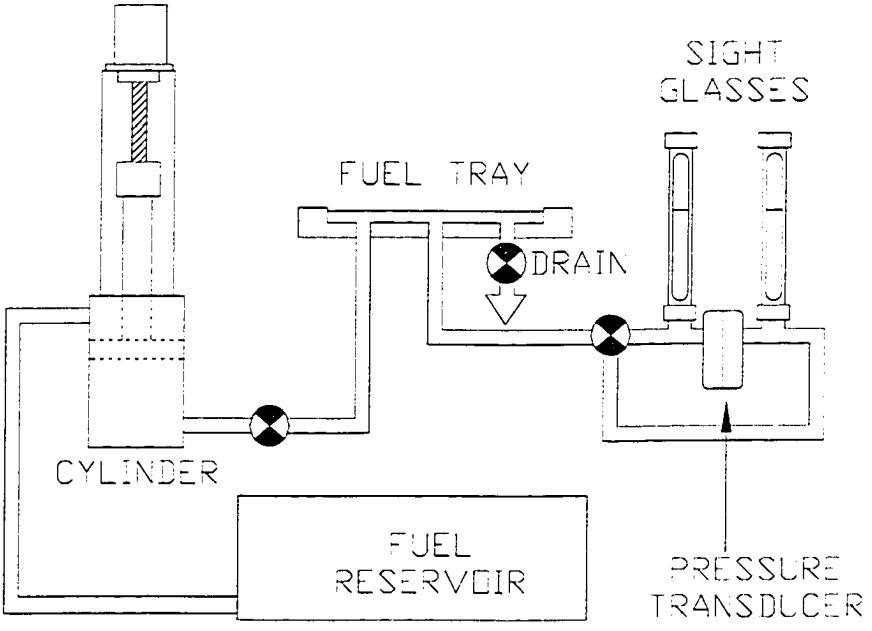

Figure 3.8: Detailed fuel delivery system

The fuel reservoir was a cylinder and piston design. Using a two-way valve the piston drew fuel from a reservoir to fill the cylinder and then turning the valve allowed fuel to be pushed out of the cylinder into the supply line and fuel tray. With all the lines bled, the fuel tray and cylinder were filled. The static pressure used for maintaining the liquid fuel level was recorded once the desired crossflow conditions were set in order to eliminate the effects caused by the dynamic pressure change crossflow would have on the fuel surface. Finally, with the crossflow speed set and the pressure set point recorded, the flame was ignited and the test commenced.

As mentioned earlier in this chapter, data were recorded in the form of a discrete time trace of mass transferred to the pan until the consumption of fuel reached steady-state. Stopping the data recording and draining the fuel tray finished the test. The fire was then allowed to burn itself out by consuming the small amount of fuel remaining in the bottom of the tray.

This procedure was repeated for all trays and crossflow speeds and each condition was repeated a minimum of two, though typically more, times to ensure repeatability of results.

The next chapter discusses the calculations and uncertainties involved in measuring the crossflow speed and the burning rate of fuel. The uncertainty in crossflow speed is a result of two factors. The first is the random errors associated with the measurement devices and the second is uncertainty due to the fluctuating nature of the tunnel fan. The mass burning rate uncertainties are a result of random measurement errors. The uncertainty in both these measurements will be included in results chapter in the form of error bars.

4. EXPERIMENTAL DIAGNOSTICS

The intent of this experimental investigation was to design relatively simple experiments in order to observe the effects of crossflow on methanol pool fires. More specifically, the main interest lies in obtaining the mass flux of fuel as a function of air crossflow speed for varying fuel tray geometries. There are numerous steps in obtaining both the crossflow speed and the burning rate. This chapter describes how these measurements were obtained and the random uncertainties associated with both those measurements.

4.1 Crossflow Speed Measurements

Experiments were conducted under crossflow conditions ranging from quiescent to approximately 6 m/s. As mentioned in the previous chapter, during any given test the tunnel crossflow conditions were set according to the percent of total fan power. The crossflow speed was measured with a Pitot-static tube placed above and slightly upstream of the test apparatus. The data acquisition system recorded the burning rate data as well as crossflow speed information. For example, when tunnel fan power was set to approximately 6% of the total capable power for at least three minutes, this produced a mean velocity measured by the Pitot-static tube of approximately 1 m/s, a maximum velocity of 1.1 m/s and a minimum velocity of 0.9 m/s (i.e. +/- 0.1 m/s). The difference between the mean, maximum and minimum was due to the fluctuations in the stream-wise speed of the wind tunnel and not from flow associated vortices (i.e. they are relatively low frequency). In addition to the uncertainty due to the low frequency fluctuation of the wind tunnel fan speed, there was also uncertainty in the instruments used to measure the crossflow speed.

A Pitot-static tube was used to measure static and stagnation air pressures and thus the crossflow speed from the following equation

$$U = \sqrt{\frac{2(P_0 - P)}{\rho}} \tag{4.1}$$

where U is the crossflow speed, P_0 and P are the stagnation and static air pressures respectively, and ρ is the air density. The static and stagnation pressures were measured with a differential pressure transducer (Make: Ashcroft Model: IXPdp). The range of the 17.44 Pa (0.07" water column) and had an uncertainty quoted by the manufacturer of 0.25% full scale.

The air density required in Equation 4.1 is obtained from the ideal gas law as follows

$$\rho = \frac{P_{atm}}{R_{air} T_{air}} \tag{4.2}$$

Where P_{atm} is the atmospheric pressure which was measured from a mercury barometer with a measurement reading uncertainty of ± 0.1 mmHg. R_{air} is the universal gas constant of air, was assumed equal to 0.2870 kJ/kg°K for all experiments and for the purpose of an uncertainty analysis is considered exact. T_{air} is the ambient temperature in the wind tunnel and was measured with a thermocouple. The thermocouple used was a Type K and had an uncertainty of ± 0.5°K (Johnson, 2001).

In order to determine the uncertainty associated with random measurement errors, an uncertainty analysis for Equation 4.1 and 4.2 has been performed. Since both equations involve powers, multiplication and division the equation can be represented in the generic form below

$$F = nA^j B^k C^m \tag{4.3}$$

The variables A, B and C each have their own uncertainties and j, k, m and n are known numbers. An uncertainty analysis of Equation 4.3 results in the generic form for the relative uncertainty

$$\left(\frac{\delta F}{F}\right)^2 = \left(j\frac{\delta A}{A}\right)^2 + \left(k\frac{\delta B}{B}\right)^2 + \left(m\frac{\delta C}{C}\right)^2 \tag{4.4}$$

The variables δF, δA, δB, δC are the uncertainties in F, A, B and C respectively. The ratio of the uncertainty of a variable over the value of a variable such as $\delta F/F$ is the fractional error, or when multiplied by one hundred is the percent error in the value. Applying this method to the crossflow speed relation in Equation 4.1 produces a form for the uncertainty in U as shown below

$$\left(\frac{\delta U}{U}\right)^2 = \left(\frac{\delta \Delta P}{2\Delta P}\right)^2 + \left(\frac{\delta \rho}{2\rho}\right)^2 \tag{4.5}$$

The uncertainty in the crossflow speed δU is the unknown and the magnitude of the actual crossflow speed is specified. The accuracy of the pressure measurement ΔP is given by the manufacturer to be 0.25% full scale and since the transducer has an output range of 1 to 5 Volts, the full scale reading occurs at the maximum output of the transducer. A pressure of 17.436 Pa results from the corresponding 5 Volt output. Therefore 0.25% of the maximum pressure results in an overall uncertainty in the pressure measurement of ± 0.0436 Pa. The actual value of ΔP can be determined by back calculating through Equation 4.1 and the values for corresponding crossflow speeds are listed in Table 4.1.

Table 4.1: Pressure Reading for Corresponding Crossflow Speeds

U, Crossflow Speed (m/s)	ΔP, Differential Pressure (Pa)
1.0	0.54
2.0	2.17
3.0	4.88
4.0	8.67
5.0	13.55
5.5	16.39

The final term on the right hand side of Equation 4.5, the relative error in ambient air density is not directly known and is derived by applying the same uncertainty analysis process on the ideal gas law in Equation 4.2. The resulting form for the fractional uncertainty in air density is

$$\left(\frac{\delta\rho}{\rho}\right)^2 = \left(\frac{\delta P_{atm}}{P_{atm}}\right)^2 + \left(\frac{\delta R_{air}}{R_{air}}\right)^2 + \left(\frac{\delta T_{air}}{T_{air}}\right)^2 \qquad (4.6)$$

The actual pressure and temperature of the air were measured for each experiment in order to calculate the air density, but the uncertainty in this air density is only weakly dependent on the particular conditions. As a result, the uncertainty associated with pressure and temperature does not significantly affect the overall uncertainty in the calculated crossflow speed. Therefore, only a maximum uncertainty in air density is calculated here and used for all experiments. The atmospheric pressure, P_{atm} for Edmonton, Alberta is on average 700 mmHg. The measurement uncertainty δP_{atm} is equal to ± 0.1 mmHg. The gas constant R_{air} is treated as exact and as such the middle term on the right hand side equals zero. Finally the temperature T_{air} is equal to room temperature, 300°K and the uncertainty associated with this measurement is equal to ± 0.5°K. By evaluating the right hand side a relationship for the ratio of the uncertainty in the density to the actual density as shown on the left hand side of Equation 4.6 can be substituted into Equation 4.5 and is approximately equal to 2.8×10^{-6}, indicating minimal uncertainty.

At low crossflow speeds the value of ΔP is small and the value of $\delta \Delta P$ is constant therefore the relative uncertainty that deals with the pressure differential is much higher at low crossflow speeds and thus the total error propagation is greater. The uncertainty in the density is essentially zero and it can be seen in Figure 4.1 that the total uncertainty in the crossflow speed is highest at lower speeds. The uncertainty in crossflow speed is omitted at 0 m/s since the fan is not operating and the tunnel is at quiescent conditions.

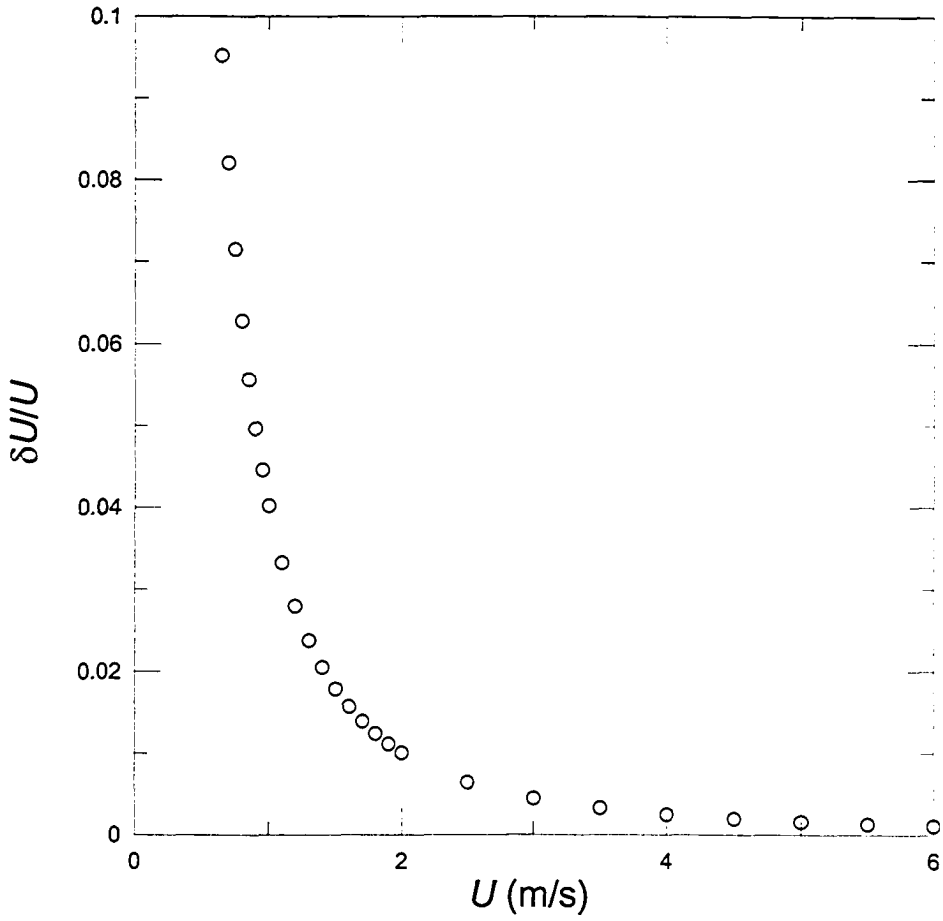

Figure 4.1: Relative uncertainties in crossflow speed measurement

In practice the relative uncertainty in crossflow speed is half of the relative uncertainty in the measured pressure difference. Table 4.2 lists the calculated values for the uncertainty in the crossflow speed. For the crossflow speeds tested, the greatest uncertainty due to measurement error occurs at 1 m/s and is equal to approximately 4%. Below 1 m/s, the relative uncertainty grows since it is inversely proportional to the square and as such the Pitot tube cannot be used to accurately measure those velocities, and thus some subjectivity is required to estimate lower crossflow speeds.

Table 4.2: Calculated uncertainties in tunnel crossflow speed measurements.

U, Crossflow Speed (m/s)	$(\delta U/U)^2$	$\delta U/U$	% Error in U
1.0	1.62E-03	4.02E-02	4.022
2.0	1.01E-04	1.01E-02	1.006
3.0	2.00E-05	4.47E-03	0.447
4.0	6.32E-06	2.51E-03	0.251
5.0	2.59E-06	1.61E-03	0.161
5.5	1.77E-06	1.33E-03	0.133

Although the instrument uncertainty is relatively low, there is also the uncertainty in the actual crossflow speed due to the fluctuating nature of the wind tunnel fan as mentioned at the beginning of this section. Figure 4.2 shows the mean crossflow speeds recorded for the various tunnel speeds tested. Velocity readings from the Pitot tube were recorded during each test and as the flow in the tunnel upstream of the pool fire was essentially uniform, velocity measurements were recorded simultaneously with each pulse sent to the stepper motor. For every second of testing approximately 10 velocity points were obtained due to the nature of the fuel delivery system. The velocity data recorded were statistically analysed and the error bars represent two standard deviations in the data above and below the mean.

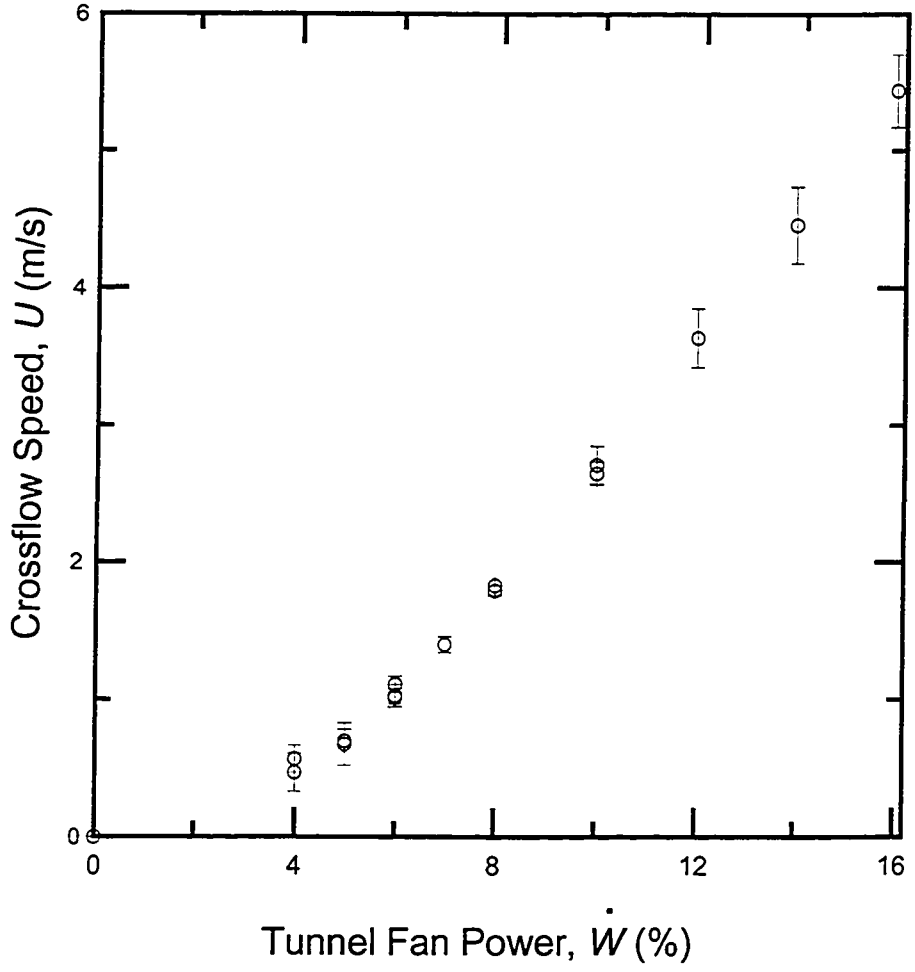

Figure 4.2: Crossflow speed of fan powers tested for 10 cm x 10 cm fuel tray.

The uncertainty due to the fluctuations in crossflow speed in this case vary from as low as 2% up to as much as 30%, indicating significant uncertainty. Table 4.3 lists examples of recorded mean crossflow speeds and corresponding percent uncertainty. The percent uncertainty is calculated from the ratio of the mean velocity subtracted from the value of two standard deviations above the mean, divided by the mean velocity. The increased uncertainty at the low-end crossflow speed is a result of the reduced capability of the wind tunnel's control system to maintain a constant rotation velocity of the fan.

Table 4.3: Crossflow speed error due to fan fluctuations

U, Crossflow Speed (m/s)	% Uncertainty
0.47	29.55
0.70	12.17
1.02	5.44
1.40	4.00
1.83	3.35
2.71	5.06
4.46	6.26
5.44	4.91

Experimental results are discussed in Chapter 5 and the error bars in crossflow speed indicated for the graphical data is the sum of both the measurement uncertainty and the velocity fluctuations.

4.2 Measurements of Burning Rate

Experimental data are presented in Chapter 5 for the burning rate of methanol pool fires or the rate at which methanol is evaporated and presumably consumed by combustion. The mass burning rate (i.e., the burning rate expressed in mass of fuel per unit time) is the key variable that is desired; however it is not the actual burning rate that is measured nor is it the evaporation rate. The burning rate in this thesis is estimated using the volumetric flow rate of fuel transferred to the trays in order to maintain a steady-state fuel level. This fuel level is in turn estimated by the hydrostatic pressure measurement. The rate of delivered fuel, which replaces the fuel that vaporizes is given by

$$\dot{m} = \rho_m \frac{dV}{dt} \tag{4.7}$$

where $\dot{m}$ the mass flow rate (hereafter referred to as the burning rate), ρ_m is the density of methanol and the derivative dV/dt is volume of fuel delivered per unit time and can also

be represented as $\dot{V}$. The mass flux of fuel is the burning rate divided by the area of the tray and is defined by

$$\dot{m}'' = \rho_m \frac{\dot{V}}{A} \tag{4.8}$$

The term $\dot{V}$ is the fuel piston's motion, which is controlled by the stepper motor and lead screw. For the piston used in these experiments, the term $\dot{V}$ can be further defined by

$$\dot{V} = \frac{A_p L_s}{t} = \frac{\pi}{4} D_p^2 \frac{L_s}{t} \tag{4.9}$$

The term A_p represents the piston surface area and L_s is the stroke of the traverse. The diameter of the piston is directly measured, the time is recorded through the data acquisition routine and the stroke of the traverse is calculated by multiplying the number of pulses by the pitch of the traverse as shown below

$$L_s = pulses\left(\frac{1\ revolution}{200\ pulses}\right)\left(\frac{1\ thread}{revolution}\right)\left(\frac{1\ inch}{10\ thread}\right) \tag{4.10}$$

which is converted to metres.

Simplifying this equation by referring to the pulse count as the variable n and the last three terms as the pitch of the traverse (P_{tr}) yields

$$L_s = nP_{tr} \tag{4.11}$$

Finally the area of the tray in Equation 4.8 is the sum of the cross-stream width multiplied by the stream-wise length. Combining all terms yields a relationship for the

mass flux of methanol that is delivered to the fuel tray in response to the evaporated fuel being consumed by combustion

$$\dot{m}'' = \frac{\pi \rho_m D_p^2 n P_{tr}}{4tLW} \tag{4.12}$$

Applying the uncertainty analysis of Equation 4.3 and Equation 4.4 leads to

$$\left(\frac{\delta \dot{m}''}{\dot{m}''}\right)^2 = \left(\frac{\delta \rho_m}{\rho_m}\right)^2 + \left(2\frac{\delta D_p}{D_p}\right)^2 + \left(\frac{\delta t}{t}\right)^2 + \left(\frac{\delta L}{L}\right)^2 + \left(\frac{\delta W}{W}\right)^2 + \left(\frac{\delta P_{tr}}{P_{tr}}\right)^2 + \left(\frac{\delta n}{n}\right)^2 \tag{4.13}$$

The terms which deal with time, traverse pitch and number of pulses are considered small or approximately exact and are neglected from this analysis, reducing to Equation 4.14.

$$\left(\frac{\delta \dot{m}''}{\dot{m}''}\right)^2 = \left(\frac{\delta \rho_m}{\rho_m}\right)^2 + \left(2\frac{\delta D_p}{D_p}\right)^2 + \left(\frac{\delta L}{L}\right)^2 + \left(\frac{\delta W}{W}\right)^2 \tag{4.14}$$

Considering the left hand side of the equation first, the term $\delta \dot{m}''$ is to be determined and the value of $\dot{m}''$ is known. On the right hand side, the density of methanol ρ_m is assumed to be at room temperature since the fuel used is drawn from room temperature containers away from any heat source. For a typical temperature of 20°C, the density is equal to 791 kg/m^3 (Methanex, 2004). Assuming the uncertainty in density is due to the variance in room temperature, the change in density for an increase or decrease in temperature can be determined from the properties of pure methanol. From Figure A.1 in Appendix A, an uncertainty of as much as 10 kg/m^3 is possible for a generous rise or drop in temperature of 5°C. The diameter of the piston is 82.6 mm (3.25") and the manufacturer

measurement uncertainty is 0.25 mm (0.01"). The cross-stream width and stream-wise length vary depending on the tray and range from 75 mm to 300 mm. The uncertainty is the same for both and a modest value of 0.5 mm is assumed since all trays were machined with a non-computer controlled mill. Inserting values yields Equation 4.15.

$$\left(\frac{\delta \dot{m}''}{\dot{m}''}\right)^2 = \left(\frac{20\ \text{kg/m}^3}{791\ \text{kg/m}^3}\right)^2 + \left(2\frac{0.01\ \text{in.}}{3.25\ \text{in.}}\right)^2 + \left(\frac{0.5\ \text{mm}}{\text{L}}\right)^2 + \left(\frac{0.5\ \text{mm}}{\text{W}}\right)^2 \qquad \textbf{(4.15)}$$

The worst-case uncertainty in the mass flux will occur when the values of L and W are smallest, meaning the smallest tray tested. A value of 1.7% is calculated for the percent uncertainty in any given value of mass flux of methanol. Increasing the values of L and W to the largest tray tested yields a minimal change to 1.4% error in the total mass flux.

4.3 Oxygen Concentration in Wind Tunnel

In order to ensure that the reduction in burning rate with increasing tray size was not an effect of depletion of oxygen in the wind tunnel, a calculation was performed at the most critical case to determine the oxygen consumption. Details of this calculation are found in Appendix B. However to summarize, for a 30 cm x 30 cm tray, tested for the full duration of the capacity of the fuel reserve, 0.5 litres of methanol are combusted. The air volume in the tunnel is approximately 350 m^3, or approximately 3 kmol of oxygen. The combustion of one half litre of methanol would consume approximately 0.02 kmol of oxygen or 0.7% of the available oxygen; hence this is not a concern.

Chapter 5 discusses the experimental results for all trays tested under varying crossflow speeds. Error bars on graphs from this point on will be a result of these calculations. For the crossflow speed measurements, the absolute uncertainty will be portrayed on data points and will be the sum of the uncertainties due to tunnel fluctuations and measurement uncertainties. The uncertainty in mass burning flux will

also be presented as error bars and will have the appropriate relative uncertainty depending on tray size.

5. RESULTS AND VISUAL OBSERVATIONS

Pool fires with varying area and geometries were tested and the burning rates for crossflow speeds ranging from quiescent to approximately 6 m/s were recorded. The burning rate was determined from the volume of fuel delivered by a positive displacement pump in response to maintaining a constant fuel level in the tray during a test. A Pitot-static tube was available for crossflow speed measurements, however, in order to maintain consistent testing from day to day fluctuations in ambient temperature and atmospheric pressure, the percent of the tunnel fan power was used as a standard that was converted to crossflow speed. Short exposure direct photographs of the flames were also collected to help interpret the burning rate data.

5.1 Transient Burning Rates

Data were obtained in the form of time series, as shown in Figure 5.1. For the illustrated case of the 30 cm x 30 cm tray with a 1 m/s crossflow, a transient trend was observed in the trace until 200 seconds had passed. After that period a steady burning rate occurred which was determined from the slope of the time trace. The shape of the time trace was similar in shape for all trays tested portraying both the transient and steady-state trends. The time needed to reach steady-state varied depending on tray size and crossflow conditions. Appendix C verifies the method for obtaining the slope of the time trace.

The mass burning rate of the flame ($\dot{m}$) can be calculated when the slope of the volume transferred to the trays with respect to time is multiplied by the fuel density. The density of methanol at 20°C was the value used and is 791 kg/m^3 (Methanex, 2004). This transient behaviour at the beginning of the test was observed for all the trays tested and was attributed to the heating of the fuel and the aluminum tray. For the remainder of this investigation the steady burning rate is the quantity of interest and for any given set of conditions will be referred to as the characteristic burning rate.

Chapter 3 discussed the tray sizes tested and the use of a base case tray for comparison purposes. For the tests conducted, the 15 cm x 15 cm tray will be considered the base case upon which increasing or decreasing the area will be compared as well as the effects of changing the aspect ratio.

5.2 Base Case Results – 15 cm x 15 cm square

The 15 cm x 15 cm base case was tested at tunnel powers ranging from 0% (quiescent) to 16 %, which corresponds to a measured crossflow speed of approximately 5.5 m/s. Figure 5.2 is the characteristic mass burning rate for the base case for the crossflow speeds tested. Error bars for both the crossflow and burning rate values are presented as outlined in Section 4.2 of Chapter 4 – Diagnostics. The relative uncertainty in the burning rate is essentially within the limits of each given data point, hence from this point on, the uncertainty in the measured burning rate will be neglected. The relative uncertainty in the crossflow speed is also small enough to neglect since the points with the highest uncertainty do not significantly overlap adjoining points, however these uncertainties will be included.

At quiescent conditions the burning rate was on average 0.26 g/s for two trials. The addition of crossflow immediately produced a 90% increase in burning rate at 1m/s crossflow to a maximum burning rate of 0.5 g/s from quiescent conditions. Further increase in crossflow and the burning rate decreased and essentially leveled out to a constant value of approximately 0.42 g/s. It is suspected that there is a transition the flow passes through around 1 m/s crossflow corresponding to a transfer from a flow dominated by buoyancy to one dominated by the momentum of the crossflow. Upon further investigation through observation of the flames, it appeared that at this point of transition, the flame was in fact detaching from the rear lip of the tray and the attachment point moved further down-stream. To define the transition for comparison with other tray sizes, the region of transition is the change in burning rate caused by increasing the crossflow speed. The amount the burning rate changes through the crossflow range is the magnitude of transition. For the illustrated base case in Figure 5.2, the transitional region

occurs through quiescent to just over 1 m/s. Following the pronounced transition region the burning rate is apparently invariant to any further increase in crossflow speed.

One goal of this research was to identify the coupling between the quantitative experimental data and the qualitative flame observations. In order to observe the flames accurately, photographs were obtained approximately 1.5 m from the flame, with a digital film speed of ISO 6400, aperture setting of F 2.5 at a shutter speed of 1/60s. The high ISO rating was required due to the low luminosity of the methanol flames. Figure 5.3 (a) illustrates the effects of the flame shape for increasing crossflow speeds. The second picture at 0.6 m/s illustrates the flame attached to the leeward side of the tray. Increasing the crossflow speed to approximately 1.1 m/s removes the attachment and the flame is swept back in the same direction as the airflow. As the crossflow speed is further increased the small fluctuation in the flame shape caused by upward buoyancy forces are slowly overcome by the increasing flux of horizontal momentum from the air. Figure 5.3 (b) gives an indication of the relative proportion of buoyancy to horizontal momentum of the flow. As the crossflow speed increases, the net flow into the flame and motion of the combustion products proceeds from buoyancy driven to momentum driven. The threshold of the separation from being attached to the rear lip of the tray to trailing downstream occurs at approximately 6% tunnel power or 1.1 m/s for the base case. This transition in the trailing flame attachment was observed for the other trays tested but occurred at different crossflow speeds with different impact on burning rate.

5.3 Burning Rates for Other Square Fuel Trays

The burning rate results for the base case produced an interesting transition as the crossflow increased. In order to further qualify the results, the effect of changing the tray area was investigated in order to determine if the trend was at all scaleable. Two smaller area trays and two larger area trays were tested using the same procedure as the base case. The smaller trays had dimensions of 7.5 cm x 7.5 cm and 10 cm x 10 cm, and the larger trays were 20 cm x 20 cm and 30 cm x 30 cm.

5.3.1 Smaller Area

Proceeding in the same manner as the base case test, the smallest tray (7.5 cm.x.7.5 cm) was tested for the same crossflow conditions. Figure 5.4 shows the burning rate for the crossflow speeds tested. Again the error bars are small and do not alter the general shape the graph of burning rate as a function of crossflow speed follows. At quiescent conditions the burning rate was on average 0.063 g/s. The rate fuel is consumed in this tray was less than that of the base case as it is one quarter the area and interestingly the burning rate was also approximately one quarter that of the base case at quiescent conditions. Increasing crossflow speed however indicated a tripling of burning rate throughout the crossflow speeds tested to a maximum value of 0.17 g/s. There was no sharp transition region observed as the burning rate increased throughout the crossflow speeds tested. However it is difficult to give a definite interpretation of the transition region in this case as the burning rate seems to continue to increase beyond the maximum crossflow speed tested. Another possibility is that the transition effect does not develop until the tray area is nearer to that of the 15 cm x 15 cm case.

Photographs were obtained and the flame images are shown in Figure 5.5 (a). Although the attachment of the flame on the leeward side of the tray is observed at crossflow speeds less than 1 m/s and the same detachment of the flame as the base case, there is no local decrease in the burning rate data. Section 2.2.1 discussed the model proposed by Hottel (1959), which states that at small diameters, conduction is dominant and the heat feedback to the fuel surface can be represented by the summation of the conduction, convection and radiative components. Hottel, in addition to Akita and Yumoto (1965) and Klassen and Gore (1994), found that the burning rate per unit area is highest for 1 cm diameter quiescent pool fires and decreases to a constant value at approximately 10 cm diameter. The size of the tray tested is relatively close to this critical dimension and the heat feedback in this case is most likely governed by conduction at quiescent conditions. Figure 5.5 (b) illustrates the relative proportion of buoyancy and momentum effects on the flame as crossflow is increased. Again it can be seen that the rising motion of the combustion products is gradually decreased as the momentum of the crossflow becomes dominant.

A second tray, smaller than the base case, was tested and had dimensions 10 cm x 10 cm square. Figure 5.6 is the resulting mass burning rates for the tray and the quiescent value of the burning rate was on average 0.12 g/s. Increasing the crossflow through the entire range produced an 80% increase in burning rate with an interesting trend at 1 m/s. The burning rate tends to increase slightly until approximately 1 m/s followed by a rapid increase and then a monotonic increase to a maximum value of 0.23 g/s. This trend when referenced to the 15 cm x 15 cm base case and 7.5 cm x 7.5 cm suggests that as the tray size decreases there is a larger effect on burning rate with crossflow speed and the transition is less sharp. The magnitude of transition is large and there is a noticeable onset of transition developing. Figure 5.7 (a) and (b) are flame images of the 10 cm x 10 cm fuel tray and crossflow vectors respectively.

5.3.2 Larger Area

The span of the transition region tends to increase and the magnitude of transition tends to decrease with larger tray area indicating that perhaps as the tray size grows the burning is limited. Also, the transition region seems to develop as tray size increases. In order to quantify this, trays were constructed and tested with the same square geometry but with larger areas than the base case. Two larger trays, one 20 cm x 20 cm and the other 30 cm x 30 cm were tested under the same conditions and crossflow speeds. Figure 5.8 shows the burning rate trend for the 20 cm x 20 cm square tray as it was exposed to crossflow ranging from quiescent to 5.5 m/s. The quiescent value obtained was on average 0.47 g/s and increasing the crossflow produced a maximum burning rate of approximately 0.69 g/s at a crossflow speed of 1.36 m/s corresponding to a 50% increase in burning rate. The burning rate then decreased and leveled out to a constant value of approximately 0.57 g/s. The transition region in this case is much like that of the base case but occurs through more of the crossflow span and the magnitude of transition has decreased. This further adds to the idea that with increasing tray area the magnitude of transition decreases and the burning rate reaches a limit.

Photographs were obtained for the range of crossflow speeds tested as shown in Figure 5.9 (a) and immediately the difference between the larger flame can be seen compared to the previous tray sizes. The flame has become more turbulent and random compared to the smoother flames of the base case and two smaller area trays. The leeward edge of the flame is again attached at low crossflow speeds but begins to slide off the back some distance before completely detaching between the 1.1 m/s and 1.8 m/s pictures. It is interesting to note however the increased rising motion of the flame at higher crossflow speeds and the increased effects of buoyancy on the plume of the flame as shown in Figure 5.9 (b). It can be seen that a crossflow speed of 2.6 m/s to 3.5 m/s is required to flatten the flame, whereas for the three smaller trays tested, the flame was flattened between 1.8 m/s and 2.6 m/s.

The tray size was increased by one more increment to 30 cm x 30 cm to get a final indication of how the transition region was developing. Figure 5.10 is the burning rate curve for the crossflow speeds tested and it can be seen that the range of transitional velocities extends beyond the crossflows tested and does not result in increasing burning rate. The magnitude of transition is thus essentially zero and the burning rate is invariant throughout the crossflow speeds tested. The quiescent value for the mass of fuel consumed was on average 1.07 g/s and the highest burning rate achieved was 1.22 g/s. Photographs shown in Figure 5.11 (a) illustrate the more turbulent and random flame structure compared with all previous trays. As in the 20 cm x 20 cm case the buoyancy of the flame is overpowering the momentum of the crossflow as shown in Figure 5.11 (b).

5.3.3 Square Geometry Normalized by Tray Area

Data with respect to area of the square geometry fuel trays were further analysed by normalizing the burning rates. Dividing each burning rate by the corresponding tray area yields the mass flux in units of g/m^2s. Figure 5.12 shows the normalized burning rates for the square trays. It is interesting to note that all the trays have quiescent burning rates with an average value of approximately 12 g/m^2s. Recalling section 2.2.1, this

tendency for a constant mass flux for methanol in fuel trays greater than 10 cm in diameter was observed in studies done by Babrauskas (1983), Akita and Yumoto (1965), and Klassen and Gore (1994). However, the effects of crossflow on burning rate for non-circular trays has not been documented, but is it is reasonable to assume that the effects would be similar and is in fact verified later on in this chapter. Therefore, it would appear that the data at quiescent conditions are reliable and only an explanation for the change in mass fluxes with the addition of crossflow remains.

The region of transition can be observed to grow as the tray size increases and the overall relative difference in mass burning rate per unit area for all the trays can be seen. The magnitude of transition, or the relative increase from quiescent mass flux to mass flux at highest crossflow speed decreases with tray area, indicating there exists an interesting phenomenon when small pool flames are in the direct path of crossflow. There are definite differences not only in the transition region of the trays tested but also in the mass flux at higher crossflow speeds. For example, the mass flux for the 7.5 cm x 7.5 cm tray at maximum crossflow is approximately 32 g/m^2s. Whereas for the 30 cm x 30 cm tray the mass flux is 12 g/m^2s for the same maximum crossflow. The difference between the 30 cm x 30 cm tray and the 7.5 cm x 7.5 cm tray indicate a near tripling in mass flux with a decrease of sixteen times the tray size for a crossflow speed of 5.5 m/s.

5.4 Burning Rates for Varying Geometry: Constant Area as Function of Crossflow Speed

The implications of maintaining tray area but altering the aspect ratio were also investigated. This was accomplished by using the area of the base case 15 cm x 15 cm tray and stretching the area to 7.5 cm x 30 cm and then orienting the rectangular shape parallel and perpendicular to the crossflow direction.

With the aspect ratio defined as the ratio of the stream-wise length to the cross-stream width. The 30 cm cross-stream x 7.5 cm stream-wise had an aspect ratio one quarter that of the base case and for simplicity will be referred to as the "wide" tray. The 7.5 cm cross-stream x 30 cm stream-wise tray had an aspect ratio of four and will be

referred to as the "long" tray. Figure 5.13 is the mass fluxes for the wide and long trays at varying crossflow speeds.

For the wide tray orientation with more flame front exposed to the crossflow, the change from quiescent burning rate to maximum was a near tripling, similar to the 7.5 cm x 7.5 cm tray. Although this fuel tray produced a much quicker ascent to a maximum burning rate than the 7.5 cm x 7.5 cm tray, the similarities could suggest a dependence of the burning rate on the stream-wise tray dimension. Clearly the wide tray possesses an onset of transition in addition to a high transition magnitude. Figure 5.14 (a) are the flame photographs of the wide tray again with the point of flame detachment from the leeward edge of the tray occurring near 1 m/s. Figure 5.14 (b) shows the impact of increasing momentum and the minimal effect of buoyancy with increased crossflow.

The long tray orientation, with only 7.5 cm exposed to the crossflow indicate a climb in mass flux at 1 m/s followed by a decrease and leveling out to a constant value of approximately 12 g/m^2s. The small increase in mass flux could be disregarded due to the small magnitude resulting in a constant, invariant mass flux across the crossflow span. Although the mass fluxes are not the same magnitude as the 30 cm x 30 cm tray, the trend is similar on a certain level again giving the indication that there may exist a dependence of the rate of fuel consumption on the stream-wise dimension.

Photographs of the long tray flames were obtained and are shown in Figure 5.15 (a). The flame appears to have more difficulty detaching from the leeward edge and in fact seems to slide down the surface the tray is mounted in. The flame structure is stronger and less sensitive to incurring any change in the net heat feedback to the fuel surface. The exchange between buoyant and momentum forces is shown in Figure 5.15 (b) and it is observed that the buoyant effects are stronger in this case then in the wide orientation.

Figure 5.16 includes the base case mass fluxes to those of the wide and long rectangular trays for the range of crossflow speeds tested. The coupling of the rate of fuel consumption was again observed as quiescent conditions as well as the overall difference in mass flux magnitude of each fuel tray. This suggests the mass flux of the wide tray is being altered by some variable in the tray shape in comparison with the long tray. At the highest crossflow speed there is a near quadrupling in mass flux between the

two trays. This may indicate that the rate at which fuel is consumed is not as dependent on area as on the frontal perimeter exposed to the crossflow relative to the stream-wise length of the fuel tray.

5.5 Circular Geometry

As a final exploration into the effects of tray geometry, a circular fuel tray was tested having the same area as the base case. In order to match the area, a circular tray with a diameter of 16.93 cm was constructed and tested. Figure 5.17 compares the mass fluxes obtained for varying crossflow speeds of the circular tray with those of the base case. The circular geometry has essentially the same overall burning rate as the base case with the added exception that it bypasses the transition phenomenon at 1 m/s. At quiescent conditions there is the coupling of mass fluxes to a constant value, fortifying the previously mentioned similarity between this work and other research. The mass fluxes are similar at the higher crossflow speeds tested but the square base case tray has the transition point at approximately 1 m/s followed by a decrease in burning rate to the constant value exhibited by the circular tray.

Further research into the differences between square and circular geometries will be left for future work however two explanations are proposed for these phenomena. The first may be due to the flame attachment to the larger frontal length (half circumference) of the circular tray compared to the one-quarter perimeter of the square tray. The second reason could possibly be the variable stream-wise length (long diameter in middle to zero length on sides) as opposed to the constant length of the square tray. The roundness allows for a more gradual detachment of the flame, avoiding the sudden drop in effective perimeter observed in square trays.

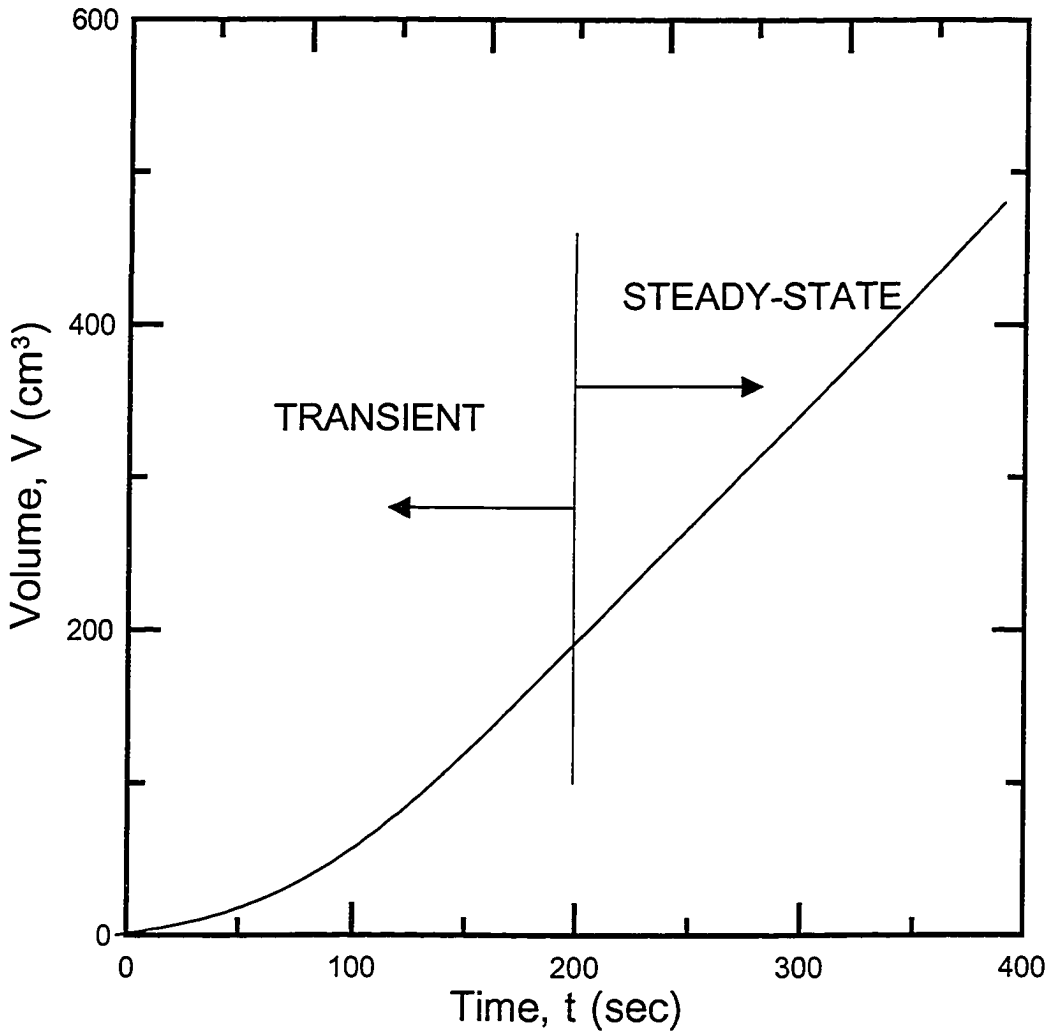

Figure 5.1: Schematic time trace of fuel transferred into fuel tray

(Appendix C is an analysis of a time trace using actual data.)

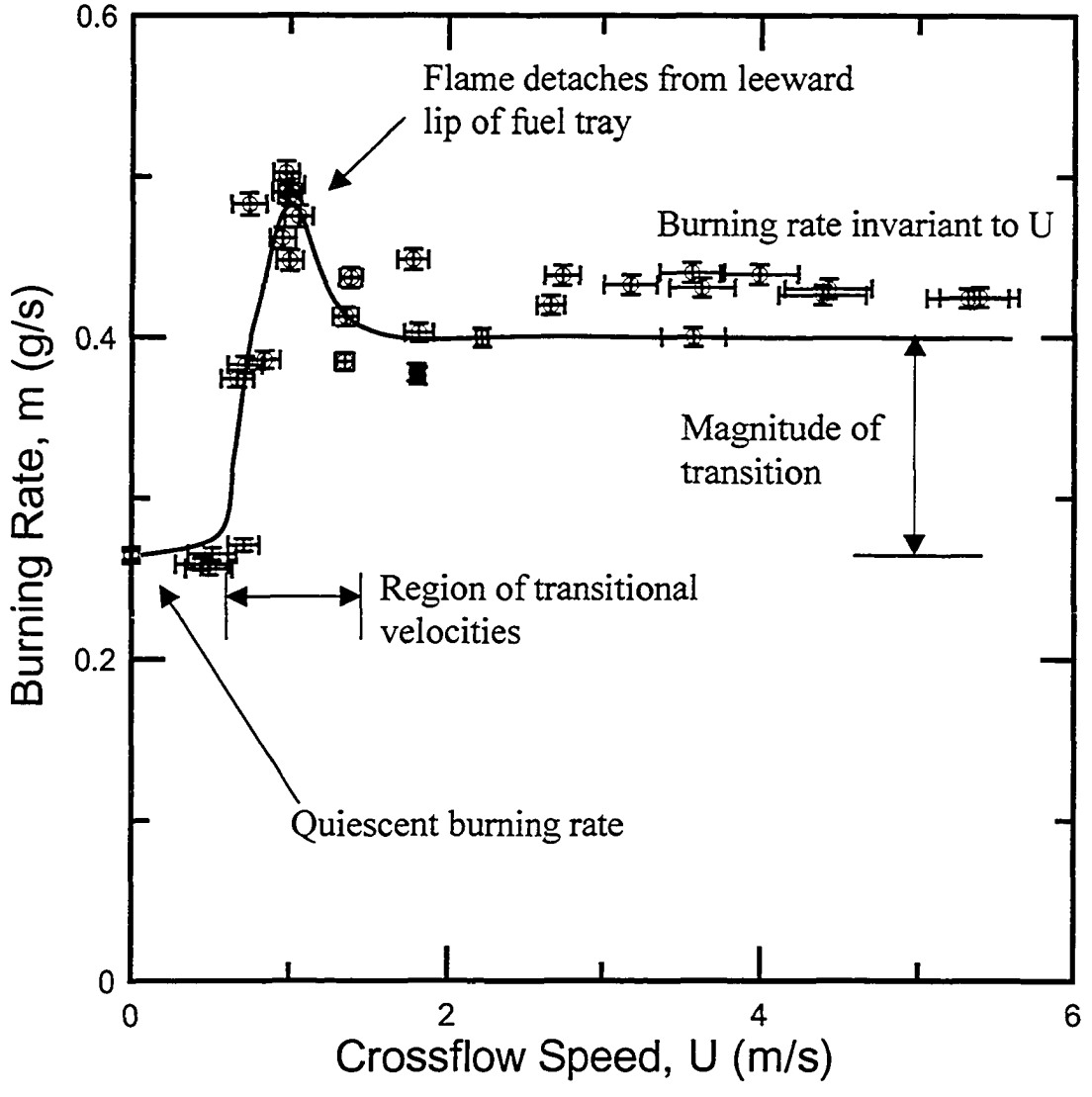

Figure 5.2: Mass burning rate of 15 cm x 15 cm square base case for varying crossflow speeds with hand-drawn trend line.

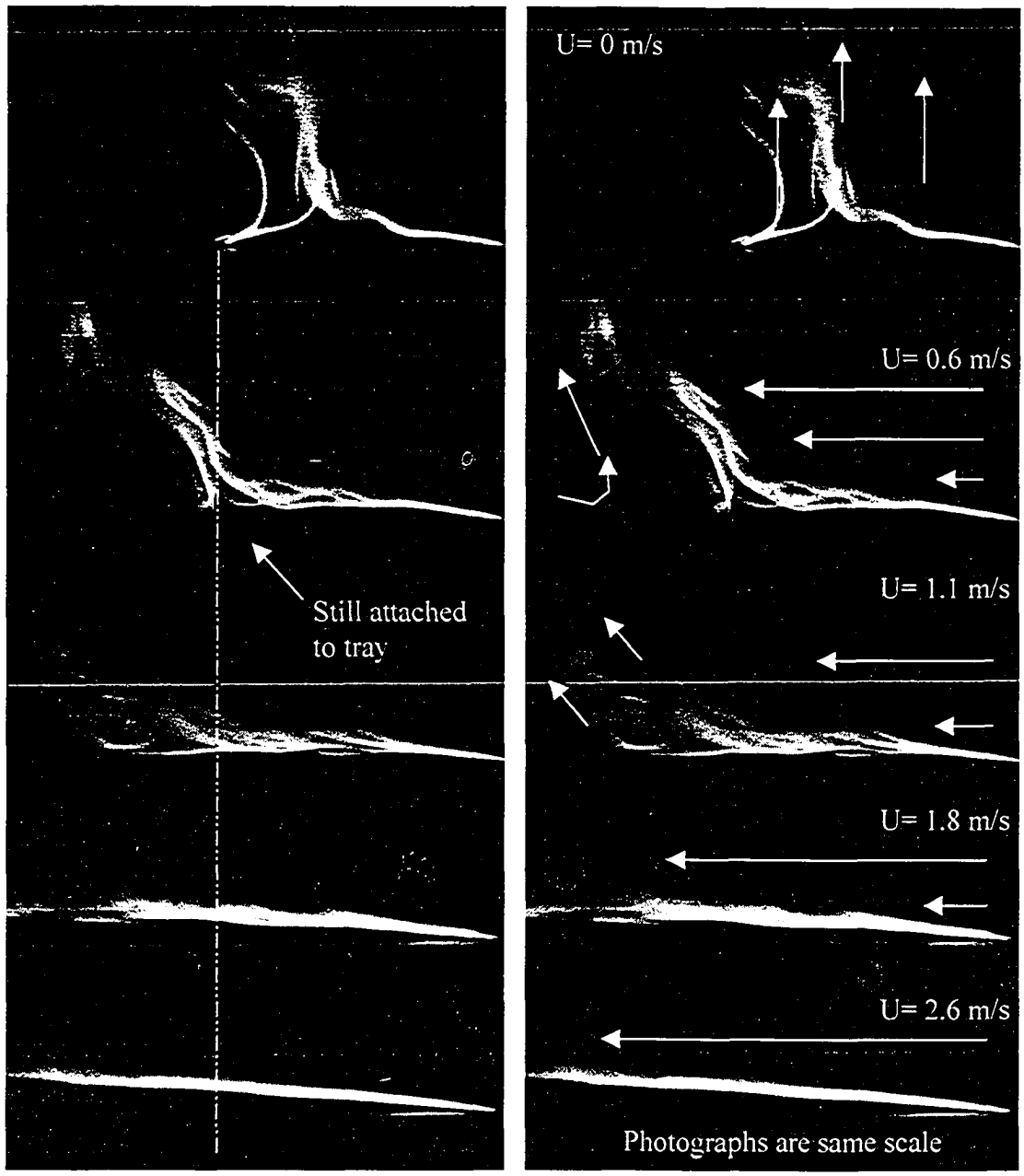

(a) (b)

Figure 5.3: 15 cm x 15 cm flame photographs
(a)Flame photographs of 15 cm x 15 cm tray under crossflow conditions.
(b) Air flow vectors indicating exchange of buoyant to momentum driven flow.

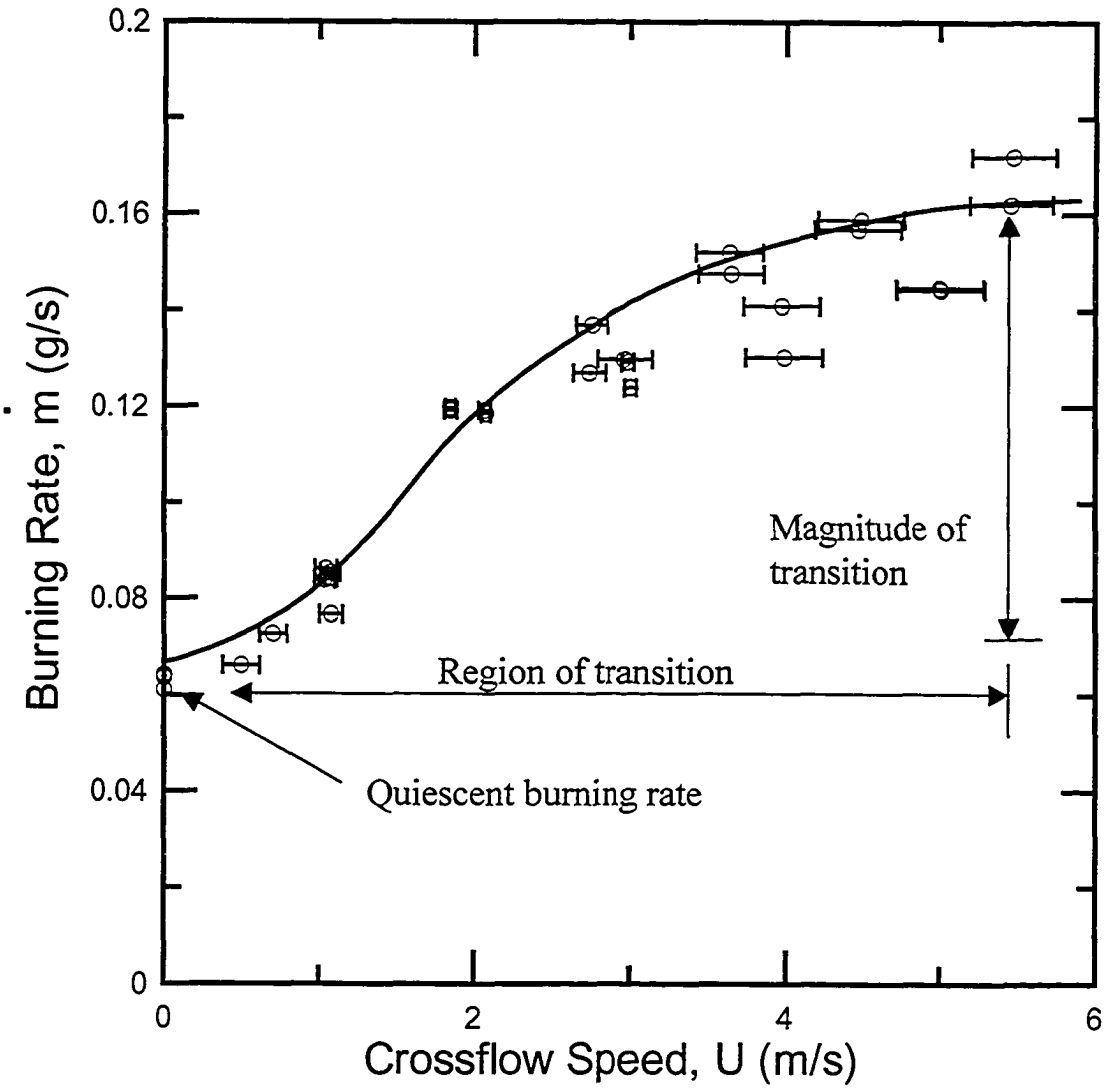

Figure 5.4: Burning rates for 7.5 cm x 7.5 cm fuel tray for varying crossflow speeds with hand-drawn trend line.

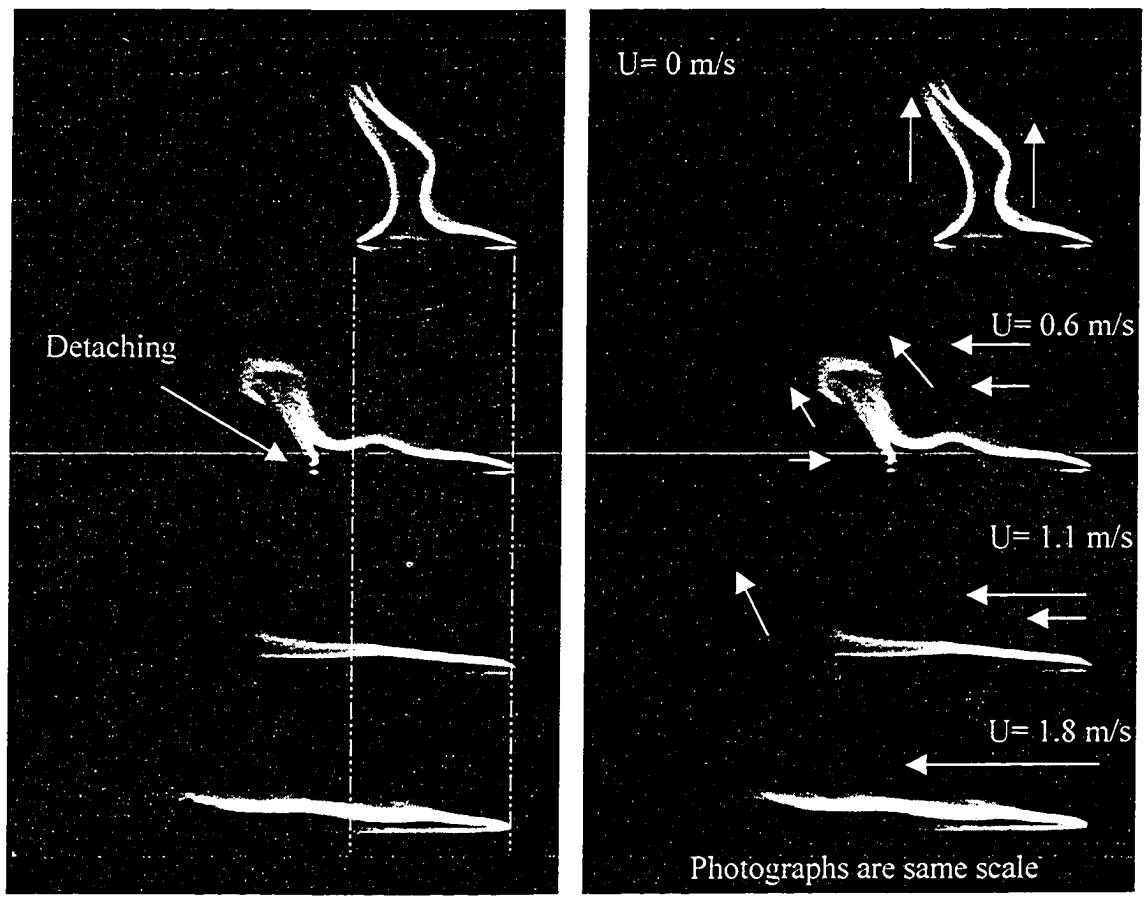

(a) (b)

Figure 5.5: 7.5 cm x 7.5 cm flame photographs
(a)Flame trailing photographs of 7.5 cm x 7.5 cm tray under crossflow conditions.
(b) Air flow vectors indicating exchange of buoyant to momentum driven flow.

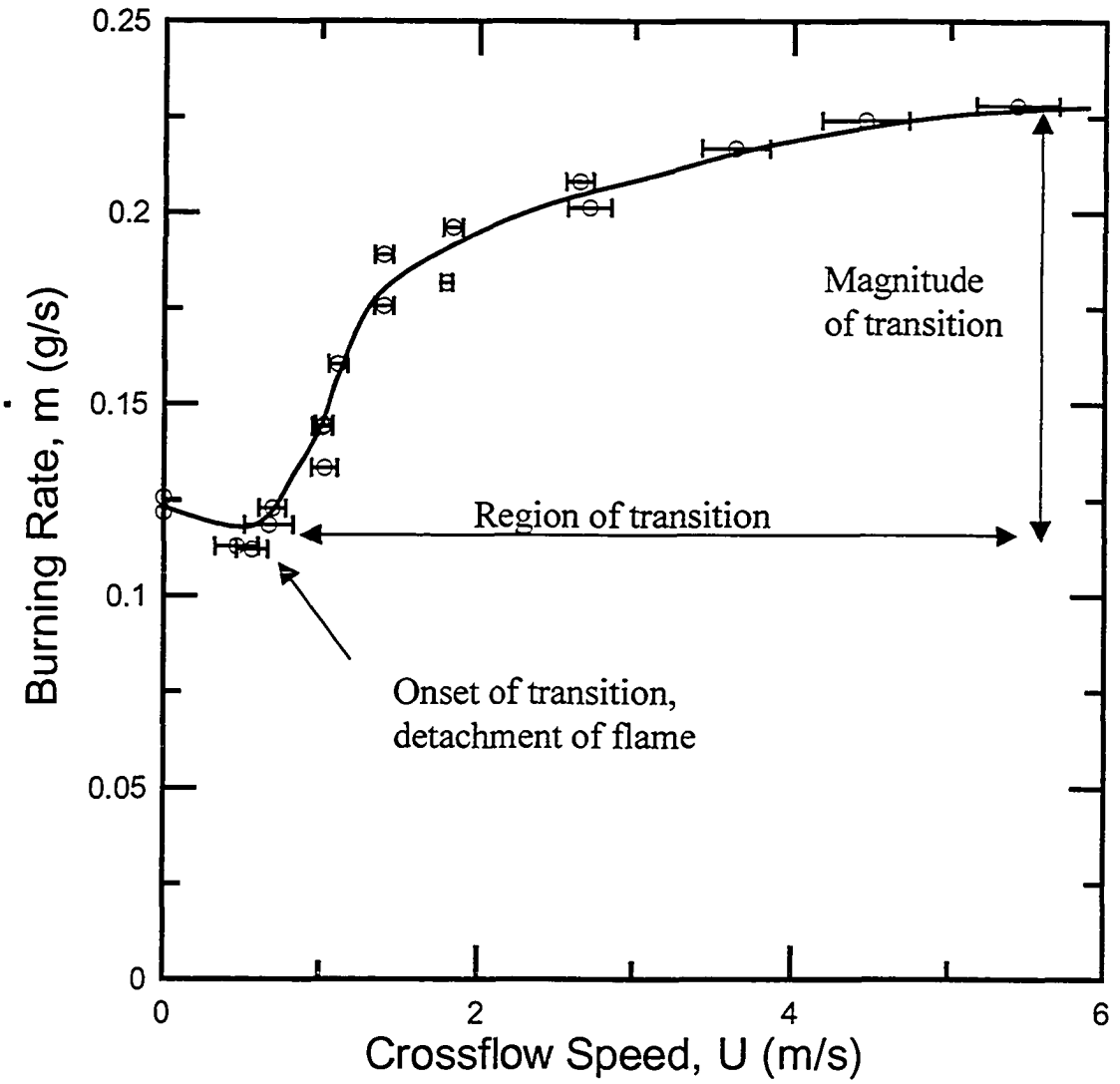

Figure 5.6: Mass Burning rates for 10 cm x 10 cm tray for varying crossflow speeds with hand-drawn trend line.

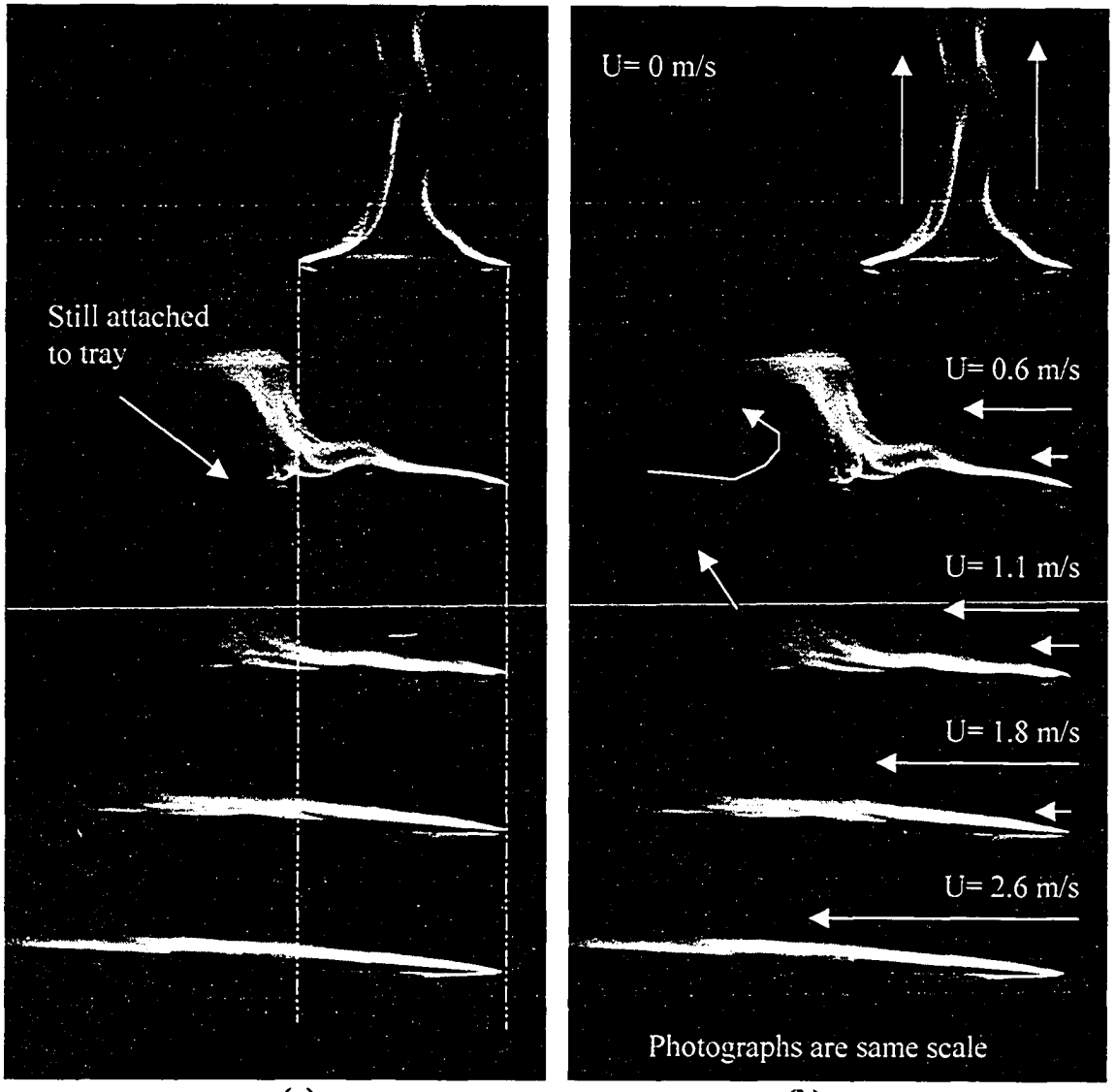

(a) (b)

Figure 5.7: 10 cm x 10 cm flame photographs
(a) Flame trailing photographs of 10 cm x 10 cm tray under crossflow conditions.
(b) Air flow vectors indicating exchange of buoyant to momentum driven flow.

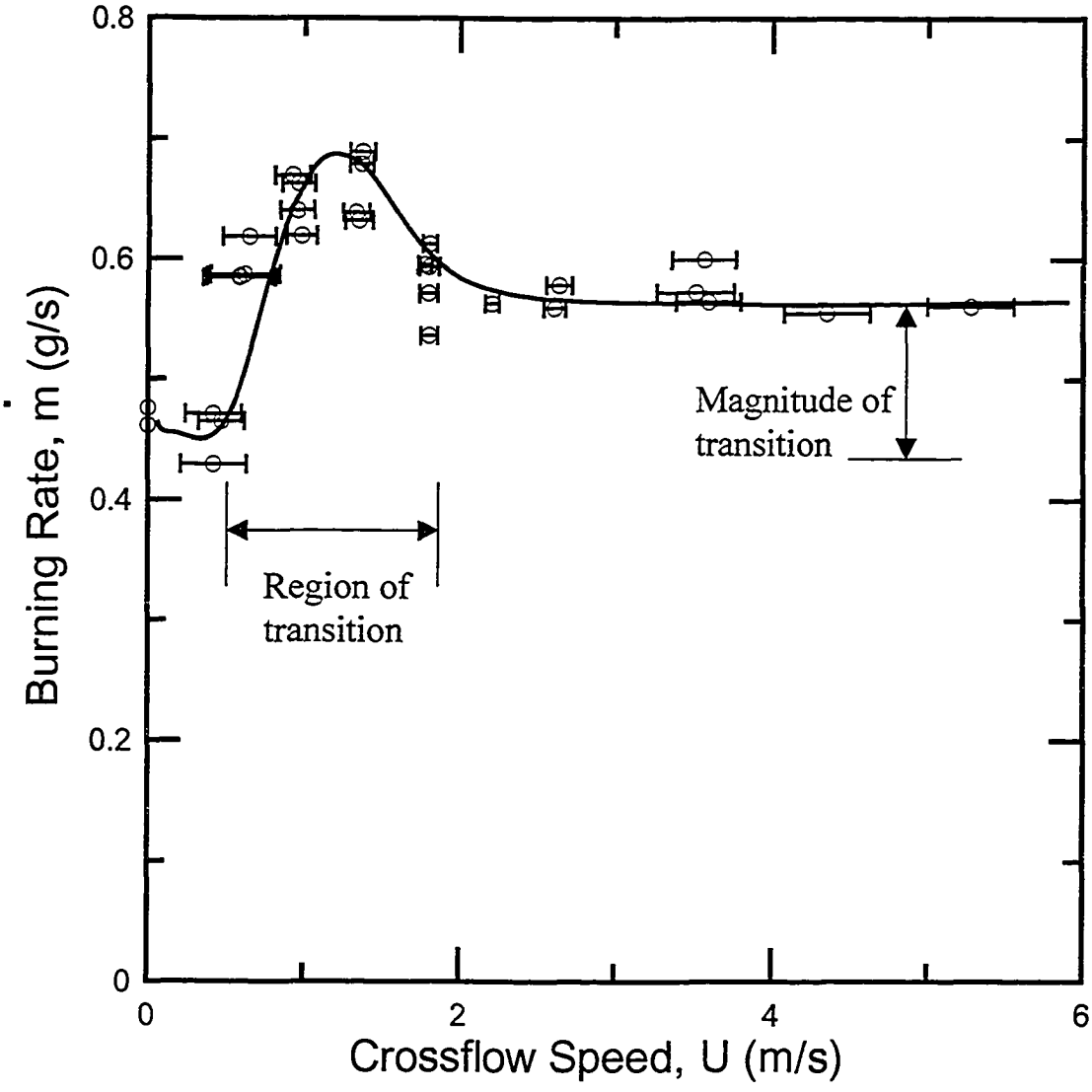

Figure 5.8: Mass burning rate for 20 cm x 20 cm tray for varying crossflow speeds with hand-drawn trend line.

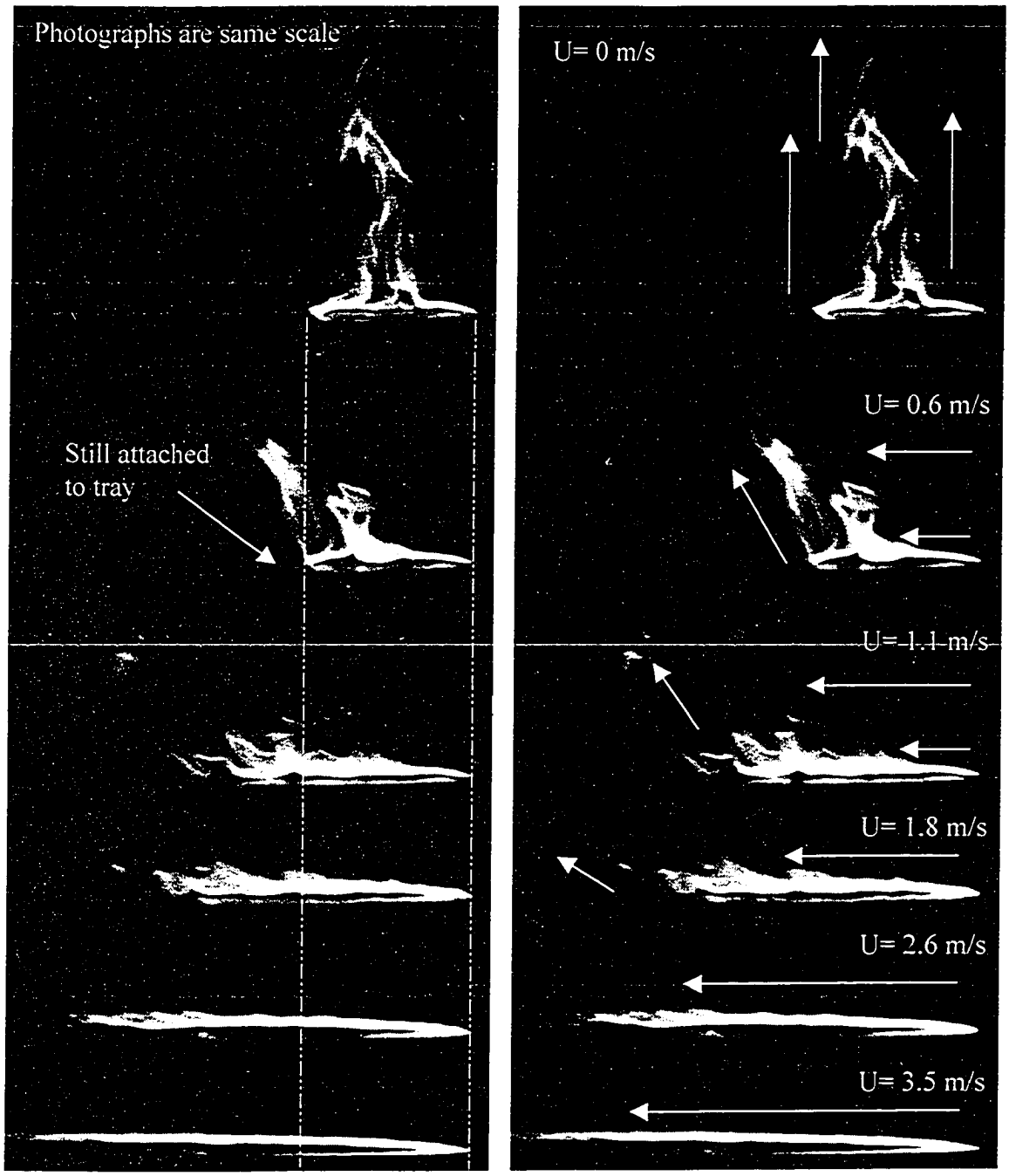

(a) (b)

Figure 5.9: 20 cm x 20 cm flame photographs
(a) Flame trailing photographs of 20 cm x 20 cm tray under crossflow conditions.
(b) Air flow vectors indicating exchange of buoyant to momentum driven flow.

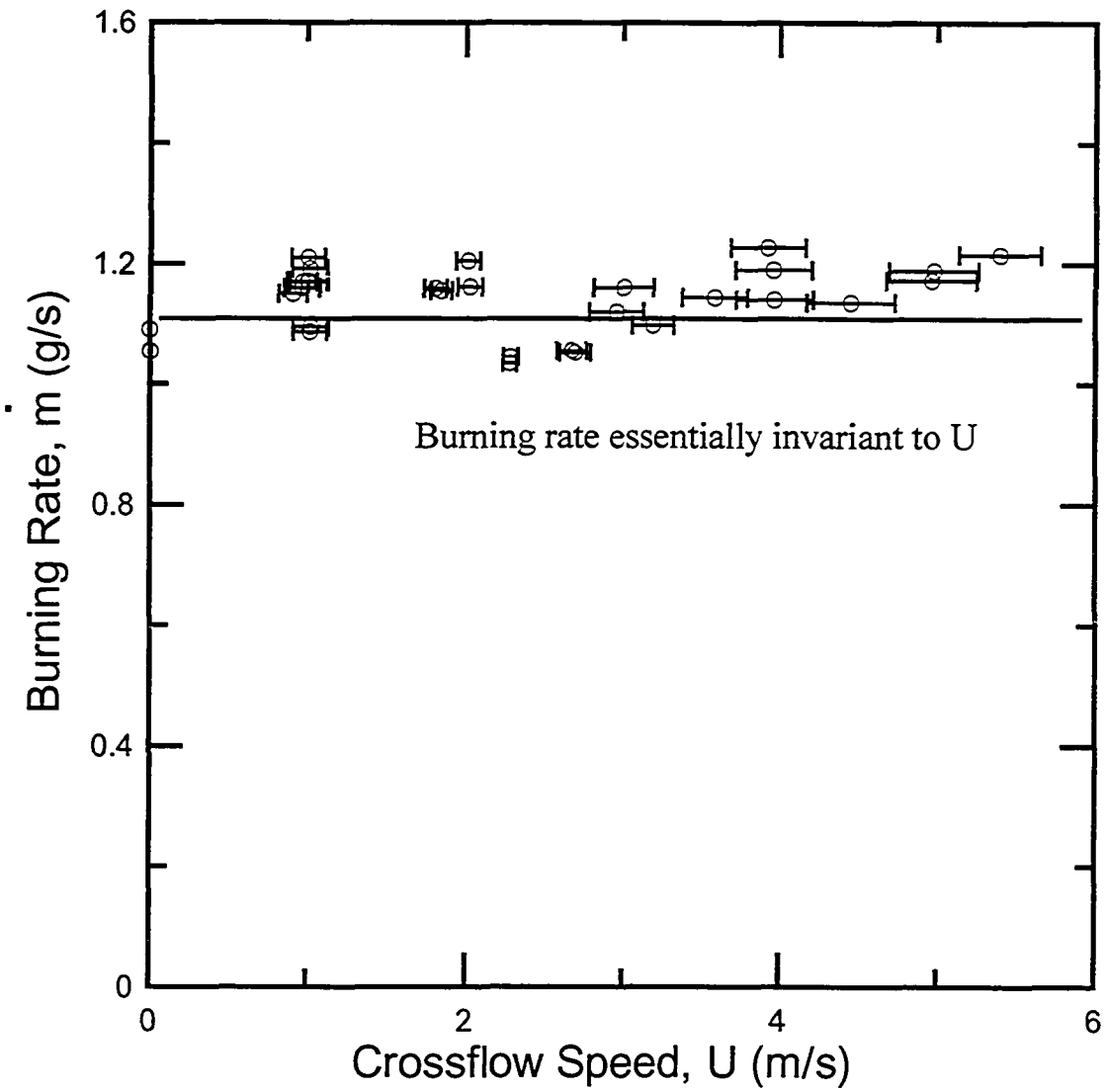

Figure 5.10: Mass burning rate of 30 cm x 30 cm tray for varying crossflow speeds with hand-drawn trend line.

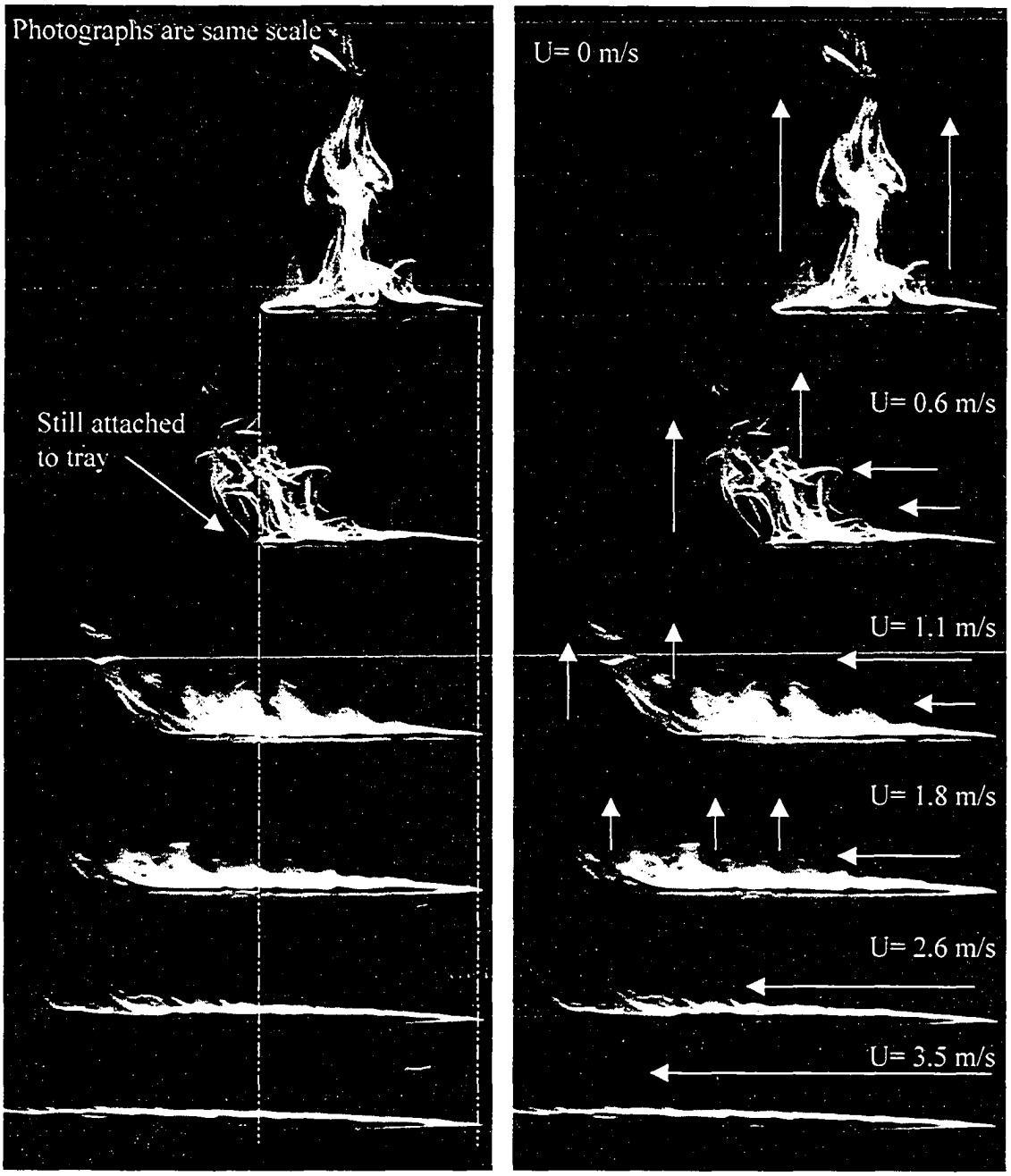

(a) (b)

Figure 5.11: 30 cm x 30 cm flame photographs
(a)Flame trailing photographs of 30 cm x 30 cm tray under crossflow conditions.
(b) Air flow vectors indicating exchange of buoyant to momentum driven flow.

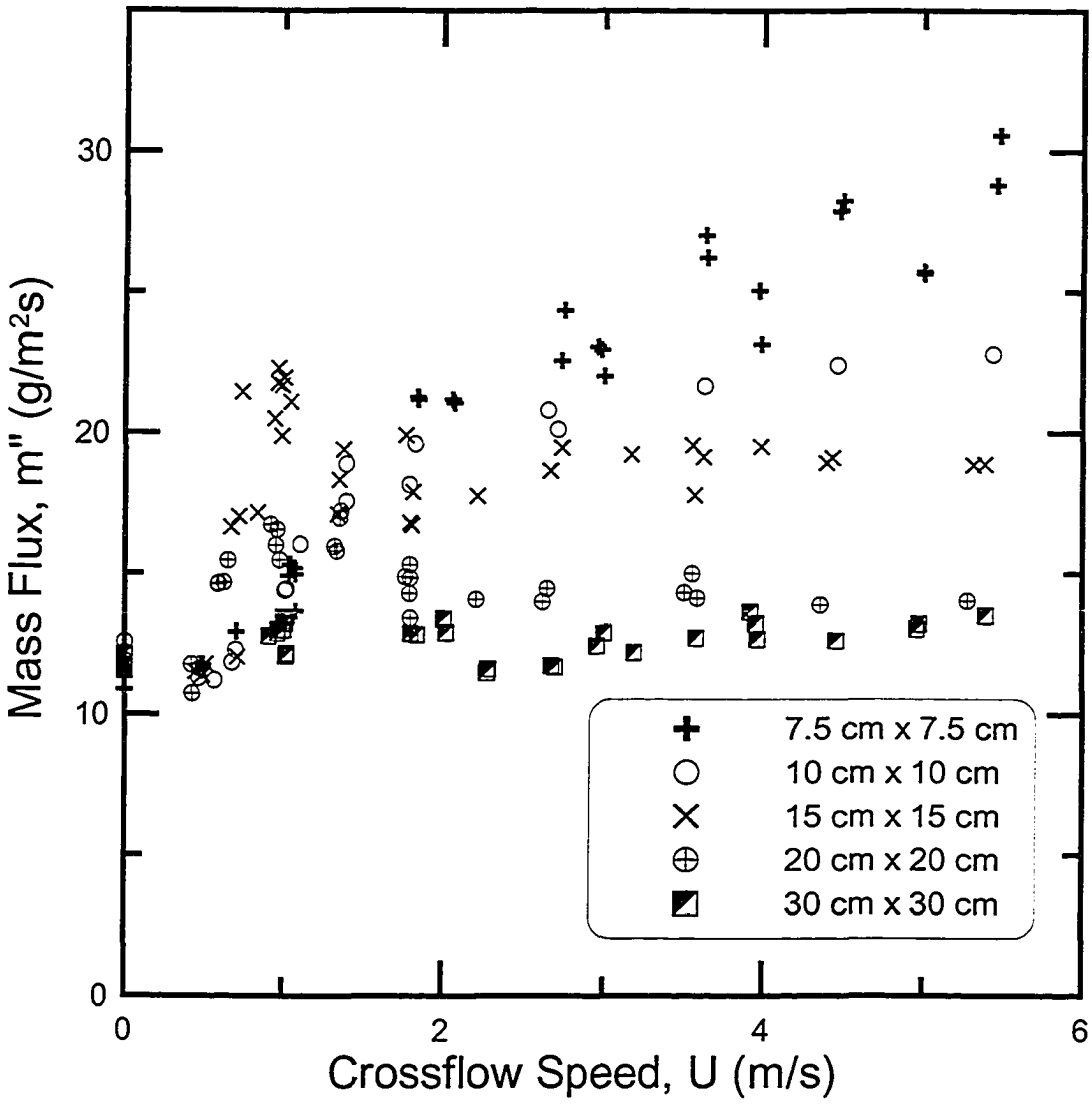

Figure 5.12: Burning rates normalized by area for square geometry trays.

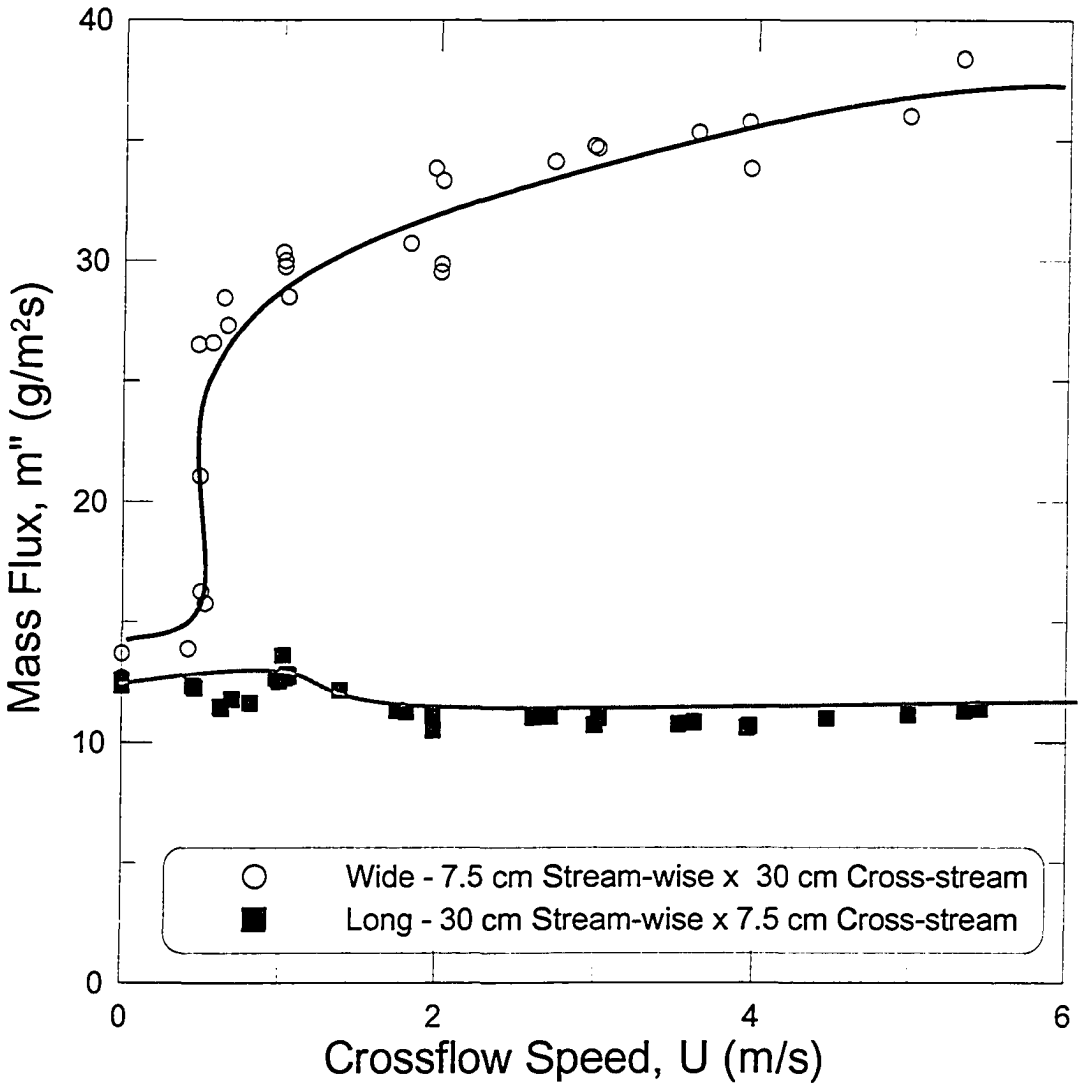

Figure 5.13: Mass fluxes for wide and long tray for varying crossflow speeds with hand-drawn trend lines.

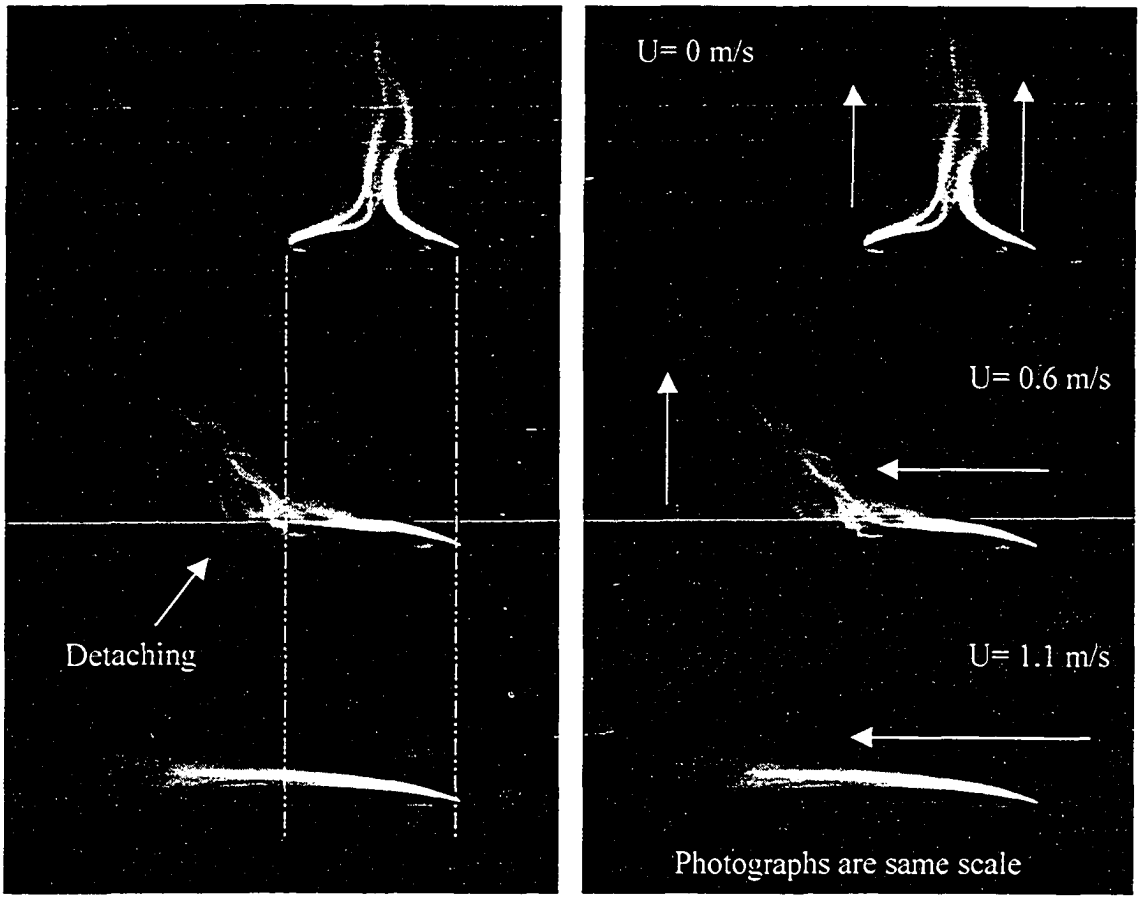

(a) (b)

Figure 5.14: Wide tray flame photographs
(a)Flame trailing photographs of 30 cm cross-stream x 7.5 cm stream-wise tray under crossflow conditions.
(b) Air flow vectors indicating exchange of buoyant to momentum driven flow.

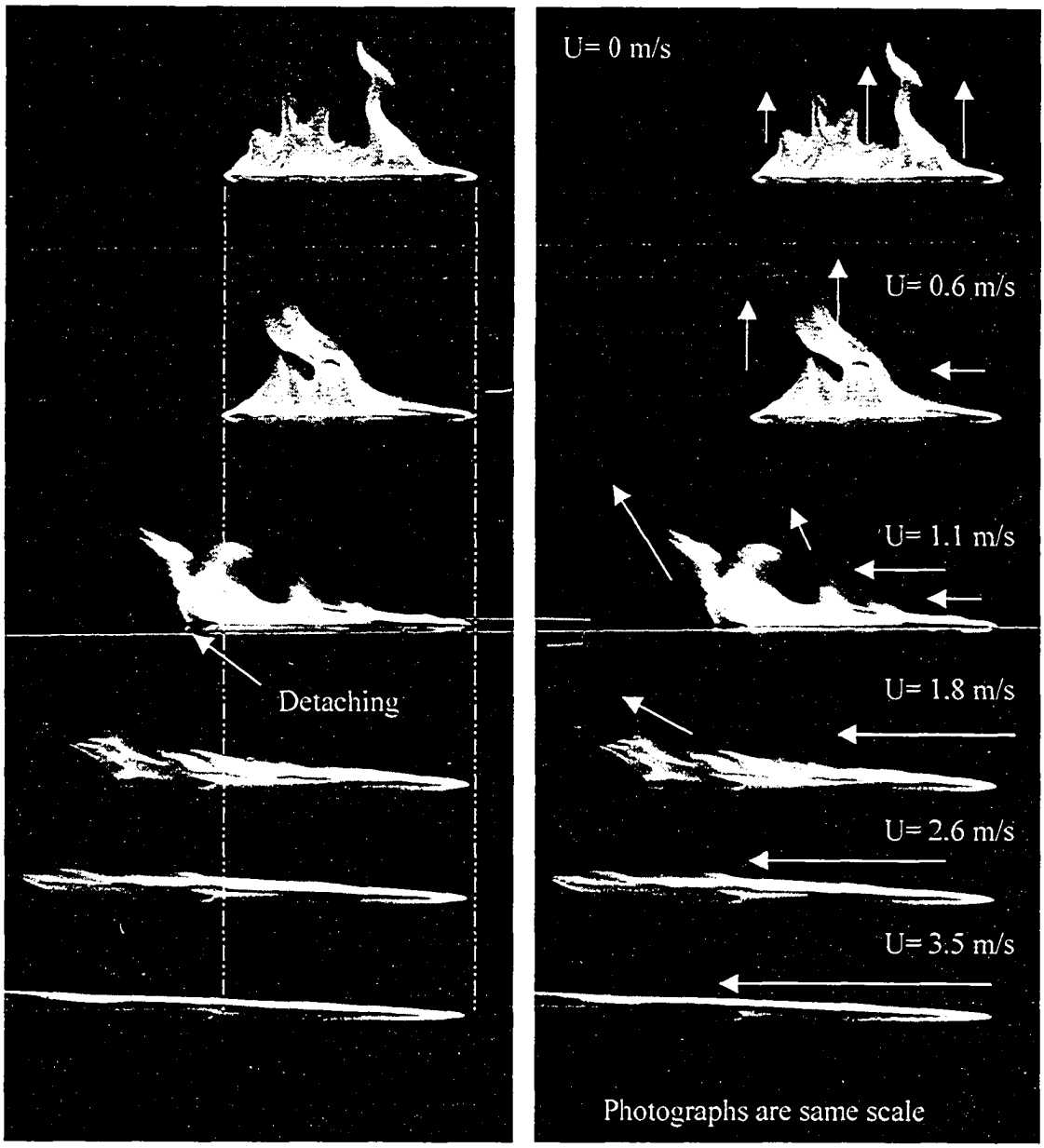

(a) (b)

Figure 5.15: Long tray flame photographs
(a)Flame trailing photographs of 7.5 cm cross-stream x 30 cm stream-wise tray under crossflow conditions.
(b) Air flow vectors indicating exchange of buoyant to momentum driven flow.

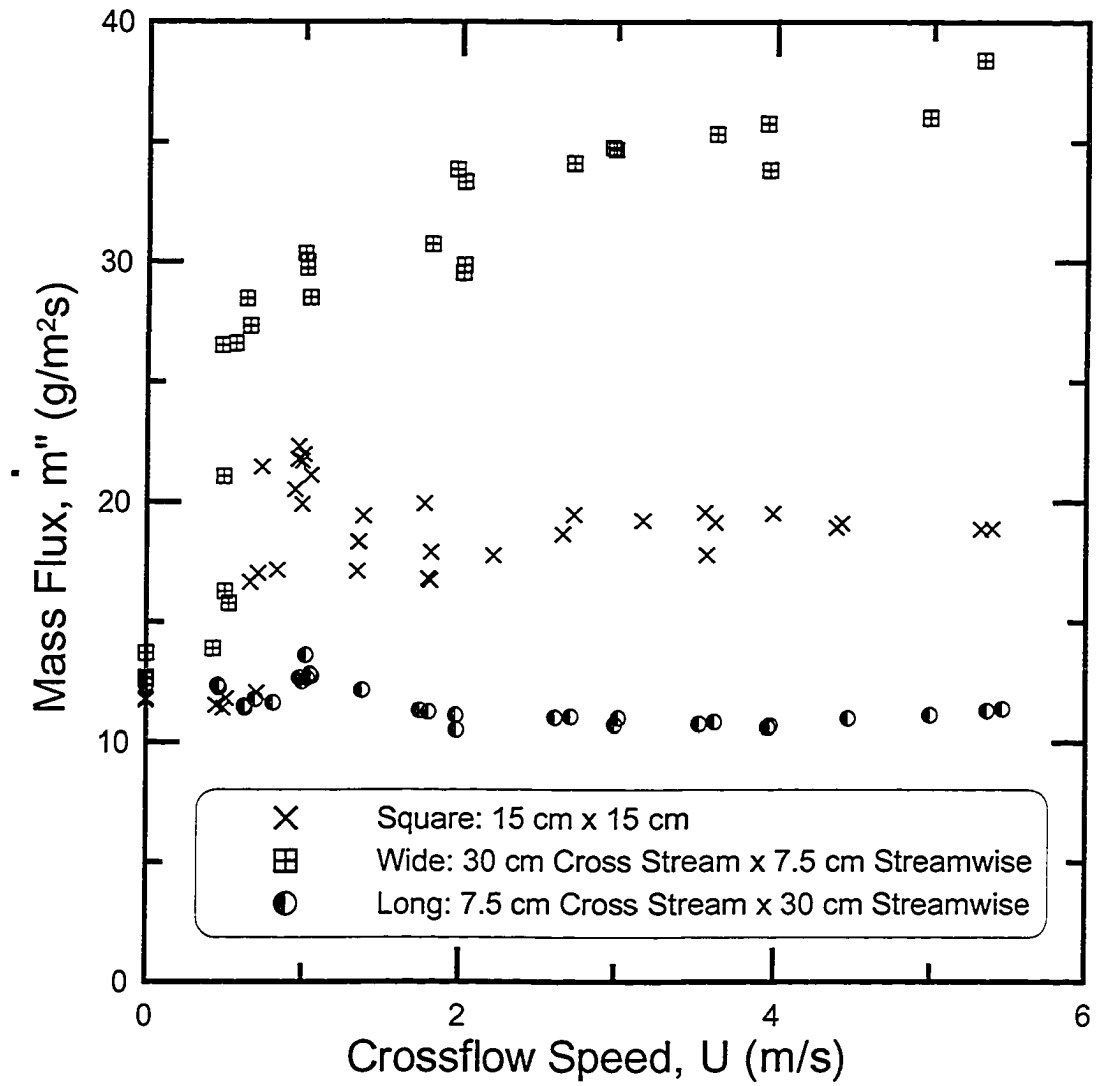

Figure 5.16: Burning rates normalized by area for varying aspect ratio.

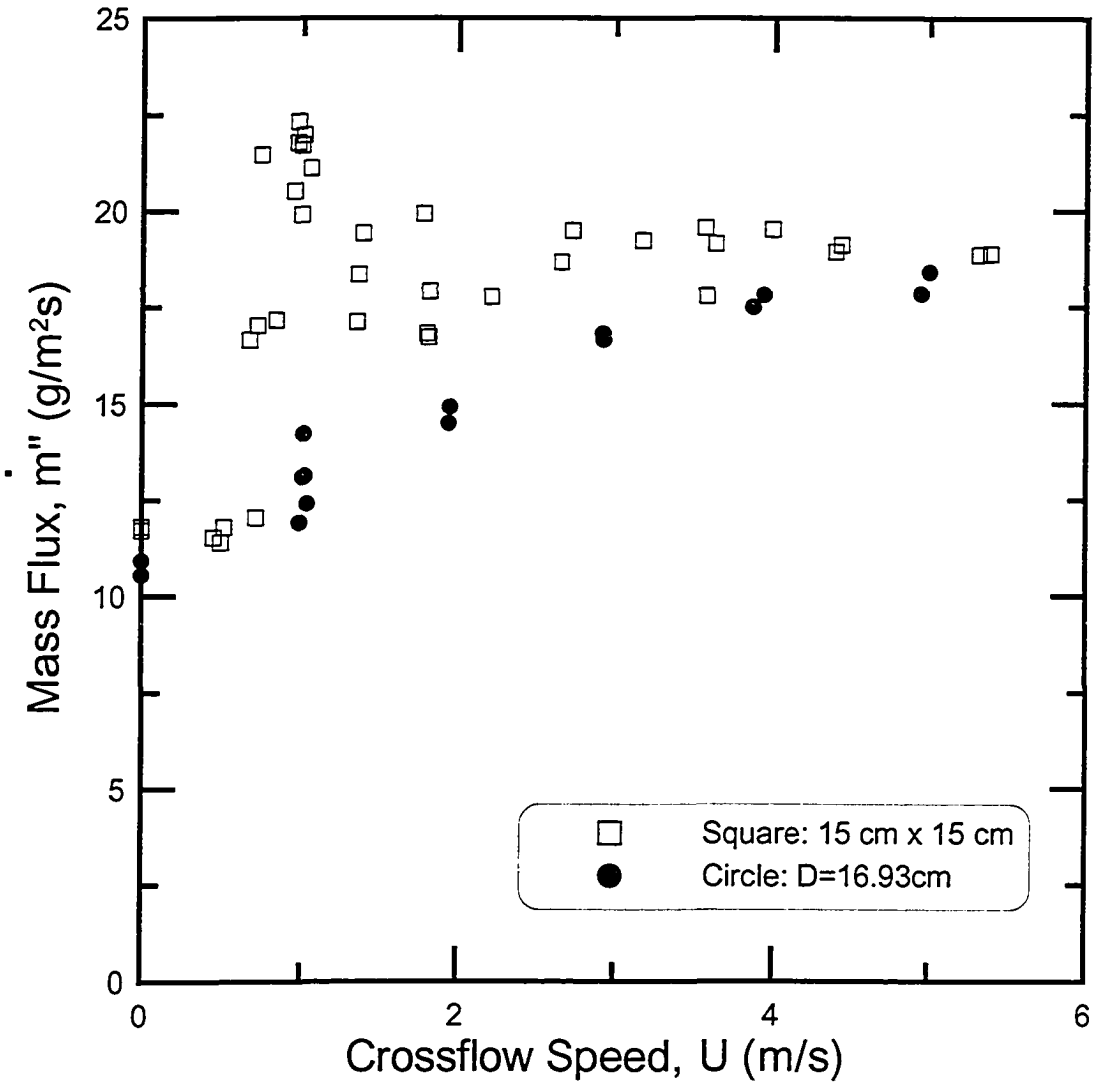

Figure 5.17: Normalized burning rates for base case and circular tray

6. CONCLUSION

This study was aimed at gaining an understanding of the effects of crossflow on pool fire burning. An experimental apparatus was designed and constructed which allowed steady rates of fuel consumption to be measured and to simplify the boundary conditions. A novel technique of maintaining and replenishing the fuel level of a burning reservoir was used and the amount of fuel required to maintain the level allowed for the calculation of the steady-state burning rate.

With a method of measuring burning rate as well as a controllable two-dimensional crossflow source, the effects of induced air flow on small rectangular methanol pool fires were studied. A better understanding was obtained of how crossflow, tray size and shape affect burning rate.

Characteristics of burning in pool fires were first observed through the use of a range of square trays ranging from 7.5 cm x 7.5 cm to 30 cm x 30 cm. For the smallest square tray, the burning rate was found to increase threefold as the crossflow speed increased from quiescent to 5.5 m/s. Increasing the tray size, a transitional effect was observed at approximately 1 m/s, which was attributed to the flame detaching off the leeward edge of the tray. This transition was defined to be the change in burning rate with increased crossflow. The region of transition was found to grow as the tray size increased and the relative magnitude of the transition decreased to the point of being negligible for the largest tray tested.

Investigation into the effects of tray geometry indicates a dependence of stream-wise length on the burning rate for rectangular shaped trays. A thinner flame normal to the crossflow resulted in a burning rate three times as large as if it were parallel to the crossflow. A circular tray was also investigated and exhibited the same burning rate as its square area equivalent but did not produce the transitional peak.

A mechanism is proposed in Appendix D to explain the results based on the primary modes of heat transfer. Heat transfer from the flame to the fuel causes the fuel to vaporize, which is in turn consumed by the flame. The total burning rate is approximated by the summation of the burning due to conduction, convection and radiation.

Future work and direction of this research are discussed in Appendix E. It includes a preliminary investigation into the effects of a turbulence grid positioned upstream of the pool fires for inducing turbulence into the crossflow.

REFERENCES

Akita, K., Yumoto, T., "Heat Transfer in Small Pools and Rates of Burning of Liquid Methanol", *Tenth Symposium (International) on Combustion*, The Combustion Institute, 1965, pp. 943-948.

Apte, V.B., Bilger, R. W., Green, J.G., Quintiere, G., "Wind-aided turbulent flame spread and burning over large-scale horizontal PMMA surfaces", *Combustion and Flame*, Vol. 85, 1991, pp. 169-184.

Arshad, M., "Investigating the Effects of Liquid Droplets, Turbulence, and Flare Stack Dimensions on the Combustion Efficiency of the Modeled Flares in Crosswind", M.Sc. Thesis, Department of Mechanical Engineering, University of Alberta, Edmonton, Alberta, Canada, 2004, 176 pages.

Babrauskas, V., "Estimating Large Pool Fire Burning Rates," *Fire Technology*, Vol. 19, p. 251, 1983, pp. 251-261.

Blinov, V. I., and Khudiakov, G.N., "Diffusion Burning of Liquids," U.S. Army Translation, NTIS No. AD296762 (1961).

Boeing commercial aircraft website, www.boeing.com, 2005.

Bourguignon, E., Johnson, M.R and Kostiuk, L.W., "The Use of a Closed-Loop Wind Tunnel for Measuring the Efficiency of Flames in Cross-flow", *Combustion and Flame* Vol. 119, 1999, pp. 319-334.

Capener, E. L., and Alger, R. S., "Characterization and Suppression of Aircraft and Fuel Fires", (WSCI 72-76), Paper presented at Western States Section Meeting of the Combustion Institute, Monterey, CA, 1972.

Chevrolet automobile website, www.chevrolet.com, 2005.

Chomiak, J., Combustion: A study in Theory, Fact and Application, Energy & Engineering Science Series edited by Gupta, A.K and Lilley, D. G., Abacus Press/Gordon & Breach Science Publishers 1990.

Emmons, H., Z. Agnew. Math. Mech., 36, 60-71, 1956.

Energy Information Administration website, http://www.eia.doe.gov, 2004.

Gaydon, A. G., Wolfhard, H. G., Flames, Their Structure Radiation and Temperature, Chapman and Hall Ltd, 1970.

H. Ingason, Report SP AR 1995:52, SP, Boras, Sweden 1995.

H. Ingason, Report SP Rapport 1995:55, SP, Boras, Sweden 1995.

Hammins, A., Fischer, S., Kashiwagi, T., Klassen, M., Gore J., "Heat Feedback to the Fuel Surface in Pool Fires", *Combustion Science and Technology*, Vol. 97, No. 1-3, 1994, pp. 37-62.

Hottel, H.C., "Review-Certain Laws Governing Diffusion Burning of Liquids, by V.I. Blinov and G. N. Khudiakov," *Fire Research Abstracts and Reviews*, Vol. 1, 1959, pp. 41-44.

Johnson, M.R., "Wake-Stabilized Diffusion Flames in Crossflow: Application to the Efficiencies of Gas Flares", Ph.D. Thesis, Department of Mechanical Engineering, University of Alberta, July 2001, 171 pages.

Joulain, P., "The Behavior of Pool Fires: State of the Art and New Insights", Twenty-Seventh Symposium (International) on Combustion, The Combustion Institute, 1998, pp. 2691-2706.

Kanury, A, M., Introduction of Combustion Phenomena, 1st Edition, Gordon and Breach Science Publishers, New York, 1975.

Kanury, A.M., Ignition of Liquid Fuels, pp. 2-188 to 2-199 in SFPE Handbook of Fire Protection Engineering, 3rd ed., National Fire Protection Assn., Quincy MA ,2002.

Klassen, M., Gore, J. P., "Structure and Radiation Properties of Pool Fires", NIST-GCR-94-651, June 1994, 153 pages.

Kolb G., Torero J.L., Most J.M., Joulain P., "Crossflow effects on the flame height of an intermediate scale diffusion flame", *Proceedings International Symposium on Fire Science and Technology* (ISFST 97), Seoul, Korea, November 1997, p. 169-176.

Lam, C.S., Weisinger, J., Weckman, E.J., "Fuel Regression of a Pool Fire in Crosswind", 2003 Spring Technical Meeting, Combustion Institute – Canadian Section, University of British Columbia.

Lapinetrucks website, www.lapinetrucks.com, 2005.

Lois, E., and Swithenbank, J., "Fire Hazards in Oil Tank Arrays in a Wind," *Seventeenth Symposium (International) on Combustion*, The Combustion Institute, Pittsburgh, 1978, pp. 1087-1098.

Magnus, G., "Tests on Combustion Velocity of Liquid Fuels and Temperature Distribution in Flames and Beneath Surface of Burning Liquid," *International Symposium on the Use of Models in Fire Research*, 1959, National Academy of Sciences, Washington (1961)

Methanex website, http://www.methanex.com, 2004

Orloff, L., "Simplified Radiation Modeling of Pool Fires," Eighteenth Symposium (International) on Combustion, The Combustion Institute, Pittsburgh (1980), pp. 549-561.

Turns, S. R., An Introduction to Combustion: Concepts and Applications, 2nd Edition, McGraw-Hill Education, 2000.

Welker, J. R., Pipkin, O. A., Sliepcevich, C. M., "The Effect of Wind on Flames," *Fire Technology*, Vol. 1, 1965, pp. 122.

Welker, J. R., Sliepcevich, C. M., "Bending of Wind-blown Flames from Liquid Pools," *Fire Technology*, Vol. 2, 1966, pp. 127-135.

Yumoto, T., "Heat Transfer from Flame to Surface in Large Pool Fires," *Combustion and Flame*, Vol. 17, 1971, pp. 108-110.

APPENDIX A

Properties of Methanol

FIGURE A.1: DENSITIES OF METHNAOL - WATER SOLUTIONS

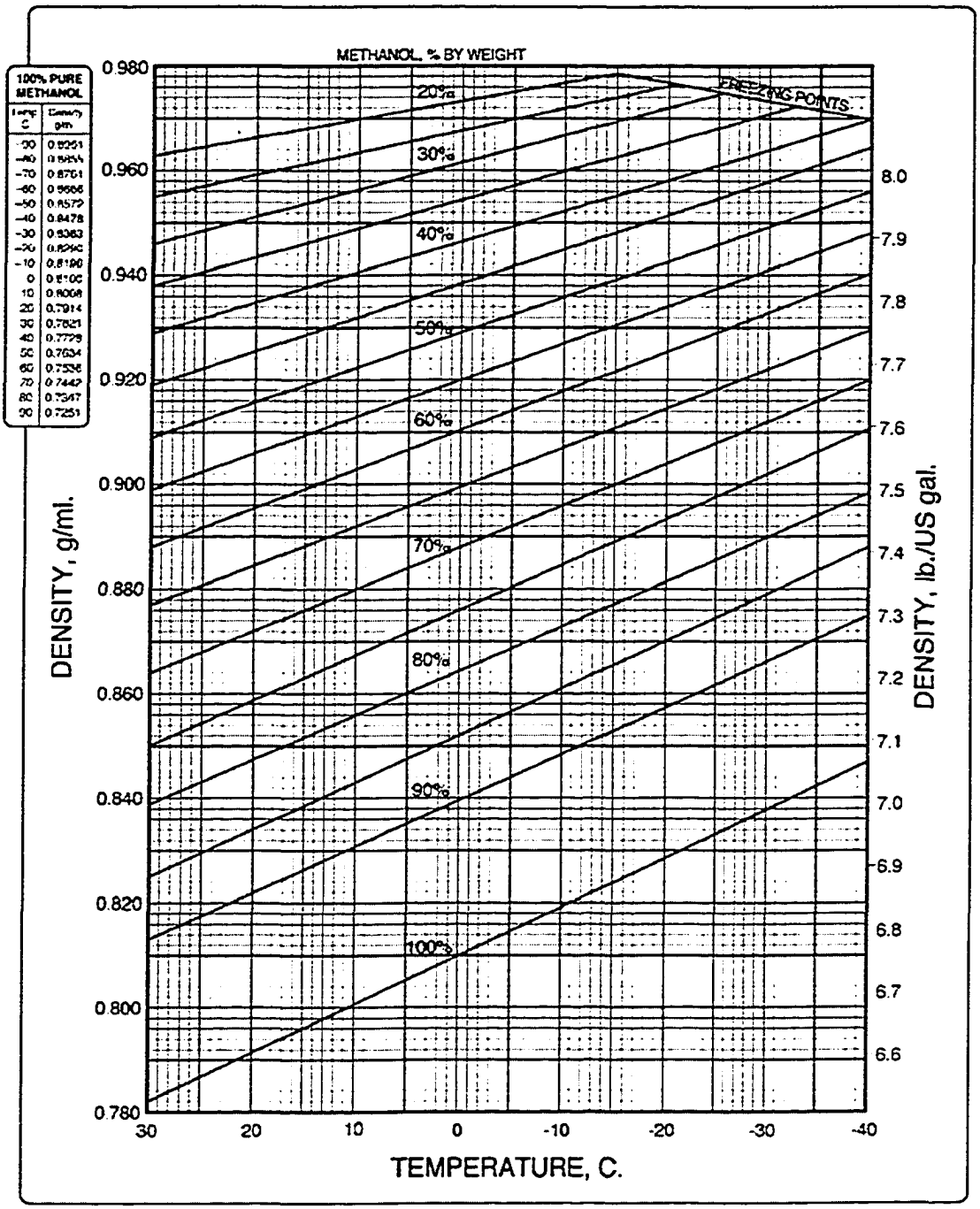

Used with permission from www.methanex.com

APPENDIX B

Wind Tunnel Oxygen Concentration

Considering the case where the most fuel and oxygen would be consumed will determine the worst case scenario for oxygen depletion in the tunnel. The largest tray tested was 30 cm x 30 cm and the fuel injection system has the capability to inject 0.5 L into the tray. For a full test duration the most fuel that could be consumed under steady-state conditions would be 0.5 L.

Obtaining the density at 20° (Appendix A) and molar mass of methanol:

$$\rho_m = 791\frac{kg}{m^3}$$

$$M_m = 32\frac{kg}{kmol}$$

Converting 0.5 L to $5x10^{-4}$ m^3 and multiplying by the density of methanol produces the total mass of methanol consumed:

$$5\times10^{-4}m^3 \cdot 791\frac{kg}{m^3} = 0.3955\,kg$$

Dividing the mass of methanol by the molar mass yields the moles of methanol consumed:

$$n_m = \frac{0.3955\,kg}{32\frac{kg}{kmol}} = 0.0124\,kmol$$

The reaction occurring is:

$$CH_3OH + \frac{3}{2}O_2 \rightarrow CO_2 + 2H_2O$$

Multiplying the mole fraction of oxygen by the moles of methanol consumed yields the moles of oxygen required to burn the fuel:

$$n_{O_2} = \frac{3}{2}(0.0124\,kmol) = 0.0185\,kmol$$

Now calculating the total number of moles of oxygen available in the wind tunnel. The tunnel has an internal volume of approximately 350 m^3. Using standard temperature and pressure in the ideal gas law yields the available moles of oxygen:

$$n_{o_2 tuunel} = \frac{PV}{RT} = \frac{100\,kPa(350\,m^3)}{\left(8.314\frac{KJ}{kgK}\right)293\,K} = 3.0177\,kmol$$

The ratio of the oxygen consumed to available oxygen is:

$$\%O_2 consumed = \frac{0.0185\,kmol}{3.0177\,kmol} = 0.006 = 0.6\%$$

Therefore, of the available 3.0177 kmol of oxygen, only 0.6% would be consumed in a test which burned a total volume of 0.5 L of methanol. Air has an oxygen concentration of approximately 21% and during the most severe case, would be reduced by 0.6% to 20.9% available oxygen. There is clearly no lack of oxygen in the tunnel and as the air is flowing in a closed loop circuit through the tunnel, the flame will not be starved for oxygen.

APPENDIX C

Analysis of Time Trace Slope

Fuel burning rates were determined from a time trace that was a direct result of fuel transferred to the fuel tray in response to a change in fuel level. Data was plotted in the form of volume transferred to the tray as function of time. Figure C.1 is a sample time trace of one experiment for a 15 cm x 15 cm tray under approximately 1.1 m/s crossflow. From the graph it can be seen that there is a transient segment at the beginning followed by a linear portion associated with steady-state burning of the fuel. For any given test, the slope was taken from the most linear portion in the steady-state zone. For the illustrated case the slope was interpreted as 0.6006 cm^3/s. The slope was calculated between 675 seconds and 1043 seconds of test duration. For any given time trace, the steady-state linear portion was estimated visually. To quantify this method for the sample trace in Figure C.1, the slope was calculated for the ranges shown in Table C.1. Comparing the calculated slopes to the actual slope used to represent the characteristic burning rate yielded a maximum difference of 4.5% occurring between 600 and 700 seconds. The high difference at that location indicates that the burning rate is not quite steady-state.

Table C.1: Slope calculated for range of experiment duration

Time Range (s)	Calculated Slope (cm^3/s)	Correlation Coefficient (R^2)	% Difference to Slope Used
600-700	0.574	0.9967	4.5%
600-800	0.5825	0.9992	3.1%
600-900	0.5897	0.9993	1.8%
600-1000	0.5955	0.9995	0.9%

It can be seen that there is not a large amount of error (< 5%) induced by visually examining the time trace and calculating the slope based on the full length of the linear section provides a good averaged estimation of the actual steady-state burning rate.

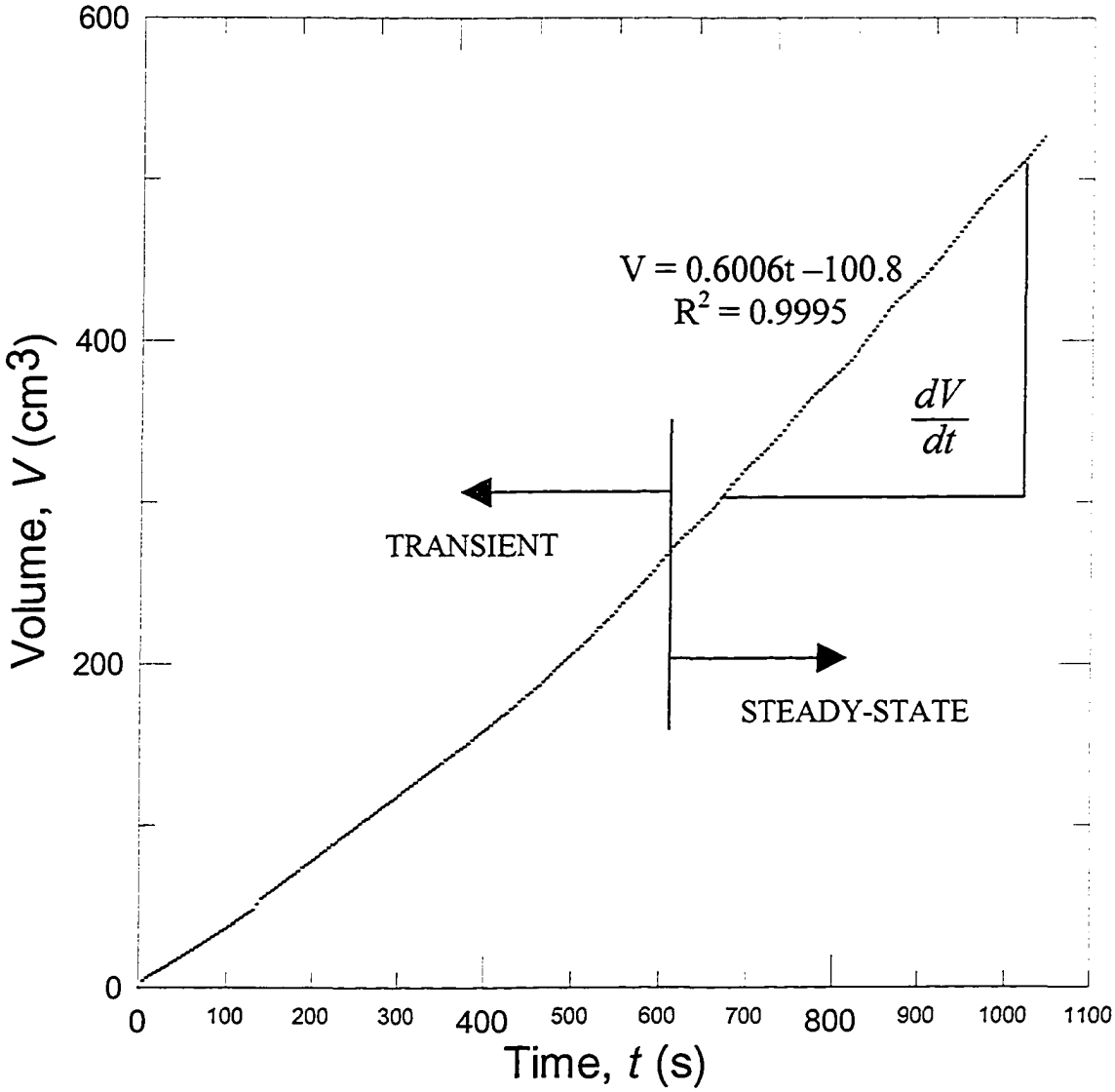

Figure C.1: Sample time trace plot - 15 cm x 15 cm fuel tray,

Crossflow approximately 1.1 m/s.

APPENDIX D

Proposed Heat Transfer Mechanism

Initially, it was assumed that the burning rate of a pool fire in a crossflow would have a relatively simple and consistent behaviour for a range of pool sizes, which could provide some insight into potential scaling relationships. The hope was to use the experimental data to create a phenomenological model that could be used to estimate burning rate of many sizes of methanol pool fires. However, these experimental pool fire findings were more complex than anticipated. Although the entirety of the problem cannot be explained at this time, a mechanism is proposed to explain the general shape of the mass flux curves.

The proposed mechanism for what sets the burning rate of a pool fire in the path of a crossflow is embedded in the heat transfer needed to evaporate the fuel. For combustion of a liquid fuel to occur, the fuel must first be vaporized and then react with oxygen. Given the abundance of oxygen available, the burning rate is limited by the vaporization process. The vaporization of the fuel is caused when the fuel is heated by conduction, convection and radiation from the flame and hot combustion products as illustrated in Figure D.1.

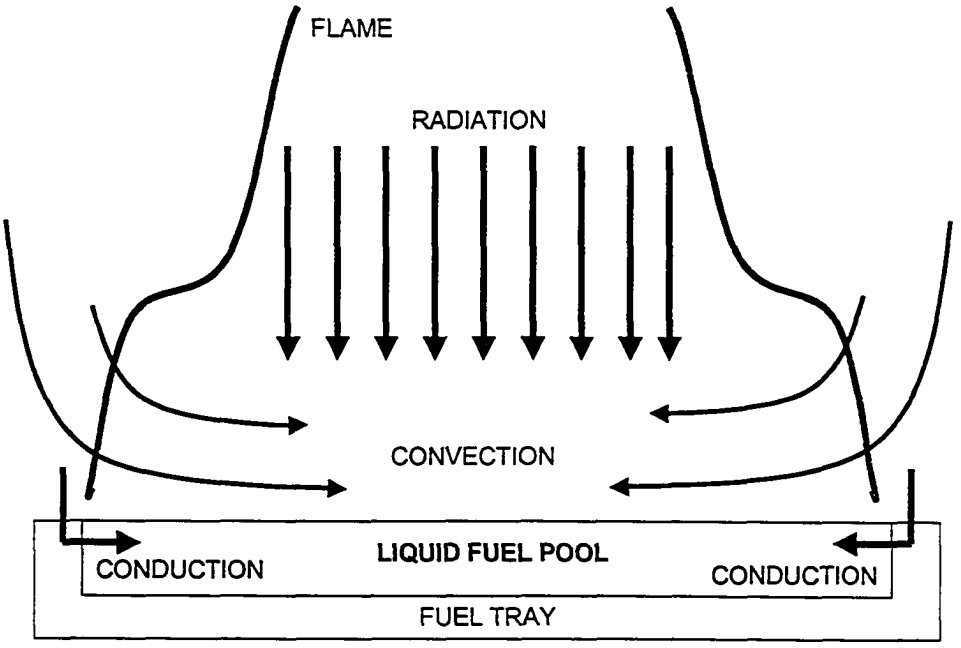

Figure D.1: Heat transfer mechanisms that cause evaporation of fuel shown for the case of no crossflow.

Evaporation due to conduction occurs when the perimeter of the tray is heated to the point where fuel at the surface in contact with the tray vaporizes. Fuel is vaporized by convection when hot gases are swept across the cooler fuel surface transferring heat and causing evaporation of the liquid. The heating of the fuel volume is further augmented when the radiative heat transfer from the luminescence of the flame is absorbed by the fuel. The net heat transfer to the liquid sets the rate of evaporation by conduction, convection and radiation once the fuel has reached its boiling point.

Referring to the normalized square tray mass fluxes of Figure 5.12 (circular geometry and effects of aspect ratio will be considered later), the transition zone discussed in Chapter 5 tends to develop with the 10 cm x 10 cm tray, showing the most distinct transition for the 15 cm x 15 cm tray. Further increase in size to 20 cm x 20 cm results in the transition magnitude decreasing and the constant burning rate following transition is also reduced. Finally for the 30 cm x 30 cm tray, the mass flux due to burning is essentially constant. One possible mechanism for interpreting these trends is

by considering the heat transfer by the summation of conductive, convective and radiative heat feedback from the flame and hot combustion products to the fuel surface.

The first assumption is how conduction and convection scale with tray size. As was found for quiescent conditions, smaller diameters are more sensitive to conduction (Hottel, 1959). Yet the experimental mass flux was found to increases significantly with increased crossflow for tray sizes smaller than 30 cm x 30 cm. The component of conductive heat transfer will scale with perimeter of the tray, as it is the sides of the tray that are in contact with the fuel. The convection component will scale with area, as it is a function of heat transfer resulting with gases contacting the pool surface. For comparison purposes, the 7.5 cm tray would have a total perimeter of 30 cm and an area of 56.25 cm^2, resulting in a perimeter to area ratio of 0.53 m^{-1}. Where as the 30 cm square tray has a perimeter of 120 cm and an area of 900 cm^2 equaling a perimeter to area ratio of 0.13 m^{-1}. A higher ratio will have a higher effective conduction component.

Considering the 15 cm x 15 cm pool fire tray size, Figure D.2 is the mass flux (g/m^2s) obtained experimentally along side the modeled conduction and convection components. Heat feedback due to the radiating flame is present but assumed to have negligible impact as the flames are relatively non-luminous. For convenience the radiation component will be considered as a part of the convection component since it scales with area.

At quiescent conditions the mass flux is approximately 12 g/m^2s. The solid line indicates the total mass flux as observed by experiment. The dotted line represents an approximate amount due to the conduction. The dashed line represents the amount due to convection. These component lines are postulations at overall magnitudes to allow a discussion of the interaction between mechanisms that are needed to create the measured burning rate.

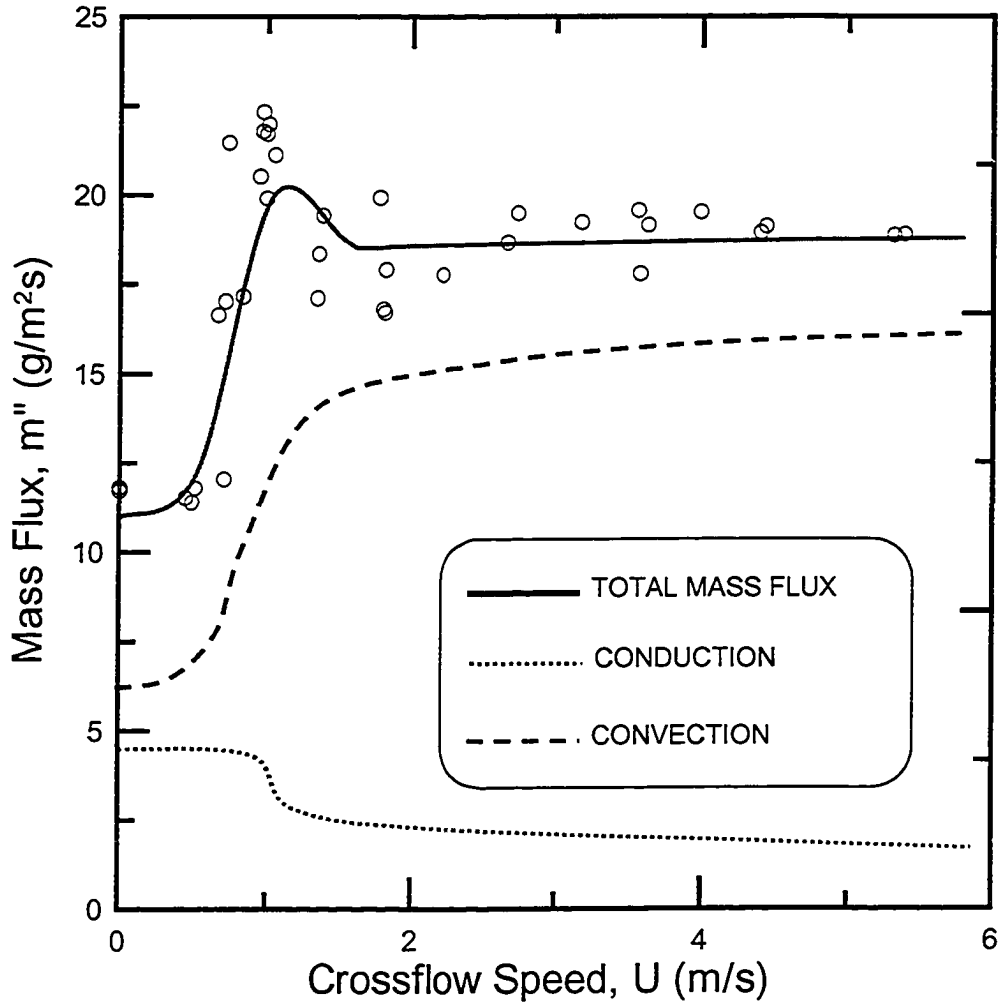

Figure D.2: Proposed heat transfer model for 15 cm x 15 cm case

The summation of the mass flux due to conduction and convection can be combined to yield approximately the total experimental mass flux. At the critical crossflow speed where the flame detaches there is assumed to be a sudden decrease in conduction, which when added to the convective term yields the bump in the total mass flux. The separation is assumed to be on the trailing edge, but it is possible there is separation along the sides as well, further adding to the sudden drop in conduction. The relative drop in conduction would be different for larger or smaller tray sizes, as the perimeter to area ratio changes. The convection component increases steeply with increased crossflow, however levels out once the flame breaks off. It is proposed that the leveling out of the convective component is a result of the heat transfer feedback loop limiting itself. In order to sustain combustion, the flame must generate heat to vaporize

fuel. Increased vaporization results in increased heat transfer, however this cannot proceed indefinitely because the upward flux of evaporating fuel limits the convection back to the fuel surface. At small flame sizes the convection is more effective because the flame is small and the distance from the flame to the tray is not great. Assuming for each tray size there is a monotonic increase in convection which subsequently decreases in magnitude for increasing tray size, as well as decreasing conduction with tray size with a distinct drop which results from the flame separation. Adding the conduction and convection together could approximately produce the experimental mass flux curves.

For the smallest size, there may not be as large of a conduction drop when the flame breaks off due to high perimeter to area ratio. Reducing the perimeter to area ratio of the 7.5 cm x 7.5 cm tray by 25% would equate to a ratio of 0.4 m^{-1}, three times as large as the 30 cm x 30 cm tray. A high ratio allows for the back edge to break off without significantly impacting the overall conduction component. In addition, the change in flame shape is less dramatic with increasing crossflow speed and the flame may only detach at the rear, whereas the larger flames may detach along the sides. The convection could possibly be considerably more effective due to the closeness of the flame to the fuel surface. Also, the ability of the flame to more efficiently transport heat by convection would be higher as the evaporation of the fuel is not limiting it. Figure D.3 illustrates the conceptual heat transfer model based on heat transfer for the 7.5 cm x 7.5 cm tray.

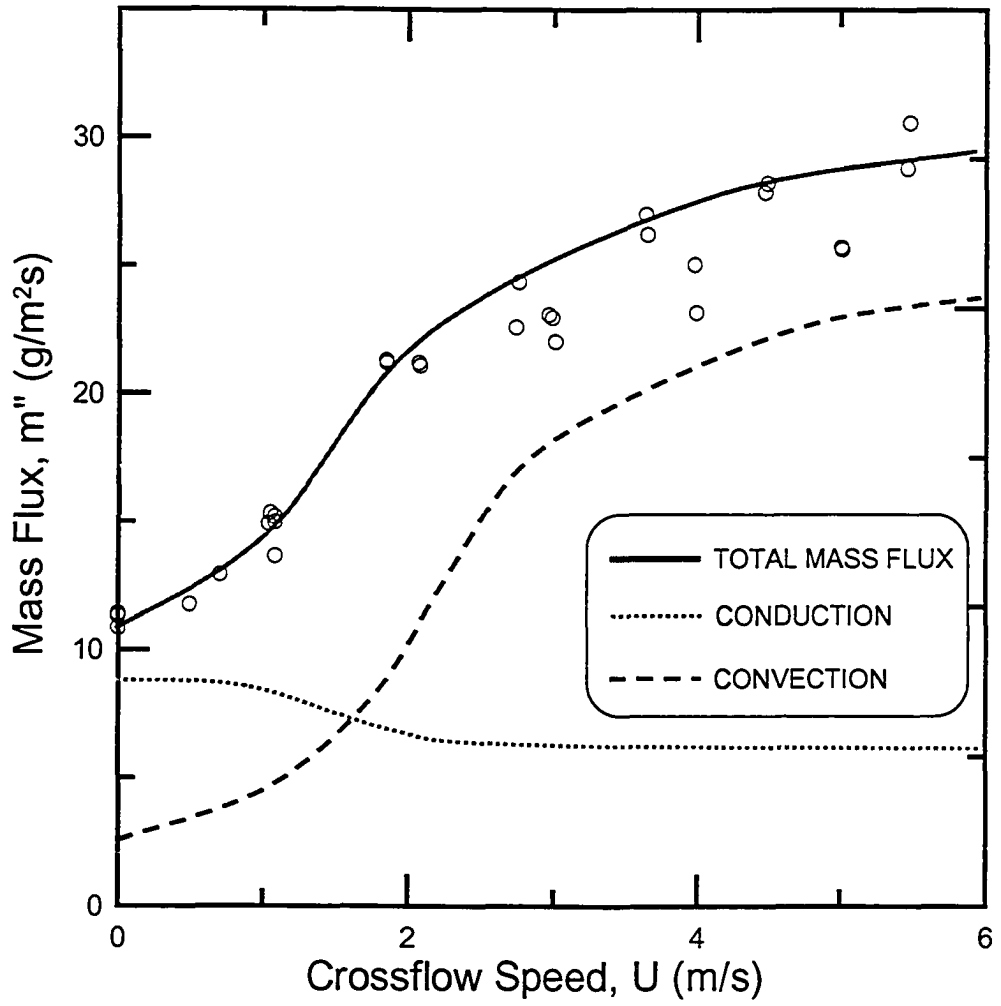

Figure D.3: Proposed heat transfer model for 7.5 cm x 7.5 cm case

As the flame becomes large (30 cm x 30 cm tray size), the turbulent nature of the flame reduces the relative effects of conduction and the flame exhibits more buoyant rising motion than the smaller trays. Following the detachment of the leeward edge, the burning rate quickly stabilizes to a constant value produced almost solely on the radiation and convective components of the heat transfer. The proposed theoretical model for the 30 cm x 30 cm tray is illustrated in Figure D.4. It is assumed that due to the size of the tray and small perimeter to area ratio that the effects of conduction are minimal. Convection and radiation must then produce the majority of the heat required to vaporize the fuel. Since the tray size is large, the convection may limit itself due to the upward buoyancy momentum of the vaporizing fuel. The resulting effects of crossflow would generate a slight increase in convection, which when added to the conduction curve,

exhibiting a slight decrease with flame detachment, would result in a relatively constant mass flux.

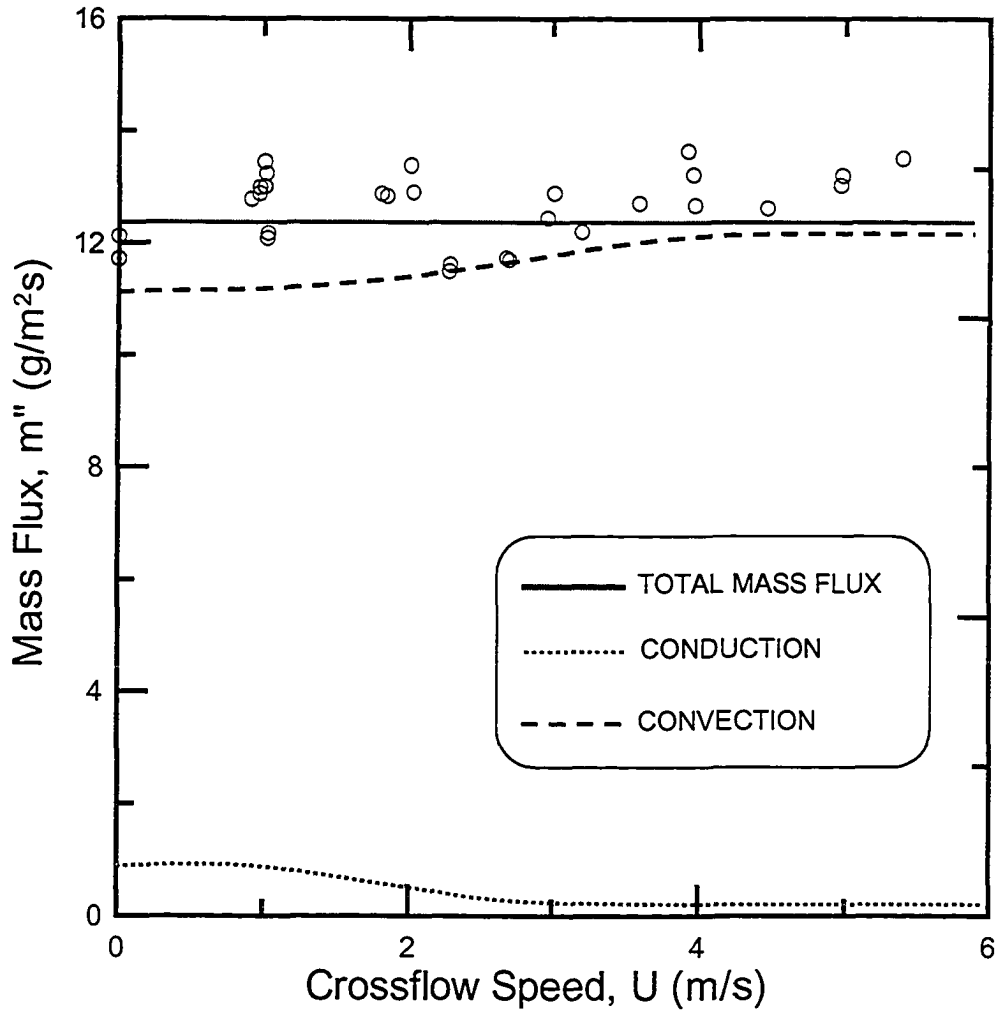

Figure D.4: Proposed heat transfer model for 30 cm x 30 cm case

Another factor that was found to be significant in these experiments was the effects of geometry. For the circular tray tested there was no bump observed as the burning rate increased, indicating that perhaps the flame did not undergo such an abrupt detachment, or loss of conduction at the back to the tray when the flame detaches. The round profile could possibly induce a more gradual detachment. Another geometry tested was that of the base case area stretched into rectangular trays. The same shaped tray, oriented parallel and perpendicular to the crossflow exhibited profoundly different

behaviour in burning rate. The wide tray (30 cm cross-stream x 7.5 cm stream-wise) behaved much like the 7.5 cm square tray, with an increase to nearly three times the burning rate at maximum crossflow compared to quiescent conditions. This may have been due to the large frontal area, and thin stream-wise length being able to accept more air into the combustion zone without limiting the amount of convection. Once the flame detached, there remained a significant amount of flame length attached to the front edge. Whereas, changing the orientation of the tray (7.5 cm cross-stream x 30 cm stream-wise) resulted in a burning rate behaviour similar to the 30 cm square tray. This orientation may have reduced airflow into the flame, and once the flame detached, there remained only the small front edge for conduction heat feedback.

Although not exact, this mechanism could be used as a starting point to describe the overall behaviour of the mass fluxes obtained for each tray size. There is no doubt that other phenomena occur which are not considered, such as effects of the fuel being injected at the center of the tray as opposed to uniformly across the entire area. This could result in higher localized heating around the edges. In order to remedy this, a plenum could be constructed below the fuel tray with many orifices to evenly distribute the fuel. Other effects may include complex mixing interfaces between incoming crossflow and the flame, or any number of unknown factors.

Summary

- At small tray sizes (7.5 cm x 7.5 cm) the burning rate is sensitive to conduction as the ratio of perimeter to area is high. Small tray sizes are also sensitive to convection as the bulk of the flame is near to the surface of the pool and an increase in convection does not significantly limit the burning rate. There is little impact on burning rate when the flame detaches and increasing the crossflow results in a relatively monotonic increase in burning rate.
- Increasing tray size and the impact that the flame breaking off has on conduction becomes more pronounced. The burning rate magnitude following transition is limited to a constant value.

- With still larger flame sizes, the heat transfer increases causing more fuel to evaporate and in turn fuel the flame. The burning rate approaches a maximum because the increasing convection component causes the heat feedback loop to limit itself, as the fuel cannot evaporate any faster.
- Further increase in tray size results in a less pronounced peak of transition and the effect of flame detachment decreases.
- Finally for the largest size tested, the decrease in conduction due to the flame detachment negates the small increase in convection with faster crossflow speed. This results in a constant burning rate.

APPENDIX E

FUTURE WORK

By simplifying the boundary condition of a combustion problem, much was learned regarding the effects of tray shape and influence of crossflow. Beginning with a simple problem allows for future work to be built upon existing knowledge. There is the potential for investigating many other variables that may influence the effects of crossflow on pool fires. Using a fuel which would produce a bright orange flame would increase the effects of radiative heat feedback and perhaps not exhibit the transition phenomenon that methanol flames produce. Other factors could also include different tray geometries and higher crossflow speeds. In this study it was found that increasing tray size decreased the magnitude of transition to the point where the burning rate was invariant to crossflow speed. This may have been due to the turbulent nature of the flame at larger sizes compared to smaller more laminar flames. One method to further investigate this effect would be to induce turbulence into the crossflow prior to flowing over the flame. This was briefly attempted by installing a turbulence grid in the tunnel upstream of the pool fires. The grid holes were 50.8 mm x 50.8 mm and the turbulence intensities as a function of downstream length were characterized by Arshad (2004). In this case the distance from the grid to the leading edge of the wing (55 cm) yields a turbulence intensity of 10% and from the grid to the tray edge a turbulence intensity of 8%. The base case tray (15 cm x 15 cm) was tested for the range of tunnel powers. During testing the Pitot-tube did not produce accurate readings as it was installed downstream of the grid (approximately 30 cm) and comparing the tunnel fan power and velocity readings to other tests without the grid confirmed this issue. Figure E.1 is the fuel consumption rate for the base case with and without the turbulence grid installed as a function of tunnel fan power. The base case tray was found to exhibit a distinct transition at 1 m/s. The addition of a turbulence grid into the crossflow reduced the magnitude of transition region and also reduced the peak burning rate, which occurs as the flame detaches from the tray leeward edge.

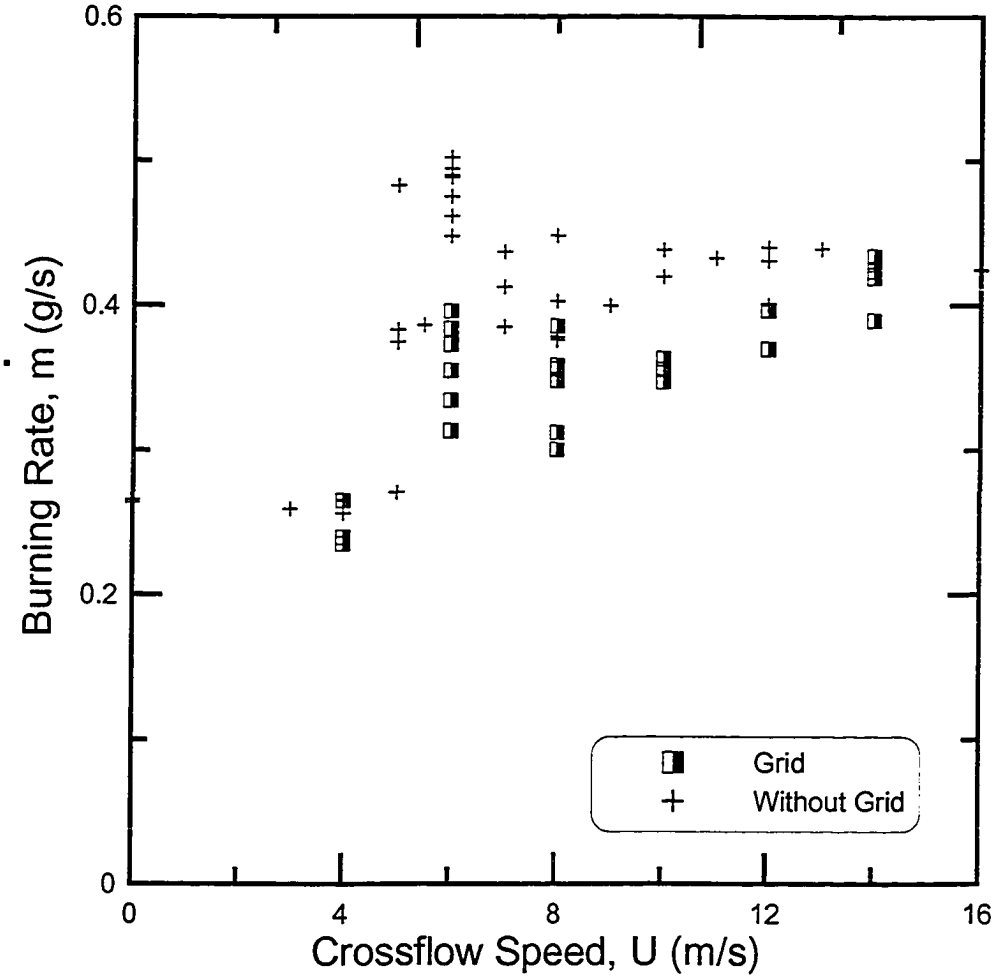

Figure E.1: Effects of turbulence grid on base case burning rate.

This effect of forced turbulence would more closely simulate an actual accidental fire, as wind is generally not produced in a uniform manner but rather it is disrupted by surrounding objects and is turbulent in nature to begin with. Further investigation into this topic could make use of smaller or larger grid spacing as well as location relative to the pool fire to perhaps produce other interesting results. However it can be seen how increasing a single variable produces different results in the behaviour of a fire and it is important to understand if it directly influences the flame or if it is being caused by some other phenomenon. Nevertheless, pool fire burning is a complex problem with many unpredictable parameters, leaving much potential for further research.